THE WEAR BEHAVIOUR OF UHMWPE AND ION IMPLANTED UHMWPE AGAINST DIFFERING COUNTERFACES

A thesis submitted to the Faculty of Engineering of the University of Cape Town in fulfilment of the requirements for the degree of Master of Science in Engineering.

By
Marcel Hohl
Department of Materials Engineering

June 1998

ABSTRACT

A study has been made of the tribological behaviour of ultra high molecular weight polyethylene (UHMWPE) and ion implanted UHMWPE during water lubricated reciprocating sliding against differing stainless steel and Yttria Partially Stabilised Zirconia (YPSZ) counterfaces. A new laboratory test apparatus was designed, built and commissioned to facilitate this research. The new apparatus is capable of simulating the reciprocating wear of a sliding couple under diverse conditions of pressure, sliding speed and lubricant environment, as well as allowing the measurement of frictional forces encountered between the two surfaces in sliding contact.

Variation in stainless steel counterface surface roughness resulted in three different types of wear behaviour. Very high wear was recorded when wearing UHMWPE against stainless steel counterfaces of surface roughness greater than 0.45 μm R_a. For wear against "moderate" surface roughnesses of between 0.05 μm and 0.45 μm R_a, an initial high *"bedding-in"* wear followed by much reduced *"steady-state"* wear was encountered, where the reduction in wear was attributed to the formation of a stable polymer transfer layer on the metal counterface. When sliding UHMWPE against polished stainless steel counterfaces (R_a = 0.02 μm), very low wear rates were recorded for the initial 50 km of sliding. After this initial period of very low wear, the wear rates were however found to increase dramatically. The increased wear against such polished stainless steel counterfaces was attributed to a subsurface fatigue mechanism known as *"macroscopic asperity wear"*.

The different stainless steel counterface topographies achieved by the different surface preparation techniques of "random" grinding or "parallel" grinding had no significant effect on the *"steady-state"* wear performance of UHMWPE. However, the *"bedding-in"* wear rates encountered against the "random" ground counterfaces was generally lower.

Tests performed against polished (R_a = 0.02 μm) YPSZ counterfaces resulted in no measurable UHMWPE wear, even after 200 km of sliding. Furthermore, the friction coefficients measured for the UHMWPE/YPSZ couple were less than half of those measured against a stainless steel counterface of similar surface roughness.

The ion implantation surface treatment of the UHMWPE wear pins resulted in a 32.6% decrease in UHMWPE wear against polished (R_a = 0.02 μm) stainless steel counterfaces over sliding distances of 20 km. It is however predicted that the surface hardened layer would be quickly worn away by the higher initial wear encountered against rougher counterfaces ($R_a \geq 0.02$ μm). Furthermore, non of the hardened layer will remain after 20 km, even when sliding against polished (R_a = 0.02 μm) stainless steel counterfaces. Under conditions of water lubricated reciprocating sliding, the current ion implantation treatment can thus be expected to yield only limited benefits over moderate sliding distances against optimal counterfaces.

ACKNOWLEDGEMENTS

I would like to thank the following people who assisted me during this research project:

Prof. Colin Allen, my supervisor, for his advice and encouragement.

Dr. Kashif Marcus for his additional advice and constructive discussion.

Prof. Anthony Ball and Associate Prof. Robert Knutsen for their continued support.

Mr. Glen Newins, Mr. Mike Dietz, Mr. Nicholas Dreze and Mr. Reginald Hendricks for their expert workmanship in machining the test apparatus, preparing the test specimens and general workshop assistance.

Mr. Dave Dean for his support in all things electrical.

Ms. Mira Topic for her technical assistance.

Mr. Adriaan Loedolff, Mr. James Petersen and Mr. Bernard Greeves for their photographic assistance.

Ms. Julie-Ann Henry for her tireless secretarial support.

My colleagues at the Department of Materials Engineering, University of Cape Town, for their assistance during the duration of this project.

I would also like to express my sincere appreciation to the Foundation for Research and Development (FRD) and Eskom for their financial support.

CONTENTS

CHAPTER 1

INTRODUCTION

Ultra high molecular weight polyethylene (UHMWPE) is one of the most frequently used polymers for sliding wear applications due to its excellent and well proven tribological and mechanical properties. Uses range from control and foil bearings in the aerospace industry and bearings, liners and seals in mechanical engineering applications, to the replacement of degenerate human couples such as hip, knee and shoulder joints in orthopaedics.

Failure of these types of bearings often occurs due to wear of the polymer surfaces so that an improvement in the wear behaviour of UHMWPE is desirable. Furthermore, the production of even small amounts of wear debris may lead to secondary detrimental effects such as the loosening of implants and consequent need for revision joint surgery in orthopaedics [1].

Modifying the polymer surface by ion implantation offers the possibility of an improvement in the wear performance of UHMWPE. The implantation process alters the near surface microstructure of polymers, leading to increased mechanical properties, which has been shown to be beneficial to the wear performance of a number of polymers including UHMWPE [2]. However, such reported work has been limited in extent and application and much remains to be evaluated.

Counterface topography and material type have also been shown to play a critical role in determining the wear performance of UHMWPE [3]. The majority of this work has been conducted against metallic counterfaces and wear of UHMWPE has generally been found to increase exponentially with counterface surface roughness (R_a) [4,5]. Unfortunately, much of the reported literature is concerned with either simulated practice for particular components such as in orthopaedics, or with testing using a pin-on-disc apparatus, which do not simulate the reciprocating type motion of conventional bearing devices.

Consequently, this present work seeks to evaluate the effect of surface roughness and topography on the wear behaviour of UHMWPE using a newly designed and built reciprocating wear apparatus and furthermore to examine the effects of both ceramic and metallic counterfaces on the wear of both conventional and ion implanted UHMWPE.

CHAPTER 2

LITERATURE REVIEW: UHMWPE STRUCTURE AND PROPERTIES

2.1 Introduction

UHMWPE molecules consist of multiple repeating units of ethylene monomers i.e. it has a structure of the type $-CH_2-CH_2-CH_2-$ (see figure 2.1). In the solid state it may be described as semicrystalline; the bulk material thus consists of both crystalline as well as amorphous regions. Many properties of polyethylene are critically dependant upon the amount of crystalline material present in the structure of the material [6,7]. Hence the molecular morphology is also expected to have a direct impact on the wear performance of the polymer.

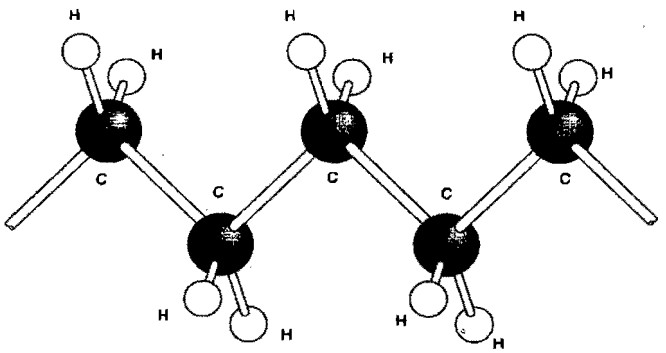

Figure 2.1 Schematic representation of polyethylene molecule [after ref. 7].

2.2 Polyethylene Crystal Morphology

Semicrystalline polymers consist of both regions of three dimensional order, or crystallites, as well as random arrangements i.e. amorphous material.

2.2.1 Crystallite Formation and Molecular Arrangement

Crystallite sizes are usually of the order of 10 nm, being much smaller than the length of a fully extended polymer chain, and are independent of molar mass [8, 9]. The essential requirement for crystallinity in polymers is stereoregularity, i.e. regions along the backbone of a significant number of macromolecules must have a regular repeating structure (isotactic or syndiotactic) [9]. Crystalline regions are

then formed from the stereoregular components of the macromolecules, representing only a portion of the overall material.

There are at present two theories describing the process of crystallisation. The older of the two, the fringed micelle theory, views the crystallite sections as bundles of regular segments from different molecules coming together to form a close packed crystalline array at localised points within the polymer (see figure 2.2a). More recently, polymer single crystal research has led to the new, and now generally more accepted theory of polymer crystallisation occurring by single molecules folding themselves at intervals of about 10 nm to form lamellae (figure 2.2b).

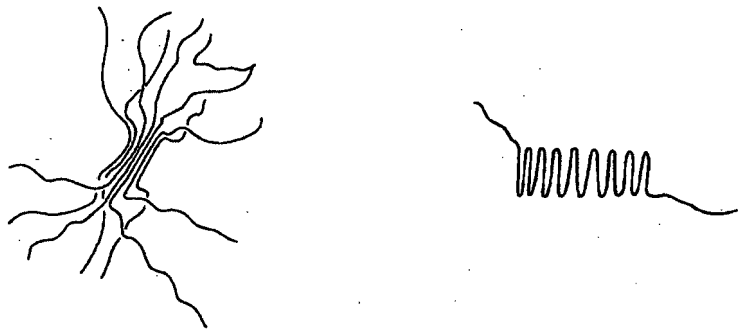

Figure 2.2 *Crystalline polymer molecular arrangements according to (a) fringed micelle and (b) lamellae theories [after ref.9].*

Both the above theories are consistent with the observed effects encountered with increased crystallinity i.e. of increased density, increased stiffness and increased softening temperature.

2.2.2 The Unit Cell

The polyethylene unit cell is orthorhombic, with the atomic arrangement within the unit cell having been researched extensively. The planar zig-zag arrangement shown in figure 2.3 results in the lowest free energy for an isolated chain [10]. The packing efficiency is quite high (73% of available space is occupied by atoms).

From figure 2.3, c is the repeat distance along the molecular chains and represents 2.53 Å; a and b equal 7.40 Å and 4.93 Å respectively, where all the unit cell dimensions are representative of cold drawn threads and rolled sheets.

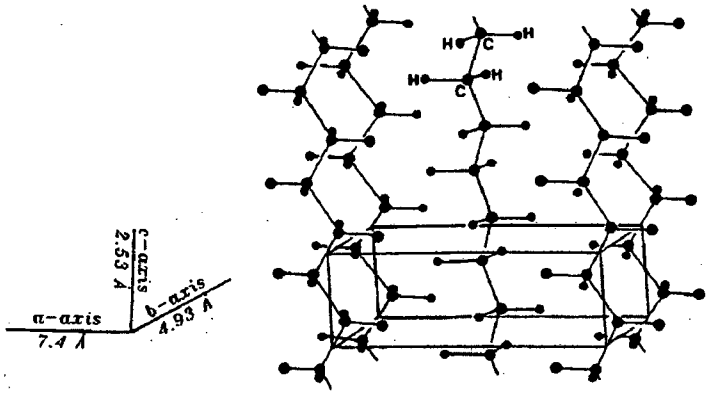

***Figure** 2.3 Packing arrangement of molecules in polyethylene crystallite [after ref.10].*

2.2.3 Polymer Single Crystals

Polyethylene is one of the few polymers known to exist as single crystals, which thus allows a detailed analysis of the polymer crystal structure.

The crystals, obtained by crystallising the polymer from an inert solvent at very high dilutions, are only visible under a microscope. They have a flat, lozenge shape [11,12]. Figure 2.4 shows the fold packing in a single crystal of polyethylene.

Electron diffraction patterns of such crystals have shown the polymer chains to be oriented perpendicular to the flat faces of the crystal. Since the average length of the polyethylene molecules is several thousand Angstroms, the chains must fold back several times within the crystal to be accommodated [13].

The unit cells of the crystallites and the relative atomic positions therein are thus well known; however, the crystallite sizes and relative distribution within the bulk material is not as clearly understood. Similar structures are however present in the bulk polymer, as evidenced by electron microscopy and x-ray diffraction studies.

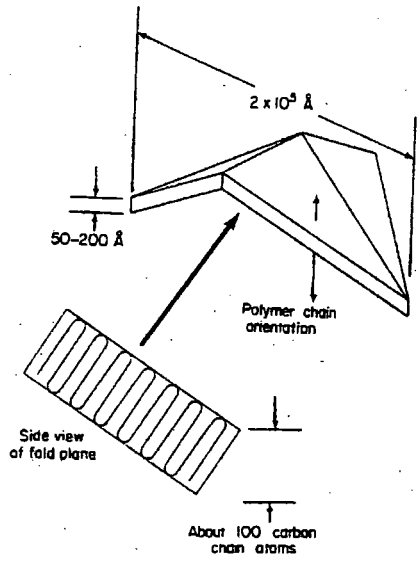

Figure 2.4a *Polyethylene single crystal fold packing arrangement. The single crystal may contain many individual molecules [after ref. 13]*

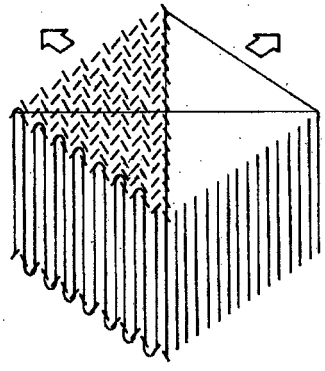

Figure 2.4b *Schematic of part of a lamellar polyethylene crystal showing the regular folded chain structure. The vertical line represents the axes of the individual molecular chains [after ref. 12].*

2.2.4 Melt Crystallized Polymer Morphology

Polyethylene, as well as many other crystalline polymers, is characterised by a spherulitic morphology. Spherulites are polyhedral entities of helically twisted lamellae radiating from a common center of nucleation, leaving amorphous

material trapped between their fold surfaces and between the spherulites themselves (see figure 2.5).

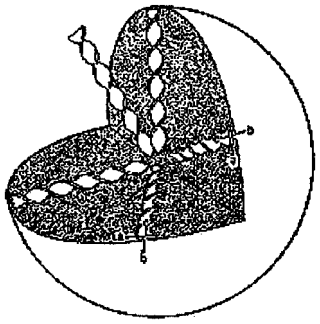

Figure 2.5 *Structural organisation within the spherulite showing orientation of crystallographic axis [after ref. 12].*

Spherulitic growth is limited by interference from neighbouring growing spherulites. Higher melt temperatures result in fewer initiating nuclei, and hence the spherulites produced are larger. Crystallisation at lower temperatures results in more spherulites of smaller size.

Figure 2.6 diagrammatically summarises the above description of the polymer morphology.

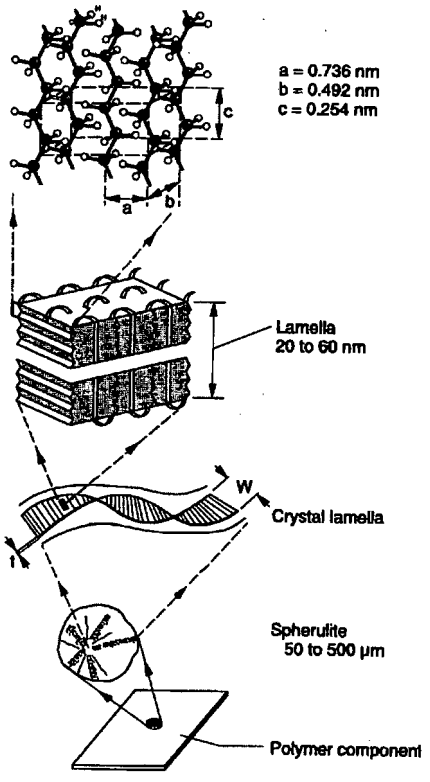

Figure 2.6 *Schematic representation of the crystalline structure and arrangement of polyethylene [after ref. 7].*

2.2.5 Molecular Orientation

The normal (i.e. no externally applied forces) crystallisation of a bulk polymer results in a random distribution of crystallite and molecular direction. However, upon subjecting the polymer to linear mechanical deformation such as drawing, the individual chains are pulled into a roughly parallel orientation, resulting in an increase in crystallinity (see figures 2.7 and 2.8) and consequently an increase in mechanical properties such as strength.

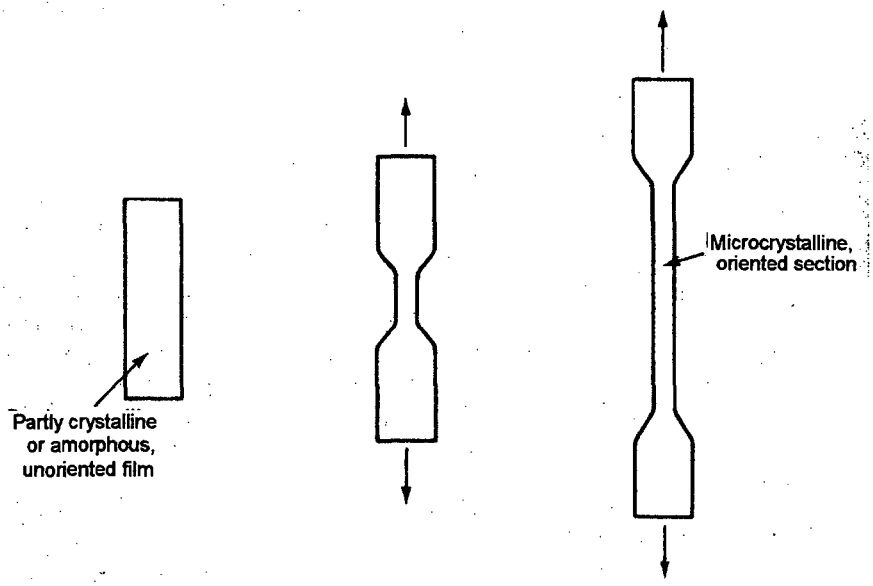

Figure 2.7 *The stretching of a polymer (as indicated by the arrows) results in an oriented section of increased crystallinity [after ref.11].*

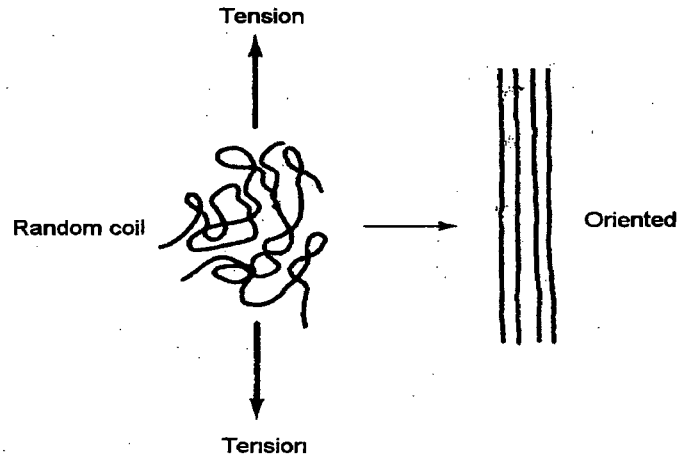

Figure 2.8 *On a molecular level, the linear mechanical deformation of a polymer results in the roughly parallel alignment of macromolecular chains, facilitating crystallisation [after ref. 11].*

Electron microscopy of bulk crystallised polymers with spherulitic structures such as polyethylene and of single crystals shows that the basic mechanism of plastic deformation contains, as the most important step, a discontinuous transformation from the unoriented material into a highly oriented fibre structure [14,15]. This structure is composed of a sequential arrangement of crystallites which are interconnected by tie molecules. Any mechanically unfolded chains will be buried by the folded crystallites. Peterlin has proposed that during deformation, multilayer lamellar crystals are destroyed, with chain tilting, slipping and breaking off of blocks of folded chains, and subsequent reformation of folded chains in the fibre [16] (figure 2.9). Figure 2.10 shows the deformation of the chain-folded domains in surface layers above the glass transition temperature (Tg) during adhesive wear. The molecules in the structure of the bulk polymer stretch and align themselves in the direction of motion [17].

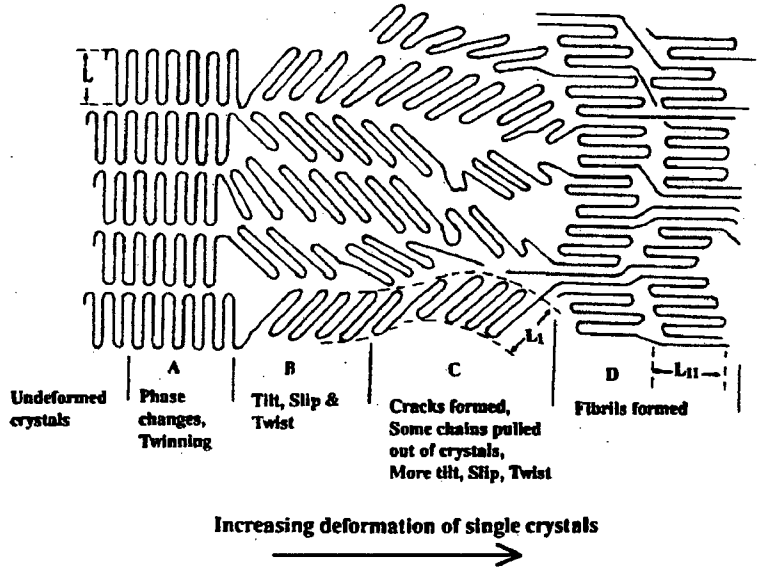

Figure 2.9 *Fibre formation by means of chain tilting, slip and breaking off of blocks of lamellae [after ref. 16].*

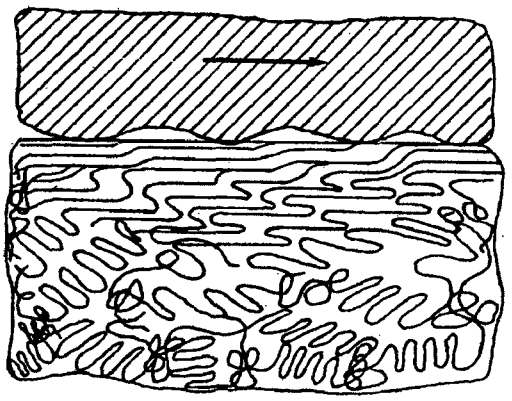

Figure 2.10 Stretching and reorientation of polymer molecules in semicrystalline polymers above their T_g during adhesive wear [after ref. 17].

2.3 Polymer Properties

The mechanical and thermal properties of all polymers are dependant on three factors that will determine whether they are essentially glassy, rubbery or fibre forming in nature [9]. These are:

- the flexibility of the macromolecule
- the magnitude of the forces between the molecules
- the stereoregularity of the macromolecules

The ability of the polymer to crystallise, the melting point of the resulting crystalline regions and the glass transition temperature are all consequences of these three factors.

2.3.1 The Glass Transition Temperature

Glass transition is a phenomenon observed in linear amorphous polymers, or in the amorphous regions of semi-crystalline polymers. Polymer properties change profoundly at the glass transition temperature (T_g), including the coefficient of thermal expansion, heat capacity, refractive index, mechanical damping and electrical properties [9]. The glass transition may be explained by the molecular rotation around single bonds becoming suddenly significantly easier at that temperature.

For semicrystalline polymers, the glass transition always occurs at temperatures below the crystalline melting point (T_m). Thus upon heating a crystalline polymer, it will first pass through its glass transition and then undergo a true phase change on melting at T_m. It has been found that features of chemical structure affecting the degree of molecular freedom influence both the crystalline melting point and the glass transition temperature, so both have similar effects on either properties. An empirical rule relating T_g to T_m has thus been formulated:

$$T_g = 0.66\, T_m$$

where T_g and T_m are given in Kelvin [7]. This general rule does, however, not apply to all polymers and should only be used with caution.

2.3.2 Mechanical Properties

In addition to the superior tribological properties of UHMWPE, its mechanical properties also determine its widespread use as a bearing material. Typical mechanical requirements of a bearing material include:

1. Adequate strength to withstand service loads.
2. Low dimensional change with load (i.e. high Young's modulus).
3. Low creep.

For biomedical applications, additional requirements have to be met:

1. The material should be biocompatible.
2. There should be minimal stress corrosion.
3. The material should be fatigue resistant in the physiological environment.
4. The material must maintain all the above properties in the physiological environment i.e. it should be stable at 37°C and should not react to the presence of synovial fluid or blood plasma.

2.3.2.1 Polymerisation Effects

The characteristic properties of polymers, especially linear polymers such as polyethylene, are largely determined by their density and molecular weight. Mechanical properties such as yield stress and stiffness are particularly dependant on the density value, while toughness and wear resistance are largely dependant on molecular length [18] (see figure 2.11).

	LLDPE	HDPE	UHMWPE
Density (g/cm^3)	< 0.94	> 0.94	0.94
Melting point (°C)	123	135	137
Tensile strength (MPa)	4.1–15.9	21.4–37.9	44
Tensile modulus (MPa)	96.5–262	414–1250	232
Elongation to break (%)	90–800	20–1300	> 350
Hardness (Shore D)	41–50	60–70	66
No. of branches per 1000 C atoms	15–25	0.5	0
Molecular structure	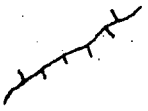		

Figure 2.11 *Property and molecular structure variations of polyethylenes [adapted from ref. 19].*

Polymer properties associated with intermolecular forces of attraction can be expected to increase as the homologous series in the paraffinic structure is ascended. The increase in general mechanical properties with increasing molecular weight is schematically shown in figure 2.12. It must be noted that these do reach an asymptotic maximum where no further gain is possible. Figure 2.13 shows that the flow temperature also rises with molecular weight. However, the degradation temperature is seen to drop with increasing molecular weight, hence complicating the choice of an ideal molecular weight for UHMWPE [7].

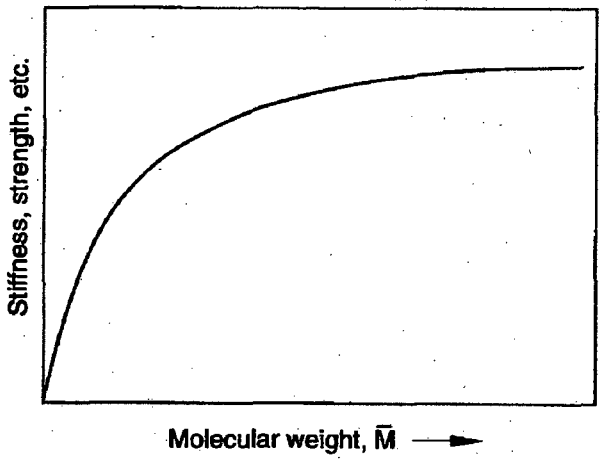

Figure 2.12 *Influence of the degree of polymerisation on the mechanical properties of typical polymers [after ref. 7].*

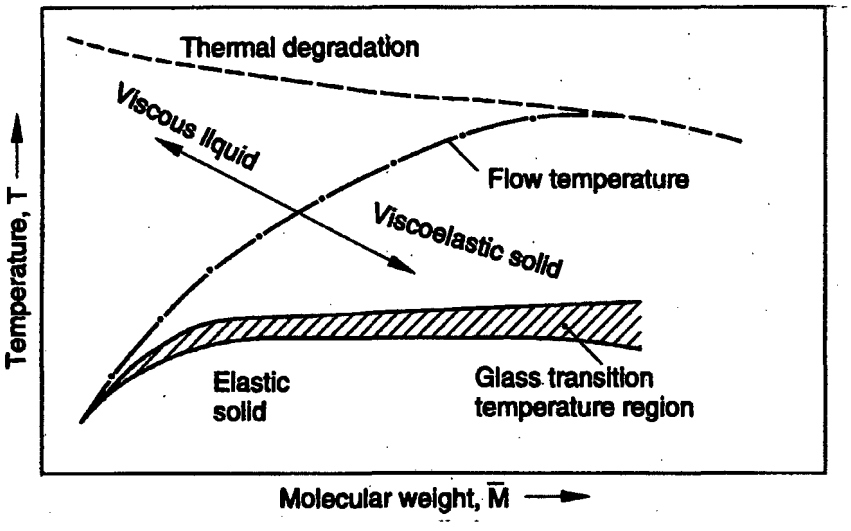

Figure 2.13 *Diagrammatic representation of the relation between molecular weight, temperature and properties of a typical thermoplastic [after ref. 7].*

2.3.2.2 Molecular Weight Distribution

Virtually all industrial polymers have the typical molecular weight distribution shown in figure 2.14. The number average is defined by

$$M_n \text{ (average)} = \Sigma m_i / \Sigma n_i = \Sigma n_i M_i / \Sigma n_i$$

where n_i is the number of molecules with molecular weight M_I [7]. The weight average can be calculated using

$$M_W \text{ (average)} = \Sigma m_i M_i / \Sigma m_i = \Sigma n_i M_i^2 / \Sigma n_i M_i$$

and viscosity average is calculated with

$$M_v \text{ (average)} = [\Sigma m_i M_i^{\alpha+1} / \Sigma m_i]^{1/\alpha}$$

where α is a material dependant parameter relating to the intrinsic viscosity of the polymer.

As the name states, UHMWPE has the highest molecular weight and consequently the best mechanical properties, resulting from a smooth, unbranched chain structure allowing a high degree of crystallisation. A comprehensive table of

properties of the grade of UHMWPE used for this research is given in Appendix A.

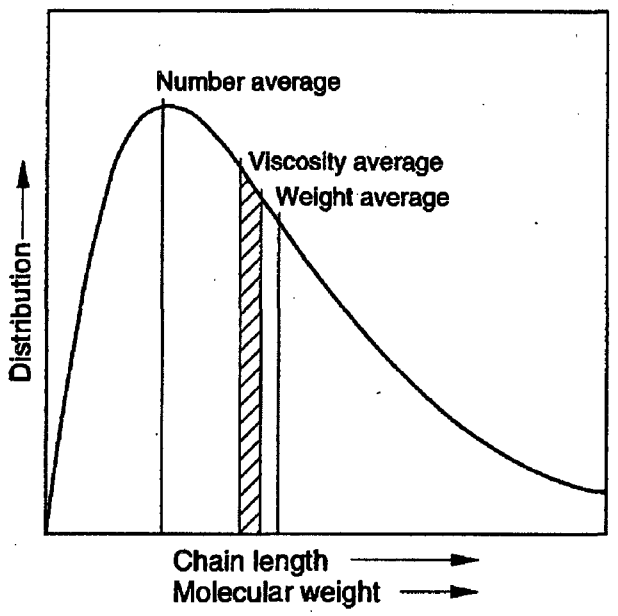

Fig 2.14 Typical distribution of synthetic polymer molar masses [after ref. 7].

2.3.3 Electrical Properties

A consideration of the electrical properties of UHMWPE is particularly relevant to its biomedical application, where the bearing material will be subject to an ionic environment. Like most polymers, polyethylene has excellent electrical insulating properties, determined largely by its primary chemical structure: The valency electrons in polymer molecules are localised in covalent bonds between pairs of atoms [12] and are thus not free to carry a conducting current.

2.4 Polymer Ion Implantation

The principles of a typical ion implanter are demonstrated in figure 2.15. Ions are generated at a source and then extracted, mass separated and subsequently accelerated towards the target, typically with an energy of 50 to 200 keV [20].

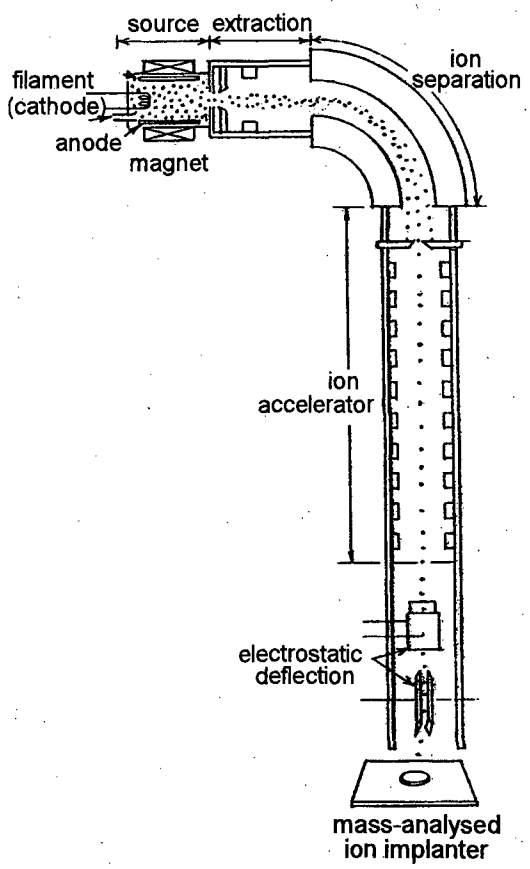

Fig 2.15 Schematic of a typical ion implantation device.

2.4.1 Structural Modifications

On striking the target polymer, the impinging, highly energetic ions lose their energy to substrate atoms mainly through ionization (by electronic excitation) and atomic collisions (by nuclear recoils) [21]. The structural modifications produced have so far proven difficult to study since they occur within a very thin (1 μm) surface layer of the bulk polymer, and crystallinity and molecular weight measurements have not yielded any accurate results [20]. The increase in mechanical properties is however attributed to the formation of a three dimensionally crosslinked structure, mainly in the amorphous region (which is where most mechanical polyethylene failure starts) [2].

Crosslinking is dominant when the polymer is ion implanted in the absence of oxygen, where oxidative degradation will be overwhelming if oxygen is present. Additional effects include scission of molecular chains, gas evolution, double bond formation and recombination of free radicals [22,23]. The free radicals generated (mainly alkyl radicals) are highly reactive and chain scission will result

from the shearing of the ruptured ends by the introduction of oxygen. Conversely, a deficiency in oxygen will cause the active ends to crosslink with other ends in the vicinity. The three-dimensionally crosslinked structures with N and functionable O elements are then consequently formed in the high dose range. However, too much energy deposition may result in a brittle, carbonized and plastically-hardened polymer structure which could lead to a lowering in wear performance.

2.4.2 Mechanical Property Changes

Ion implanted polymers have registered significant increases in near surface mechanical properties. Rao *et al.* registered surface hardness increases (to 100 nm) of nearly 50 times for implanted poly (ether ether ketone) (PEEK) and polystyrene (PS) at Ar^+ doses of 5 x 10^{19} ions.m^{-2}. Rao's results also indicated that the hardness initially increases as a function of fluence but seem to level out at higher doses [21].

Liao *et al.* have studied the effect of ion implantation to various doses on the hardness and elasticity in the near surface regions of UHMWPE. At the highest dose tested (1.4 x 10^{17} ions.cm^{-2}), the nanohardness increased from 0.079 GPa to 1.236 GPa at a depth of 30 nm, representing a factor of increase of 15.6 times. Similarly, modulus of elasticity increases of 7.4 times were measured. A transformation from plastic to elastic behaviour was also found [2].

The mechanical property changes caused by ion implantation decrease dramatically with surface depth and are also very dependant on the implantation dose used. Tables 2.1 and 2.2 illustrate the hardness and modulus of elasticity changes registered at different depths for varying implantation doses.

dose (ions/cm^2)	displacement-depth nanohardness (GPa)				
	30 nm	50 nm	100 nm	200 nm	500 nm
0	0.079	0.068	0.05	0.036	0.03
5.00E+13	0.09	0.08	0.06	0.04	0.03
2.00E+14	0.11	0.1	0.09	0.04	0.03
1.00E+15	0.14	0.13	0.08	0.05	0.03
1.00E+16	0.692	0.572	0.34	0.174	0.072
1.40E+17	1.236	0.894	0.49	0.19	0.09

Table 2.1 *Nanohardness measurements for ion implanted UHMWPE at various doses and depths [after ref. 2].*

dose ions/cm^2	displacement-depth modulus of elasticity (GPa)				
	30 nm	60 nm	85 nm	110 nm	remark
0	1.95	1.62	1.43	1.16	plastic
5.00E+13	2	1.67	1.52	1.21	plastic
2.00E+14	2.09	1.71	1.57	1.24	plastic
1.00E+15	6.9	4.44	3.17	2.43	elastic
1.00E+16	8.96	5.82	4.23	3.33	elastic
1.40E+17	14.5	10.1	7.42	5.81	elastic

Table 2.2 *Modulus of elasticity changes for ion implanted UHMWPE [after ref. 2].*

2.5 Summary

This chapter has shown that the mechanical properties of polyethylene are critically dependant on the crystalline structure of the polymer and, since the mechanical properties are expected to influence the wear performance of polymers, a consideration of their structure is thus important when examining the wear behaviour of UHMWPE.

However, polymer crystallinity is not only governed by the structural arrangement of the molecules created during fabrication, but may also be influenced by bulk mechanical effects such as the stretching and wearing of the polymer. Additionally, post-fabrication techniques such as ion implantation may be used to alter the near surface structure of the polyethylene and thus further enhance its mechanical properties.

CHAPTER 3

LITERATURE REVIEW: THE FRICTION AND WEAR OF POLYMERIC MATERIALS

3.1 Introduction

Tribology is the science of contacting surfaces in relative motion. Tribological investigations are necessarily complex, involving examinations of the interactions of friction, wear and lubrication. Because of the complexity of the surface interactions, various simplifications and approximations must be made [24]. Hence different tribological models are used to describe the many forms of sliding contacts observed, such as abrasion and adhesion, but it must be remembered that these models are system dependant and will not actually operate in isolation.

3.2 Friction

3.2.1 Introduction

The frictional force is the force resisting the relative motion of two solids in contact. The force required to initially move the two contacting bodies relative to each other is termed the static frictional force (F_s), while the dynamic frictional force is the force required to maintain this relative motion (F_d). The dynamic frictional force is normally lower than the static frictional force. Both depend on the real area of contact as well as various system factors such as sliding velocity, normal load (W), temperature and surface roughness [25].

3.2.2 The True Area of Contact

Real surfaces are microscopically rough and often have Gaussian asperity-height distributions [26]. Figure 3.1 shows a smooth surface in contact with a rough surface of varying asperity heights. It is clear that the real area of contact A_r is much less than the apparent projected area of contact A_o, or

$$A_r = \sum_{i=1}^{n} A_r^i << A_o$$

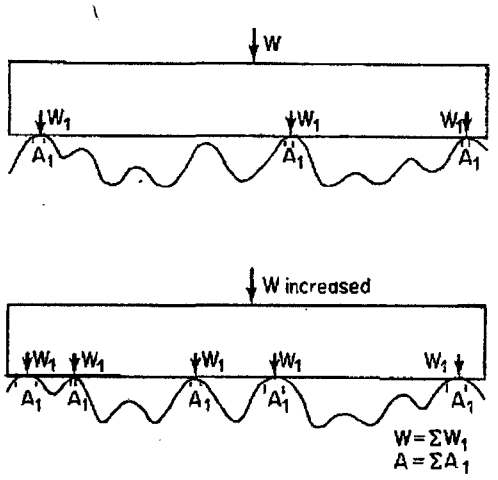

***Figure 3.1** Rough and smooth surface interaction with increasing load W [after ref. 26].*

At low interface loads, contact will occur only at the highest asperity tips. As the load is increased, the discrete areas of these initial contacts are increased and new contacts are created with lower asperities (see figure 3.1). Assuming the Gaussian asperity-height distribution, the most important surface interaction observations [26] are thus:

1. The mean area of a contact spot remains constant with increasing load (as the smooth area compresses the rough area); the total real area of contact A_r divided by the number of contacts remains constant, with both A_r and the number of contacts increasing.

2. The relationship of applied load to total real area of contact (A_r) is linear for both elastically and plastically deforming surfaces. It must be noted that this result would be very different for an equal asperity height distribution.

4. The maximum surface roughness compression usually encountered in engineering practice is less than 10%. At greater loads, the underlying material is stressed beyond its yield stress and hence plastically deforms. From [26], the applied load W produces a mean contact pressure of $3P$ at the asperity contacts when these are plastic, where P is the total applied pressure ($=W/A_o$). Consequently,

$$W = 3PA_r.$$

Within the bulk material W produces a stress P as the material becomes plastic , so

$$W = PA_o .$$

Thus for the often occurring condition of 10% compression,

$$A_r = (1/3)A_o .$$

3.2.3 Junction Growth

The true area of contact is not only affected by the applied load W but also by the tangential forces. Figure 3.2 shows a block of material loaded against a rigid plane surface, thus representing a very idealised form of asperity contact. In figure 3.2a, the block is subjected to uniaxial compression by a normal stress p_0 and is assumed to be on the point of yielding when nearly all the asperity contacts are plastic. When a tangential stress is applied to the block (figure 3.2b), the material will experience an additional shear stress τ and thus for the material to remain at the point of yielding the normal load must be reduced to a value of p_1. If the normal load remains constant, the area of contact must grow; hence the phenomenon of junction growth [36].

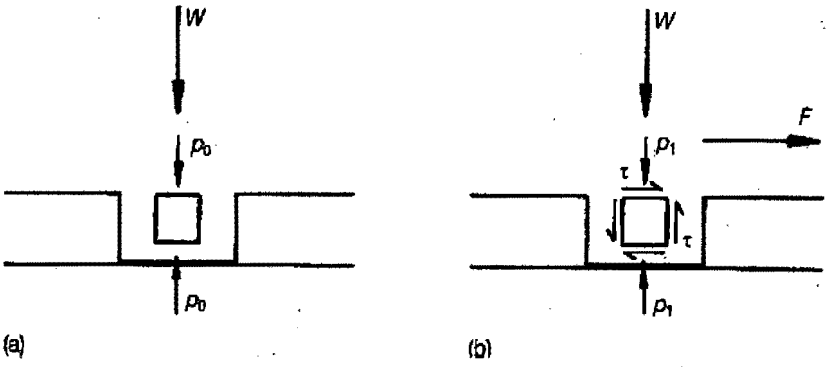

***Figure 3.2** An idealised asperity being pressed against a rigid plane surface with (a) no tangential load and (b) tangential force applied [from ref. 36].*

Polymers, however, deform predominantly elastically and thus the normal stress is likely to reduce the value of τ, causing yielding rather than junction growth.

3.2.4 Friction Models

Amonton formulated the following basic laws governing friction:

- the frictional force is independent of apparent contact area
- the frictional force is directly proportional to applied load

which Coulomb then described in mathematical terms as

$$F_{friction} = \mu W$$

where μ is a constant known as the coefficient of friction.

Polymers usually do not obey Amontons law very well, so that the frictional force is not linearly dependant upon the applied load and the following relation is thus used more frequently

$$F_{friction} = kW^n$$

or

$$\mu = F_{friction}/W = kW^{(n-1)}$$

where n and k are constants. Generally, the friction coefficient will decrease with increasing load, and for branched polyethylene, n is approximately 0.74.

The frictional force experienced by one solid sliding over another is usually considered to be a combination of various frictional modes, or

$$F_{total} = F_{adhesion} + F_{deformation} + F_{cohesion} + F_{viscous}$$

where $F_{adhesion}$ and $F_{deformation}$ have the greatest influence (figure 3.3); $F_{viscous}$ is the viscous drag under wetted conditions and $F_{cohesion}$ is the contribution of wear to the bulk frictional losses [27]. The adhesion and deformation components will thus warrant further explanation.

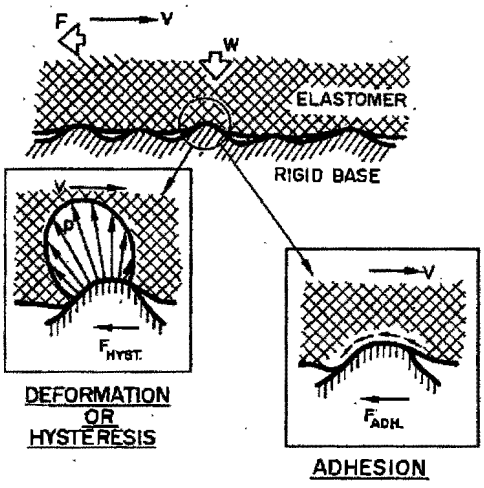

Figure 3.3 The principle components of polymer friction [after ref. 27].

3.2.4.1 Adhesion

The adhesive component of friction arises from the molecular bonding of exposed surface atoms of the two interacting surfaces at their real areas of contact (A_r) [28]. With metals, adhesive frictional forces will thus be associated with metallic bonds, for ceramics there may be valency bonds, and with polymers these forces will be due to electrostatic forces, van der Waals forces and Hydrogen Bonds [29].

When polymers are worn against suitably smooth hard surfaces, the adhesive forces are often larger than those existing between the polymer molecules themselves thus resulting in shear within the bulk polymer and the deposition of polymer onto the counterface. After multiple traversals across the counterface, a stable, thin film of polymer, or transfer layer, may thus form on the counterface, resulting in the polymer eventually sliding against it's own deposit and not the original counterface [30]. Thus for the case of a polymer shearing a short distance from the wear surface, microscopic plastic flow is envisaged [25]. The shearing stresses are transmitted by adhesive forces operating at ranges below 0.1 nm, the interfacial adhesive zone being up to 100 nm thick [25,31,32], as shown in figure 3.4. For polymers such as PTFE and polyethylene, high interfacial pressures can distort their linear molecules and orient their chain structure in the direction of sliding, which has a profound effect on wear [33,34].

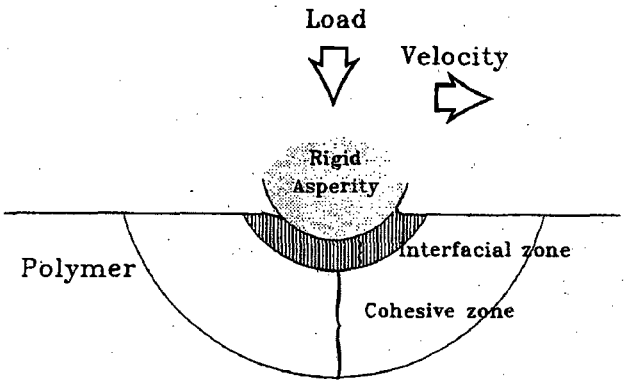

Figure 3.4 *The two adhesion affected zones for polymers sliding against a hard, rigid surface [after ref. 31] .*

3.2.4.2 Deformation

The deformation component of friction is caused by the asperities of the harder material ploughing through the softer material [35]. A numerical estimation of this term supposes a conical asperity of semi-angle α sliding over a plane surface (figure 3.5). The flow pressure needed to displace it is taken as the indentation hardness H of the surface material multiplied by the cross sectional area of the groove [36]:

$$F_{deformation} = Hax = Hx^2 tan\alpha.$$

The normal load supported by the asperity is given by

$$W = H\pi.a^2/2 = 0.5H\pi x^2 \tan^2\alpha$$

and thus the coefficient of friction due to ploughing is

$$\mu_{deformation} = F_{deformation}/W = (2/\pi)cot\alpha.$$

Similarly, using a plain strain model, where the asperity is taken to be a wedge of semi-angle α, will lead to [13]:

$$\mu_{deformation} = cot\alpha.$$

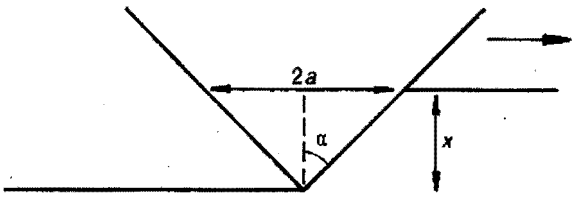

Figure 3.5 The deformation model of friction, where a conical asperity of semi-angle α ploughs through a softer material [after ref. 36].

For elastomers, the indentation caused by an asperity will experience a delayed recovery, thus giving rise to what is generally known as hysteresis friction, and thus

$$F_{deformation} = F_{hysteresis}.$$

3.3 Wear

3.3.1 Introduction

Wear may be described as being the removal of material from one or both solid surfaces in moving contact with one another. In nearly all cases, the life of rubbing mechanical parts is determined by some sort of wear process [29]. The wear of polymers may be divided into four main groups [37]:

- adhesion
- abrasion
- fatigue
- chemical degradation

These mechanisms will normally not operate in isolation so that failure will be caused by a considerable amount of interrelationship between the various processes [14].

Briscoe made the even more general wear classification, *viz.*, cohesive wear and interfacial wear [31], where cohesive wear processes are governed by the cohesive strength of the polymer and interfacial wear involves the dissipation of frictional work in a thinner region at the interface (see figure 3.4). For cohesive wear processes, the frictional work is dissipated in fairly large volumes adjacent to the interface by the interaction of surface forces or the interlocking of asperity

contacts. An investigation of cohesive wear necessitates an understanding of the polymers' mechanical properties, where the wear rates may be correlated with strength, toughness or fatigue properties which are obtained from bulk deformation experiments [19]. An examination of interfacial wear, on the other hand, will focus on the chemistry and surface forces of the interacting solids. Polymer transfer and chemical wear are examples of interfacial wear, whereas abrasion and fatigue may be categorised as cohesive processes.

3.3.2 Adhesive Wear

The adhesive wear mechanism results from the adhesive forces generated between the atoms of the surfaces in real contact (see 3.2.4.1) and is likely to be the predominant wear process if the harder of the two contacting surfaces is relatively smooth. The likelihood of strong interatomic bonding at the sliding couple interface increases with increasing applied load W; indeed, extremely strong bonding may result from high loads being applied to atomically clean surfaces in contact [38]. Thus, for relative movement to occur, interfacial shear must occur in order to rupture these adhesive bonds. However, it is often not the interfacial bonds themselves that rupture, but rather the bonds of the cohesively weaker material. This fracture product then forms a third body deposited onto the cohesively stronger material and may form a stable film, known as a transfer layer. The formation of transfer layers is extremely important in achieving low wear rates in many polymer sliding wear situations and will be dealt with in greater detail in Chapter 3.4.

Periodically, the softer of the two materials will find a "flaw" in the harder material and this will result in a portion of the harder material being removed. The debris may then be back transferred or be abraded by other features of the harder surface, or become further involved in the sliding process as a third body and lead to third body abrasion.

3.3.3 Abrasive Wear

Abrasive wear is caused by the asperities of the harder of the two materials in sliding contact displacing material of the softer, or by hard particles moving or imbedded between the two surfaces causing material displacement. Abrasive wear can thus be divided into two categories, namely two body abrasive wear and three body abrasive wear (see figure 3.6).

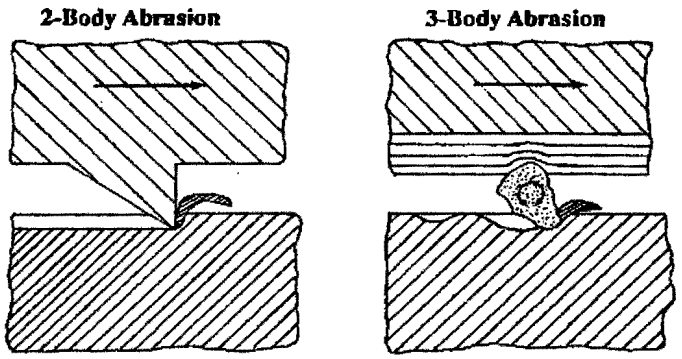

Figure 3.6 *Schematics of two- and three body abrasive wear [after ref.17].*

An idealised model of two body abrasive wear consists of a hard conical indenter of base angle θ penetrating and ploughing a groove into the softer material. For the case of hard surface asperities penetrating the surface and removing material by the shearing or cutting of a rigid polymer, the following theoretical relationship has been derived [31,37]:

$$z = k(W/H)\tan\theta$$

where z is the volume of material removed per unit sliding distance
W is the normal load
k is the probability of formation of a wear particle (since only a portion of the material undergoing deformation appears as loose wear debris
H is the hardness and
θ is the base angle of the indenting asperity.

For metals, plastic deformation occurs at all angles of θ, but for polymers this is only true for angles greater than 30°, i.e. when the apex angle is small.

The abrasive deformation of polymers is usually partly plastic and partly elastic, the roughness of the counterface determining which of the two will dominate [39]. The product $S\epsilon$, which is essentially related to the area under the stress-strain curve, appears to be an important material parameter influencing wear. Lancaster and Ratner have shown the single traversal wear of various polymers over relatively rough steel counterfaces to be proportional to $1/S\epsilon$ where S is the rupture stress and ϵ the elongation to break [40,41].

Giltrow has linked the cohesive energy density, which indicates the strength of secondary bonding in polymeric materials, to the abrasive wear behaviour of polymers. The abrasive wear of thermoplastics was shown to be inversely proportional to the square root of their cohesive energies as shown in figure 3.7.

The relationship was however only observed when the predominant mode of deformation was plastic [42].

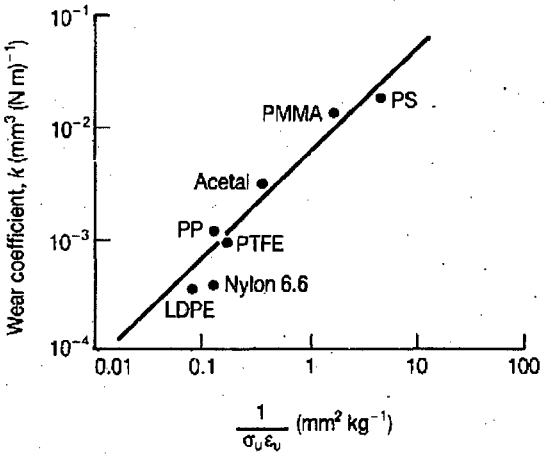

Figure 3.7 *The Ratner-Lancaster correlation relating single-pass abrasive wear rates of polymers and the reciprocal of the energy parameter* $S\epsilon$. *Tests were performed over rough steel surfaces of* R_a = *1.2 μm [from ref.36].*

3.3.4 Fatigue Wear

Fatigue wear results from strong adhesive forces between the surface layers of the two solids in sliding contact. Damage is however cumulative, so that several contact cycles of compression and recovery across the same portion of material are required to fully detach a fragment piece.

Wear due to fatigue results from the formation of cracks associated predominantly with elastic deformation. The cracks grow and intersect with repeating numbers of cycles and wear debris is consequently formed [36]. Thus, in a simple model of fatigue wear, the wear rate would be expected to correlate with the rate of fatigue crack growth and consequently be determined by the Paris equation

$$da/dN = A(\Delta K)^n$$

where a is the crack length,
N the number of cycles,
ΔK the range of stress intensity to which the growing crack is exposed during each cycle,
A and N are empirical constants and
da/dN thus being the increase in crack length per stress cycle.

Fatigue wear becomes increasingly more significant as the counterface becomes smoother and the polymer more elastic. Shallow pits and cracks perpendicular to the direction of sliding have been associated with fatigue wear in UHMWPE [19].

3.3.5 Chemical Wear

Chemical wear is analogous to stress corrosion and hence occurs in a chemically active system subjected to an applied stress. Some form of chemical degradation will almost always be present in all wear processes, often causing mild chain scission in polymer wear situations [19]. Polymer cracking may thus occur below accepted critical value stresses. Although chemical wear is a very important tribological process, it's precise role and bearing on the overall wear behaviour of polymers is little understood.

3.4 The Transfer Layer

The transfer of one material onto the counterface of its sliding couple is a characteristic exhibition of the adhesive or adhesion induced fatigue mechanism of wear [43]. Many polymers sliding against hard counterfaces, for example metals, form detectable transfer of polymer on these counterfaces. Indeed, the wear behaviour of these polymers may be critically dependant on the formation of such a transfer layer.

Most thermoplastics deposit a polymer film onto the counterface when wearing against a harder material. Under "normal" transfer conditions, repeated sliding over the counterface will lead to a progressive build up of the transferred layer which eventually becomes detached. For these conditions, polymer is deposited onto the counterface without significant chain scission or chemical degradation usually in lumps, typically 0.1 to 10 μm thick [36]. Transfer of the debris back onto the polymer also occurs frequently. Polymers do not readily transfer more polymer onto the transfer layer, so that in most cases the rate of wear is dictated by the rate of removal of the transfer layer. Thus, if the transferred material adheres strongly to the counterface, even after removal of the normal load W, low wear rates can be expected.

Under certain conditions, some polymers such as PTFE, HDPE and UHMWPE form slightly different transfer layers associated with very low friction and wear rates. Very thin but stable transfer films of thicknesses between 5 to 10 nm may be formed [36]. The polymer chains in this layer are highly orientated. Sliding,

subsequent to the formation of such a stable transfer layer, will occur only between the similarly oriented polymer and its deposit, so that the polymer will not directly interact with the harder counterface. The variation of the friction coefficient of a HDPE/glass sliding couple with increasing sliding distance, as seen in figure 3.8, demonstrates the effect of such a stable transfer film. The initial transferred layer is quite thick, of the order of a few micrometers, and the friction coefficient is high at around 0.2 to 0.3. With the formation of the stable, thin transfer film and the molecular orientation of the polymer and transfer layer, the friction coefficient is seen to drop to a much lower value. The conditions conducive to the formation of these very thin and "low wear" transfer layers are very sensitive and the above mentioned "normal" transfer will again be predominant if for instance the surface roughness or sliding velocity is increased. Factors influencing the formation of stable, low wear transfer layers are discussed in the following sections.

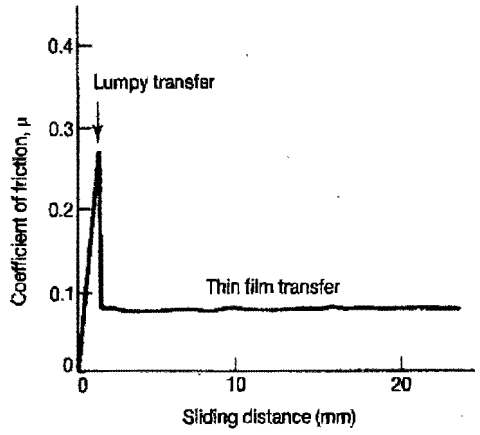

Figure 3.8 *The variation of coefficient of friction with sliding distance for high density polyethylene (HDPE) sliding against glass [after ref.36].*

3.4.1 Counterface Topography

The ability of transfer films to adhere tenaciously to the counterface strongly depends on the topography of the counterface [4,44,45,46]. Smooth counterfaces are more likely to support stable transfer films due to the more intimate contact between polymer and counterface causing greater adhesion, and the surface energies of the couple will dominate the transfer process. Rough surfaces, on the other hand, will suppress the formation of stable transfer films [37,47]. Marcus reported the difficulty of UHMWPE to form a stable transfer layer when sliding in the direction of grinding, thus resulting in different wear behaviour to that observed when worn normal to the direction of grinding, where stable transfer

layer formation was easily achieved for the same value of surface roughness [19]. Very low UHMWPE/steel wear rates were reported by Clarke for counterfaces of roughnesses between 0.25 and 0.6 μm R_a and were attributed to an "extensive valley transfer film" [46].

3.4.2 Lubrication

Lubricants can often inhibit the formation of a stable transfer layer and thus lead to increased wear. Polymer-metal sliding wear in aqueous environments is unaffected if the couple does not produce a stable transfer layer during dry sliding, whereas wear rates increase for normally transfer layer forming couples in aqueous environments [37,48]. The wear rates of PTFE and UHMWPE have been shown to be significantly affected by the presence of water, especially for rougher counterfaces [45,49].

3.4.3 Chemical Effects

The formation of a stable transfer layer can be aided by improving its adhesion to the counterface. Suitable polymer fillers have been shown to do this; the incorporation of lead and copper oxides into HDPE have lead to performance improvements when wearing against steel, although it is unclear exactly how the adhesion of the transfer layer is improved in this case [36]. Some fillers such as carbon particles are thought to improve the wear performance of polymers against rougher counterfaces by slightly abrading their surfaces, leading to a smoother and cleaner counterface and consequent better transfer layer adhesion.

Some transition metal oxide fillers are thought to induce mild degradation of the polymer and thus create strong valence bonds between the transferred layer and the counterface [31].

3.4.4 Further Influences

Applied load (W), environment temperature, counterface temperature and type of motion have all been shown to have an effect on the formation and adherence of a stable transfer layer. Rhee *et al.* and Tanaka found increases in the thickness of the transfer film with increases in load, which then suppressed the onset of severe wear to a higher temperature [50,51]. Tests using independent temperature controls for polymer and steel counterfaces established that the uniformity of the

transfer film was temperature dependant and that uniformity, in turn, had an effect on polymer wear [52]. Higher counterface temperatures were found to promote the formation of a stable transfer layer.

The nature of the sliding motion also influences the attainment of stable transfer films, for example wear debris will not leave the contact zone as easily during oscillatory motion as it does when sliding in a uniform direction (as is the case for a pin on disc testing apparatus), and thus the transfer layer will form more readily during oscillatory wear [52].

3.5 Lubrication

3.5.1 Introduction

A lubricant is a substance introduced between surfaces in sliding contact and having a lower shear strength than the surfaces themselves, which reduces friction between the sliding couple. Ideally, the lubricant will prevent all direct contact between the two sliding contacts, but this is not necessarily the case; many lubricated systems may still experience asperity contact and hence junction formation. Both instances, however, are normally expected to lead to lower rates of wear. Liquids are most commonly used as lubricant due the their "low shear" properties and the fact that they may be shorn an infinite number of times without failing from wear or fatigue [53]. Different types of liquid lubrication may be distinguished:

3.5.2 Hydrodynamic Lubrication

Under hydrodynamic lubrication, the mating surfaces are separated by a relatively thick fluid lubricant so that none of their asperities will be in contact. The pressure to support the normal applied load W is generated hydrodynamically which necessitates the surfaces being conformal i.e. the opposing surfaces are closely matched in dimensions and separated by a small gap over a relatively large area.

The hydrodynamic pressures arise due to the viscosity of the fluid (due to the relative motion of the surfaces) and the convergence of the gap between the mating surfaces. The pressure distribution is described by the Reynolds equation for fluid flow, which assumes the flow to be laminar, the separating gap small compared with the other system dimensions and the prevailing forces being viscous. Despite these simplifications, the equation remains extremely complex.

For the case of uniform tangential sliding of two planes, as shown in figure 3.9, and the flow being incompressible and the viscosity uniform, the variation of pressure p with distance x is given by the simplified Reynolds equation as [36]

$$dp/dx = -6\eta U(h-h^*)/h^3$$

where η is the fluid dynamic viscosity,

h^* is the separation of the surfaces at the point of maximum pressure ($dp/dx = 0$),

U is the sliding velocity,

and the other quantities are as defined in figure 3.9.

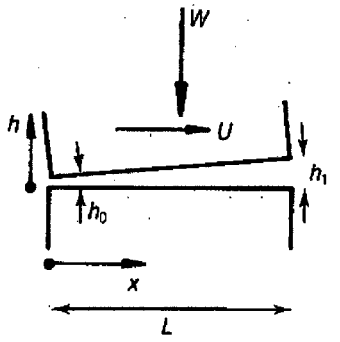

Figure 3.9 *Mating surface couple under conditions of hydrodynamic lubrication. The degree of convergence has been exaggerated for clarity [after ref. 36].*

By setting the boundary conditions such that $p = 0$ at $x = 0$ and $x = L$, further integration gives the normal load W supported be the bearing per unit width as:

$$W = 6\eta KU\,(L^2/h_o^2)$$

and

$$K = [\ln(1+n)/n^2] - 2/[n(2+n)]$$

where $n = h_1/h_o - 1$. The numerical value of K thus depends on the ratio of the inlet and outlet film thicknesses only and is actually quite insensitive to this ratio. The maximum load capacity will hence occur when $K = 0.027$.

3.5.3 Elastohydrodynamic Lubrication

Under conditions where the mating surfaces are not conformal but rather counterformal, involving nominally line or point contacts, local pressures in the contact zone may become much higher than those encountered during hydrodynamic lubrication. Under these high pressure conditions, elastic deformation of the bearing surfaces and variations of fluid viscosity with pressure become increasingly important and lubrication in these circumstances is considered elastohydrodynamic (EHL). EHL explains why much higher loads can be supported by a bearing couple, without asperity contact occurring, than may be predicted by hydrodynamic theory: Very high pressures will increase the local viscosity of the lubricant and thus increase the film thickness and secondly, surface regions subjected to high pressures will deform elastically and asperity contact will thus be decreased.

The latter effect is particularly important in "soft" EHL, where one or both of the mating surfaces are softer and deformation occurs at relatively low pressures and viscosity increases do not play a significant role [36].

3.5.4 Thin Film or Mixed Lubrication

For lower sliding velocities or lubricant viscosities, the hydrodynamic film thickness decreases. In thin film lubrication, surface asperities penetrate and disturb the laminar flow conditions so that only part of the applied load is carried by hydrodynamic action whilst the remainder is carried by the interacting surface asperities. The frictional force will thus be due to both the shearing of the lubricant film and asperity interaction [54].

3.5.5 Boundary Lubrication

Under very high loads (W) and very slow sliding speeds hydrodynamic effects are completely absent. Unless the bearing surfaces are protected by a suitable boundary lubricant, asperity contact and consequent very high wear will occur. Boundary lubricants prevent asperity contact and associated adhesion and junction growth by forming absorbed molecular films on the surfaces, the repulsive forces of which then carry the applied load. Figure 3.10 shows the typical operation of a boundary lubricant, for example a long chain carboxylic acid on a metal surface. The lubricant molecules are absorbed with the polar end groups adhering strongly to the oxide layer present on the metal. The molecular chains align themselves

perpendicular to the surface due their mutual repulsion and dense layers of hydrophobic chains 2 to 3 nm long are thus formed. Most of the load is thus carried by the interactive forces of the hydrocarbon chains and only small areas of naked asperity contact occur [36].

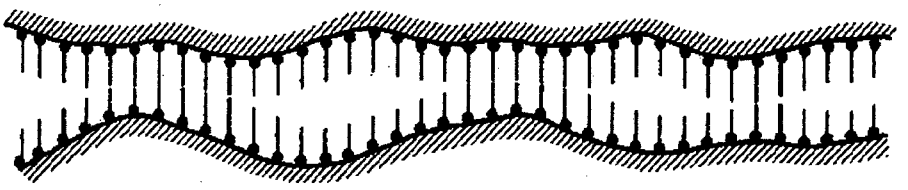

Figure 3.10 *An example of operation of a boundary lubricant [after ref. 36].*

Lubricating systems are highly complex and only the hydrodynamic and elastohydrodynamic regimes are satisfactorily understood [36], unlike mixed and boundary lubrication, where the lubricating environment can be influenced by all aspects of the materials involved, such as metallurgy, nature of oxide films and physicochemical properties of the lubricant etc. [55]. The variation of the coefficient of friction through the various lubricating regimes with the changing quantity $\eta U/W$ is illustrated in figure 3.11; the relation is known as the Stribeck curve.

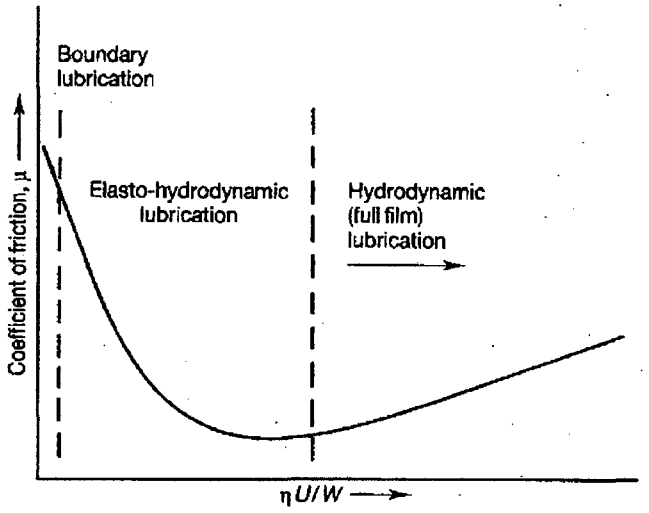

Figure 3.11 *The Stribeck curve relating frictional drag* μ *with the quantity* $\eta U/W$ *[after ref. 36].*

3.6 The Friction and Wear Behaviour of UHMWPE

3.6.1 Introduction

Thermoplastic polymers are often classified into three different groups distinguished by their friction and wear behaviour [56]. The "smooth molecular profile" polymers such as HDPE, UHMWPE and PTFE exhibit excellent sliding properties, unlike the "normal" polymers such as LDPE and polypropylene (PP), and the amorphous polymers like polymethylmethacrylate (PMMA) and polyvinyl chloride (PVC) [57]. Furthermore, the frictional characteristics of the linear chain polymers are different to those of the branched chain polymers: While the coefficient of friction for linear structured polymers is sensitive to the relative motion of the polymer-counterface couple, branched chain polymers do not show this motion-direction dependency [30].

3.6.2 UHMWPE-Counterface Surface Interaction: Molecular Orientation

The motion dependency of smooth molecular profile polymer friction and wear occurs because the linear polymer chains can orient themselves at the sliding interface (molecular orientation), whereas branched polymers cannot do so because of steric hindrance [58]. Recent studies on the wear of UHMWPE under water lubricated and *in vivo* simulated conditions have indicated its wear performance to be greatly influenced by the type of sliding contact. Linear motion, either unidirectional or reciprocating, results in very low rates of wear, whereas multi-directional motion under the same conditions will result in much higher wear [59,34,60].

Direct evidence of the molecular orientation phenomenon on worn surfaces of UHMWPE has been identified by Wang *et al.* [61] by means of plasma etching and scanning electron microscopy. By etching worn tibial and acetabular UHMWPE surfaces with ion plasma, they revealed a preferential orientation of crystallite lamellae in the direction normal to that of principal motion. A common observation on worn UHMWPE surfaces is the appearance of surface stretching in the form of fibril formation or fibrillation which Wang *et al.* has also ascribed to molecular orientation; the fibrillar structure is readily formed on worn surfaces by surface traction forces, where this oriented structure will be harder (not brittle) in the orientation direction and weaker or softer in the direction normal to sliding. Hence for unidirectional motion, UHMWPE becomes orientation hardened, whereas for multiaxial motion it becomes orientation softened.

3.6.3 System Parameters Affecting UHMWPE Wear

3.6.3.1 Counterface Roughness and Topography

Counterface roughness plays a critical role in determining UHMWPE wear. Generally, UHMWPE wear decreases with decreasing counterface roughness, although some workers have found a certain optimum counterface roughness, below which the UHMWPE wear rises sharply; Dowson *et al.* found this minimum to correspond to a counterface surface roughness of about 0.03 μm R_a for wear against stainless steel under dry sliding conditions [62] (figure 3.12). It would appear that this optimum exists only for those instances where transfer layers are formed to achieve low wear rates [37] i.e. for UHMWPE wearing against ceramics such as Yttria Partially Stabilised Zirconia (YPSZ) no such minima is expected.

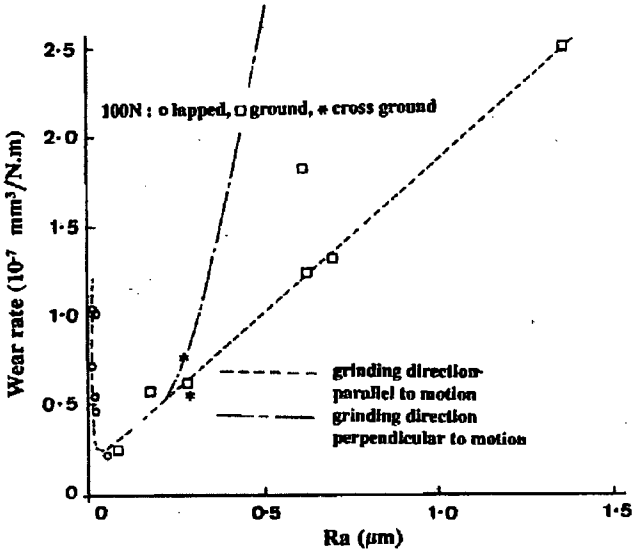

***Figure 3.12** The effect of counterface roughness on the wear rate of UHMWPE under dry reciprocating sliding against a stainless steel disc, showing a wear minima at a surface roughness of 0.03 μm R_a [after ref. 62].*

The increase in wear rate with increasing counterface roughnesses at higher R_a's is not linear under water lubricated conditions. Lloyd *et al.* found the wear rate for UHMWPE sliding against stainless steel (ground in the direction perpendicular to the direction of sliding) under water lubricated reciprocating motion to increase by approximately three orders of magnitude from 0.1 to 1.0 μm R_a and proposed the following relation for surface roughnesses between 0.1 and 1.0 μm R_a [63]:

$$Specific\ Wear\ Rate\ (mm^3/N.m) = 1.1 \times 10^{-8} \exp(7.7R_a).$$

The topography of the metal counterface also affects wear. Hollander and Lancaster showed the wear rate to decrease with increasing counterface asperity average radius [64]. Marcus *et al.* found wear to be higher when sliding occurs in the grinding direction due to the inability of the polymer to form a stable transfer layer on this type of topography (for tests conducted under water lubricated reciprocating sliding conditions at an average sliding speed of 0.25 $m.s^{-1}$) [19]. Counterface roughness and topography effects are thus very complex and are further interrelated with the other system parameters such as lubrication, pressure, temperature and sliding speed.

3.6.3.2 Lubrication

For crystalline polymers which rely on the formation of a stable transfer layer to reduce their rates of wear, the introduction of water as a lubricant often has a deleterious effect on wear performance. The fluid disrupts the transfer film and exposes the original surface topography, leading to higher wear [65].

However, successful water boundary lubrication may be achieved if the counterface is hydrophilic. Steel counterfaces can allow the formation of weakly held water films and thus lead to friction decreases [66]. Tanaka found transfer occurring for both dry and water lubricated conditions although the characteristics of the worn surfaces were different. The increase in wear under water lubrication may result from a change in the surface structure of polymers by the water rather than the change in transfer layer behaviour [67].

3.6.3.3 Interface Pressure

The steady state wear rate of unfilled polymers is generally little affected by pressure increases up to a critical interface pressure which is typically one third of the compressive strength of the polymer [68]. Dumbleton *et al.* showed that while the initial wear rate of UHMWPE increases greatly with increasing pressure, the steady state wear remains fairly constant [69] even to pressures of 1635 $lb.in^{-2}$ (11.27 MPa) (figures 3.13 and 3.14).

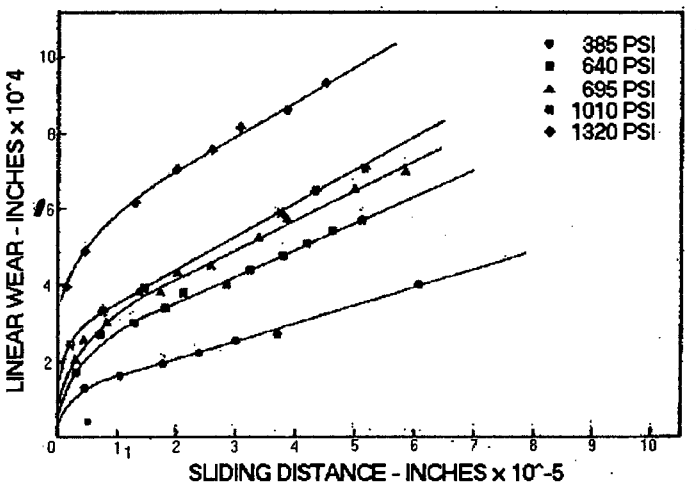

Figure 3.13 The effect of pressure on the wear of UHMWPE sliding against stainless steel in water [after ref. 69].

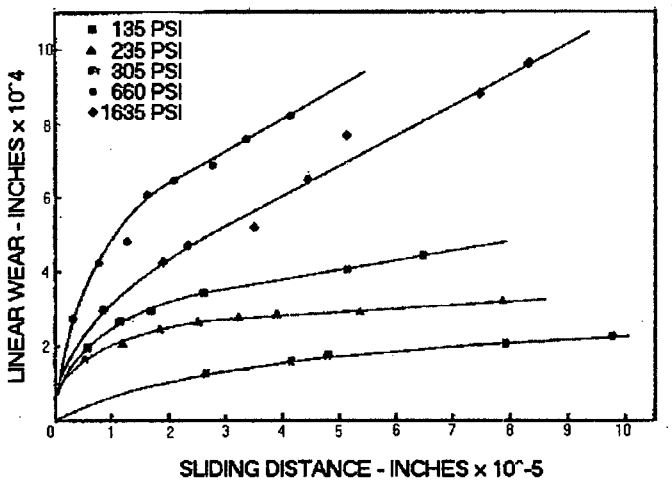

Figure 3.14 The effect of pressure on the wear of UHMWPE sliding against stainless steel in water [after ref. 69].

3.6.3.4 Temperature

The mechanical properties of all polymers are usually adversely affected by an increase in temperature because of the weakening of the intermolecular bonds between the molecular chains as the temperature rises, so that their wear performance can be expected to decline concurrently [19]. The wear behaviour of polymers is particularly influenced by temperature effects because of their low thermal conductivities (hindering frictional heat dissipation) and their low melting points. Conversely, an increase in counterface temperature may aid the formation

of a thicker transfer layer and thus lead to decreased wear. The results of Evans *et al.* indicated that the wear rate and friction increases with decreasing counterface temperature or increasing pin temperature in the 15-45° C temperature range [52].

Above a certain critical temperature, the wear rate has been found to rise rapidly because of thermal softening leading to extrusion and gross polymer flow [70,71]. Challen and Dowson have presented an analytical thermal analysis for the calculation of the maximum interfacial temperature in a pin-on-disc wear tester for UHMWPE and showed that severe wear occurred for temperatures exceeding 125° C [70]. Rhee and Ludema, however, disagree with the general finding that the polymer melting point can be taken as the onset of severe wear, as their analysis of polyoxymethylene sliding wear showed that the polymer surface temperature can be appreciably higher than the melting point of the polymer and may reach the decomposition temperature of the polymer [72].

3.6.3.5 Sliding Speed

The influence of velocity on wear can be attributed mainly to surface temperature effects [73]. After a critical sliding velocity, corresponding to a critical interface temperature, is reached, wear can be expected to increase abruptly as the polymer starts to soften and melt. Below the critical sliding velocity, UHMWPE wear is little affected by variations in speed (figures 3.15 and 3.16).

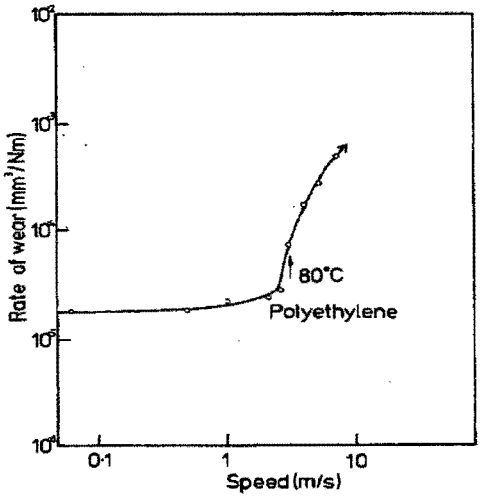

Figure 3.15 *The variation of polyethylene steady-state wear with sliding speed. Tests were conducted using a pin-on-ring apparatus against mild steel of 0.15 μm R_a [adapted from ref. 73].*

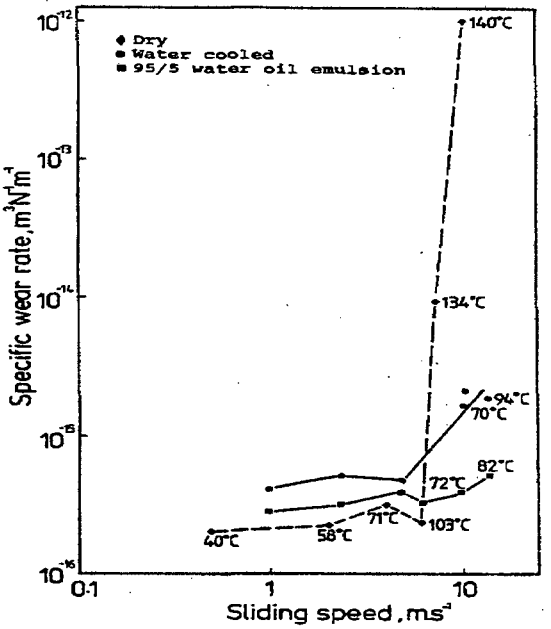

Figure 3.16 *The variation of UHMWPE specific wear rates with speed (for wear against a steel disc). The temperatures given are a summation of the measured surface temperature and the calculated flash temperature at each velocity [after ref. 68].*

3.6.3.6 The "PV" Limit

The product of interfacial pressure and sliding velocity, or *PV*, is frequently used in bearing design and specification to define the allowed conditions under which a polymer bearing may operate. The *PV* limit is the product of pressure and velocity below which reasonably low friction and wear occurs. Shen and Dumbleton [74] established a *PV* of 5400 $lb.in^{-2}.ft.min^{-1}$ (203.6 $kPa.m.s^{-1}$) for RCH 1000 of viscosity average molecular weight 1.25 x 10^6. For lubricated sliding, the attainable *PV* may be much higher still, Dowson *et al.* having carried out testing at *PV* values of 100 000 $lb.in^{-2}.ft.min^{-1}$ (3770 $kPa.m.s^{-1}$) without catastrophic wear occurring [75].

Dumbleton and Shen investigated the effect of *PV* on the wear factor *K* for UHMWPE sliding against stainless steel of 0.127 μm R_a under distilled water lubrication. The *K* value is not constant but passes through a maximum in the region of 500 $lb.in^{-2}$ (3.45 MPa) (figure 3.17).

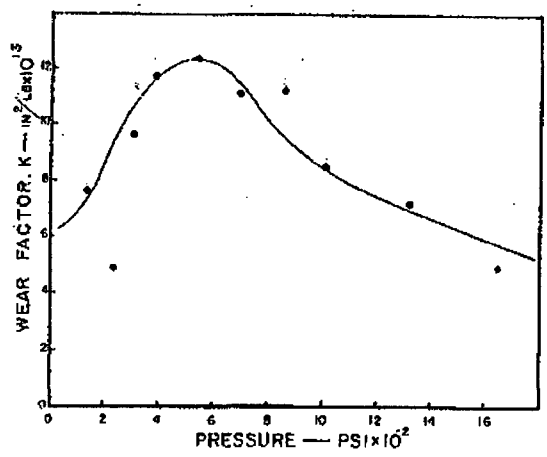

Figure 3.17 Wear factor K *vs.* PV *for UHMWPE tested against stainless steel of surface roughness 0.127* μm R_a *under water lubrication [after ref. 69].*

The current author, however, considers *PV* values and limits of limited use because of the multitude of influences having an effect on the wear performance of UHMWPE.

3.7 Summary

The polymer wear process has been shown to be very sensitive to a multitude of system parameters such as temperature, pressure, sliding speed and lubrication type as well as the nature of the counterface. Indeed, by manipulating these parameters, the actual nature of material removal can be changed and associated differences in wear rate can thus be expected to be great. It is thus important in the design of experiments and interpretation of results that due cognisance is taken of these variables.

CHAPTER 4

THE NEW RECIPROCATING WEAR TESTING APPARATUS

4.1 The Design of a New Reciprocating Wear Testing Apparatus: Problem Definition

4.1.1 Design Statement

A new wear testing apparatus capable of simulating the sliding wear performance of two materials wearing against each other under varying conditions of reciprocating sliding is to be designed.

4.1.2 Design Requirements

The design must:

- provide for two independent tests to be performed simultaneously
- permit the speed of reciprocation to be adjustable to a maximum average velocity of 0.2 $m.s^{-1}$
- provide for a maximum load of 1000 N to be applied onto the reciprocating plain of the test specimens
- feature a loading system for which the load applied onto the test specimen will not fluctuate with increasing wear of the specimen
- provide for the applied load to be varied according to test demands
- permit tests to be performed in liquid-lubricated or dry environments
- prevent the liquid lubricant temperature from rising due to frictional heat generation
- provide for the interface environment to be isolated so as to eliminate third body effects and allow accurate wear debris analysis to be performed
- facilitate that both test specimens are readily accessible and that locating and securing the specimens in position is easily achieved
- feature a specimen loading device which will allow no relative movement between the test specimens other than along the axis of the applied load (except for specimen location and retrieval)
- guarantee the test specimens to be repositioned in their identical relative positions after retrieval to ensure the test specimens remain perfectly matched

- count and monitor the number of cycles completed so that test sliding distances can be calculated and set
- enable the frictional force between the wearing interfaces to be measured
- permit specimens of a simple, previous design to be used so that these can be manufactured along the simplest and most cost effective manufacturing route or used from stock.

4.1.3 Design Constraints

The design must:

- incorporate materials which are readily available to the workshop of the Department of Materials Engineering, University of Cape Town
- for the relevant areas, use materials that can withstand harsh operating environments, as well as the elevated temperatures which may be used in some tests
- allow for all wearing components to be readily accessible for routine inspection or replacement
- incorporate within itself the required precision for reproducible testing such that the machining tolerances on test specimens may be relaxed
- not require any special workshop facilities
- not involve any exceedingly difficult fabrication and hence excessive manufacturing time
- use a simple and comparatively cheap drive mechanism.

4.1.4 Design Criteria

The design should:

- be as simple to operate as possible
- use standard material dimensions wherever possible
- utilise as many standard components as possible, particularly for the wearing components
- minimise noise generation
- be of compact design so as to use only moderate laboratory space

4.2 Concept Formation of the New Reciprocating Wear Testing Apparatus

There are two types of wear testing apparatus, which are generally used to test the overall wear performance of materials.

4.2.1 Pin-On-Disc Tribometer

The pin-on-disc is the simplest wear testing apparatus. Figure 4.1 shows a typical pin-on-disc apparatus layout. The counterface disc is mounted onto a shaft or disc driven by an electrical motor. The wear pin is forced against the counterface disc by means of a simple pivot/counterweight arm system. The interfacial pressure can thus be adjusted by simply altering the pivot load. The counterface/wear pin friction may be measured by a strain gauge device located on the pivot arm or, alternatively, by a push button type load cell restraining the tangential movement of the specimen clamp (provided the pivot is otherwise free to rotate accordingly).

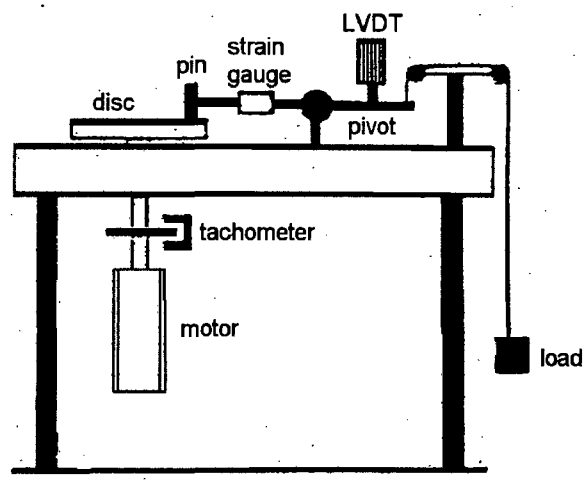

Figure 4.1 Schematic view of a basic pin-on-disc wear testing apparatus layout.

The benefits of the pin-on-disc type wear testing apparatus include:

- simple mechanical design
- easy friction measurement
- uncomplicated loading technique
- constant speed

There are however some major drawbacks to this system:

- the topography of the counterface disc changes with the rotational angle of the disc (unless the surface finishing technique is completely directionally random or perfectly circular or radial)
- wear debris is easily removed out of the interface path due to the outward flow of lubricant, which might hinder the otherwise natural build up of transfer layers etc.
- the counterface discs must be fairly large if linear motion is to be approached
- the sliding velocity will vary across the wear pin surface due to the circular motion of the counterface disc.

4.2.2 Reciprocating Wear Testers

Reciprocating type wear testing apparatuses are also frequently used to test wear performance. The schematic of figure 4.2 shows the relative specimen motions typical of such a wear rig. The counterface specimen is mounted onto a shuttle base, which is forced to reciprocate along an axis normal to the wear pin applied load. The wear pin itself is clamped stationary and forced against the counterface.

Reciprocating wear testers do not suffer from any of the drawbacks listed above for the pin-on-disc types. However, the design of reciprocating wear testers is more complex than that of pin-on-disc types. Furthermore, although the type of motion associated with reciprocating type apparatuses is linear, the sliding velocity is sinusoidal, which may be undesirable in certain wear simulations.

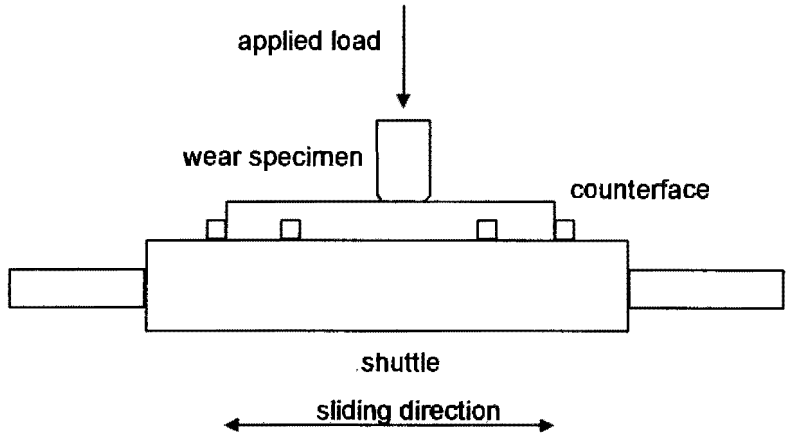

Figure 4.2 Schematic representation of the relative motions of a reciprocating wear tester.

4.2.3 Existing Wear Testing Apparatuses

Two reciprocating wear rigs were already in operation at the Department of Materials Engineering, University of Cape Town [19,76].

The central component of the apparatus shown in figure 4.3 consists of an aluminium housing in which the wear pin is clamped in a holder so that it is able to reciprocate continuously against the desired counterface. The stainless steel housing is constrained to reciprocate along the desired axis by a bushing mechanism sliding on two hardened steel rods (two bushings on each rod).

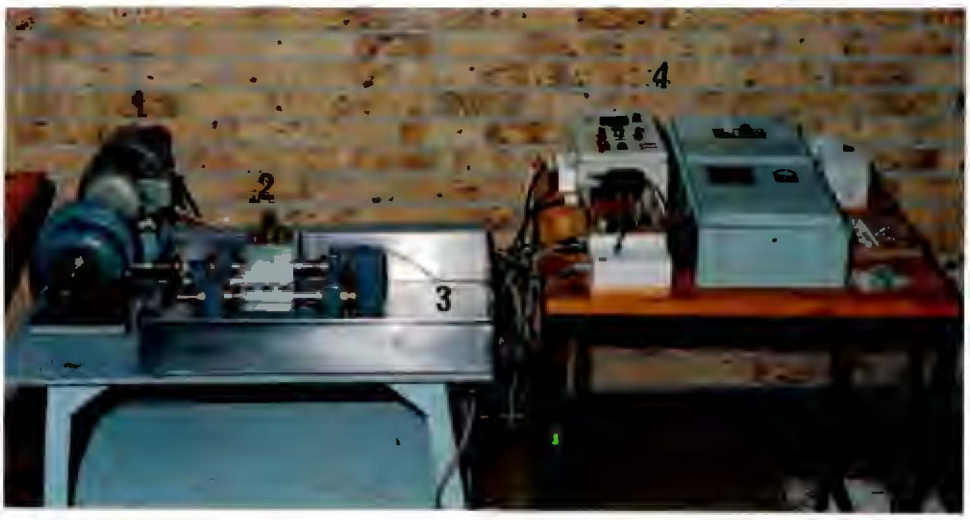

Figure 4.3 *The reciprocating wear testing apparatus as used by Marcus et al. with (1) motor/gearbox, (2) wear specimen housing, (3) lubricant bath, (4) control equipment.*

Figure 4.4 is a schematic of the pin housing and its loading mechanism as well as the stationary counterface. The force is applied onto the wear specimen by a pre-calibrated steel spring and loading screw which may be adjusted to obtain the desired load.

The reciprocating speed of the specimen housing mechanism can be controlled by a thyristor controller which regulates the speed of the electric motor. The desired sliding distances to be covered can be set on a preset counter which sends a signal to the control unit stopping the motor once the required distance has been traversed. The frictional forces can be measured by a friction transducer and the friction signal displayed and stored on an oscilloscope. A stainless steel bath allows tests to be performed under suitable lubricant conditions.

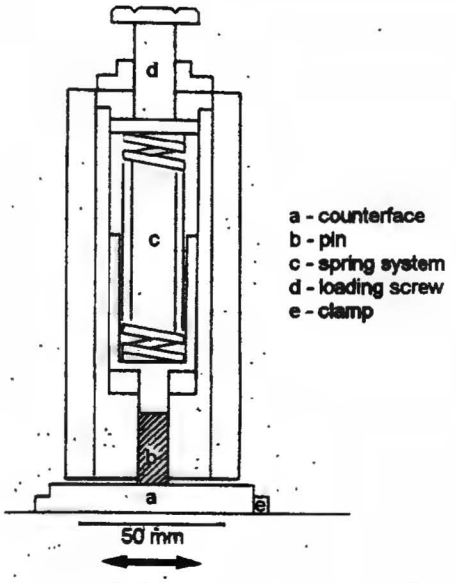

Figure 4.4 A schematic of the pin housing and counterface used on the test reciprocating test rig shown in figure 4.3.

The main disadvantages associated with this wear tester are:

- unreliable spring loading mechanism
- highly cumbersome specimen location/retrieval
- exposed lubricant environment leading to probable third body interference
- design allowing only a single test to be performed at a time
- open bushings located over lubricant bath resulting in probable contamination of the lubrication fluid by bushing oil

The wear tester shown in figure 4.5 is of generally more sophisticated design.

Figure 4.5 The reciprocating wear testing apparatus as designed by Kienle with (1) reciprocating shuttle, (2) force applying load cell, (3) motor.

However, this rig also relies on a crank slider mechanism to achieve the desired relative reciprocating motion of wear specimen to counterface. Figure 4.6 shows the essential mechanical constituents of this design. The wear counterface is clamped onto a shuttle which oscillates on two parallel shafts secured in the horizontal plane. To the other side of the vertical backing disc is a crank slider arrangement driven by an electric motor and supported at the same level as the reciprocating shuttle. The wear pin is clamped stationary and the force is applied onto it by a load cell mechanism.

The original design included the use of a perspex chamber to allow the submergence of the entire shuttle, shuttle locating and wear pin clamping mechanisms in the desired lubricant. However, adequate sealing of this chamber proved difficult, and complete submergence of the entire reciprocating assembly and wear pin clamping mechanism is undesirable. The original chamber was thus replaced by a bath assembly surrounding the shuttle and subsequently the entire reciprocating assembly up to the level of the wear pin/counterface interface is submerged with the desired lubricating medium.

A beam type load cell transducer allows the friction between the wear pin and counterface to be measured. The friction signal can be displayed and stored on an oscilloscope.

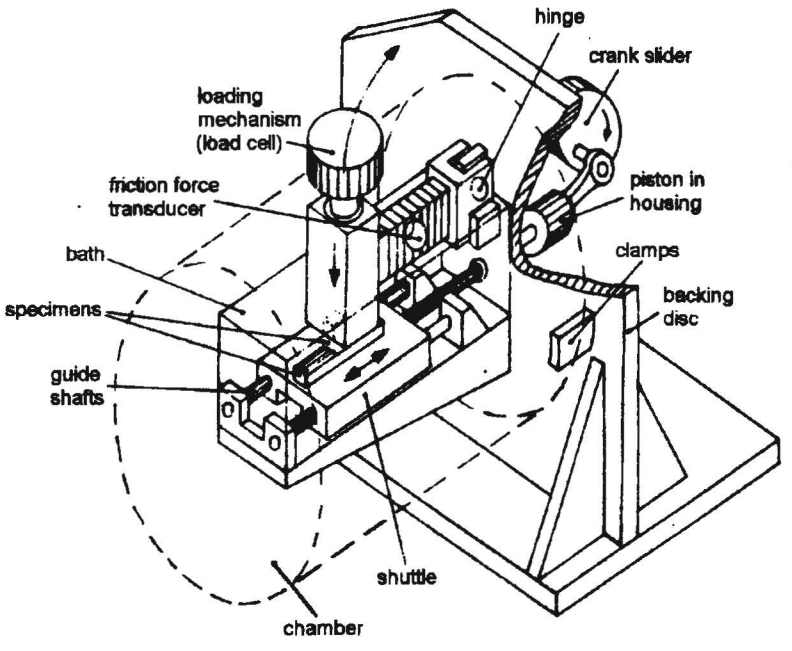

Figure 4.6 Schematic sub-assembly of the reciprocating wear tester designed by Kienle.

The most significant disadvantages associated with the this test apparatus are:

- low maximum applied load of 100 N, necessitating the use of small interface areas to obtain the desired high pressures which increases the inaccuracies associated with measuring low wear mass loss
- complex loadcell load technique
- low capacity lubricant bath possibly resulting in frictional heating of lubricant
- the placement of the bearing/shaft assembly inside the lubricating bath environment leading to
  - rapid degradation of the bearings/shafts necessitating very frequent and lengthy service
  - possible ingestion of bearing debris as third body particles between the test interface
  - inaccurate wear debris analysis due to possible presence of bearing debris
  - interference of the bearing lubrication with the testing environment
- design allowing only a single test to be performed at a time

A new wear testing apparatus was thus built, the design of which was broadly based on the concept used by Kienle [76], involving a crankshaft driven reciprocating shuttle containing the desired lubricating environment sliding on a linear bearing/shaft mechanism. The same arrangement of mounting the reciprocating assembly and wear pin clamping and loading mechanism to one side of a vertical backing plate, with the crankshaft and associated assembly on the other (see figure 4.6) was used in the new design. The new design features the following innovations to overcome the disadvantages associated with the previous rigs:

- duplication of all the relevant mechanisms to allow two tests to be performed simultaneously
- lubricant environment isolated from all surroundings including linear bearing assembly
- lubricant recirculation into a large reservoir to ensure a constant temperature
- simple and reliable lever arm/dead weight load application up to 1000 N

4.3 Solution Specification for the New Reciprocating Wear Testing Apparatus

Description:

A laboratory test apparatus to be used for investigations of wear and friction of two material surfaces sliding against each other under reciprocating, single axis motion in differing environments.

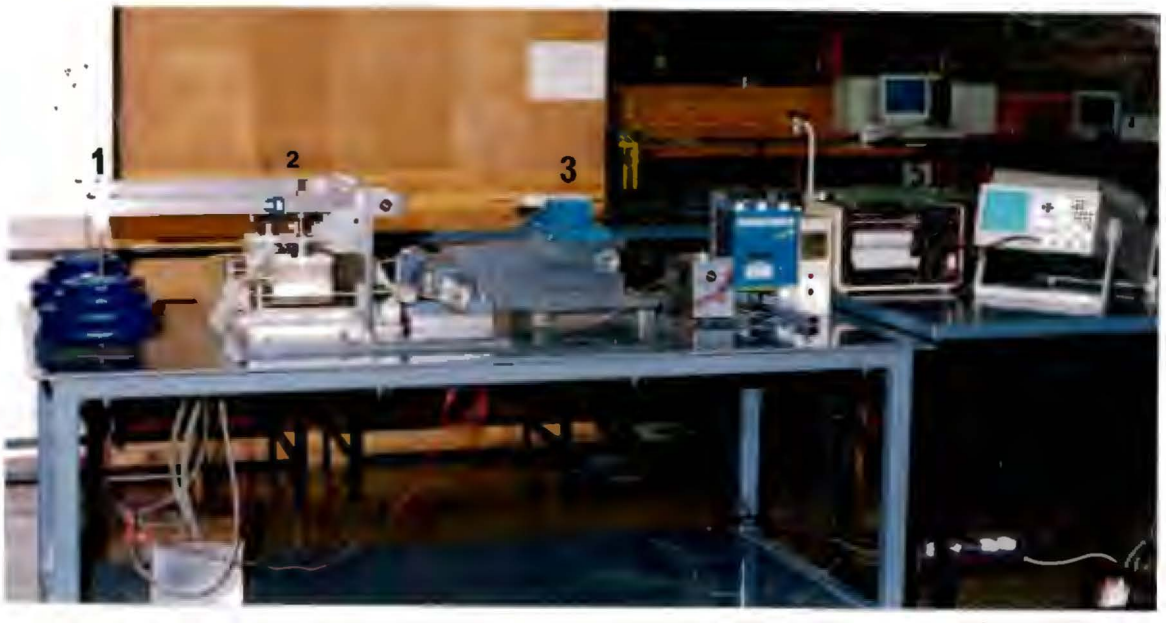

Figure 4.7 The new reciprocating wear testing apparatus with (1) dead weights/lever arm, (2) wear pin holder (static) and reciprocating shuttle, (3) motor, (4) pump control, speed control and cycle counter, (5) chart recorder and digital storage oscilloscope.

Hardware:

- overall dimensions: (including table) — length = 2005 mm; width = 1000 mm; height = 1260 mm
- primary drive: — Renold Crofts 1.5 kW 380/240 V 3 Phase, 4 Pole Electric Motor c/w
- primary transmission: — Renold Crofts Ritepower 2D Gearbox Ratio 7.52 : 1
- speed controller: — Renold Crofts Renvert Junior RVJ 150-2

AC Variable Speed Drive
220 V single phase in, 220 V three phase out
c/w programming module

- reciprocating drive: belt driven crank slider
- stroke length: 50mm
- velocity profile: sinusoidal

Test Specimens:

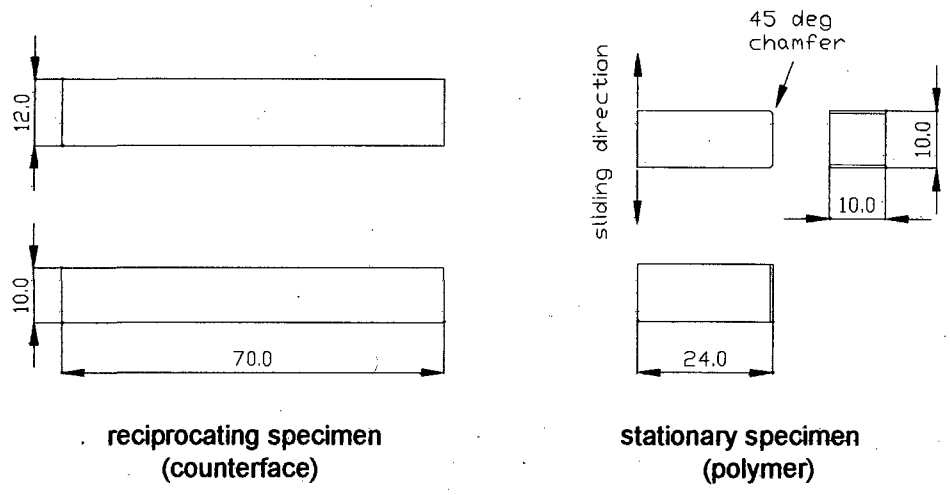

Figure 4.8 Recommended Test Specimen Dimensions

Operating Parameters:

- reciprocating speed: 0 – 2 Hz (Liquid Lubrication)
  = 0.2 $m.s^{-1}$ average sliding velocity
  (larger fan must be fitted for prolonged low speed operation)
- loading of specimens: lever arm/dead weight adjustable 50 – 1000 N

Testing Environments:

- dry
- bath filled with desired medium, recirculated or stagnant

Features:

- friction force readout, to a maximum combined frictional and secondary force of 1000 N,
- repositioning in an identical position is guaranteed for both test specimens after each and every test run; the reciprocating surfaces will therefore remain matched even during interrupted testing.

Options:

Provision has been made in the design to allow certain components to be changed or modified in order to expand on some of the existing specifications:

- stroke length adjustable between 0 – 50 mm if the crankpin holder is remanufactured accordingly
- applied loads of less than 50 N are possible if the lever arm is modified to allow counterweight balancing of the arm

Materials Used:

• internal workings of test cell:	grade AISI 316 stainless steel
• test cell surrounds:	grade AISI 316 stainless steel, grade AISI 431 stainless steel, Acetal, Perspex
• supporting mechanisms:	grade AISI 316 stainless steel, grade AISI 431 stainless steel, brass, stainless steel square tubing
• backing plate:	grade AISI 316 stainless steel
• base plate:	3CR12 steel
• table structure:	BS 070M20 mild steel

4.4 Discussion of the New Reciprocating Wear Testing Apparatus

The design of the new reciprocating wear testing apparatus is capable of meeting all the requirements, constraints and criteria as discussed in Chapter 4.1. Due to its complexity, the design will be discussed under several subheadings with reference being made to the sub-assembly drawing at the end of this section. For greater clarification, reference can be made to a series of photographs showing the wear rig at the end Chapter 4.5.2.

4.4.1 The Basic Layout

Reference should be made to the subassembly drawing at the end of Chapter 4.4. The vertical backing plate (14) forms the central part of the test rig. All the test cell components holding the specimens and facilitating load application are on the same side of this plate. Most components used here are exposed to or in proximity to the test environment, and hence only materials with good resistance to corrosion were specified. The adjustable weights (1) are an exception, as they are well clear of the test environment due to the length of the weight/lever arm (2).

The other side of the vertical backing plate is bolted to gusset stands (13) which secure it in position on the base plate (10). All the mechanical drive components are also found on this side of the backing plate: A 1.5 kW electric motor drives the crankshaft via a timing belt/pulley. The crankshaft is connected to two connecting rods on either side, which drive the reciprocating shafts (11) forcing the shuttles and all their associated attachments to reciprocate. A diaphragm type tension/compression load cell rated to 1000 N forms part of the reciprocating shaft (11) and thus enables friction measurements to be performed.

4.4.2 The Reciprocating Drive Mechanism

As discussed in Chapter 4.3, much of the current design was based on that of an existing reciprocating wear rig designed by U. F. B. Kienle, in which a crank-slider type mechanism was chosen to produce the desired sinusoidal velocity profile.

Figure 4.9 shows the main elements of the reciprocating drive mechanism. The crankshaft is driven by a timing belt, the timing pulley being keyed onto the shaft off center to accommodate a third bearing/plumber block. This additional plumber block was added to decrease the bending moment on the shaft caused by the tension exerted onto it by the timing belt. On each side of the timing belt/pulley are located the main bearings and their plumber blocks. The crankpin holding plates are bolted on each end of the shaft. The crankpins themselves are located 25 mm off center so that the resultant stroke will be 50 mm. Furthermore, the two crankpins were mounted 180° out of phase with each other in order to balance primary forces.

Connecting rods link the crankpins to the reciprocating shafts (11). Due to the severe fluctuating loads placed on the two components, a high strength martensitic stainless steel (AISI 431) was chosen for the conrod and crankpin.

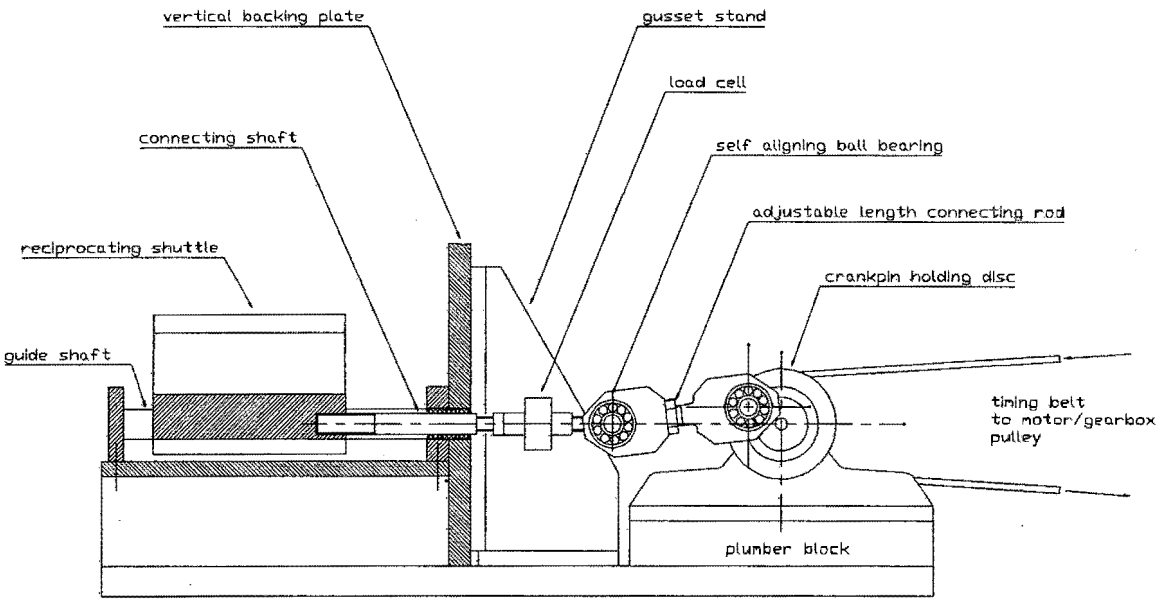

Figure 4.9 A drawing of the main elements of the reciprocating drive mechanism.

The reciprocating shafts linked to the conrods are fastened onto diaphragm type tension/compression load cells (12), which form part of the reciprocating shafts. These reciprocating shafts move through holes in the vertical backing plate (14) and onto the shuttle bases (9) and which in turn force the bases to reciprocate. The shuttle bases are each supported by four linear ball bearings rolling on 20 mm diameter guide shafts. The ball bearings were chosen over bushes as the formers' friction coefficient is much lower, thus reducing mechanical forces and allowing more accurate friction measurements to be performed.

4.4.3 The Reciprocating Shuttles

The reciprocating shuttles hold the counterface specimens in their positions and isolate the desired testing environments (7) (see figure 4.10). The bath bases, bolted onto the shuttle bases (9), are manufactured from acetal. These bases slope away from the vertical backing plate (14) to facilitate lubricant drainage and cleaning of the baths. Perspex was specified for both walls, permitting some side observation of the bath interior.

The counterface specimens are placed into the recesses of elevated stainless steel blocks (protruding out of the acetal bath bases), each featuring two locating screws. The baths are covered by acetal lids, which have elongated center sections cut out to allow the free movement of the (static) specimen clamps (4). Attached to the sides of the lids, and perpendicular to the reciprocating direction, are small

platelets to reduce the oscillating flow of the lubricant and hence prevent spillage (not shown in drawing).

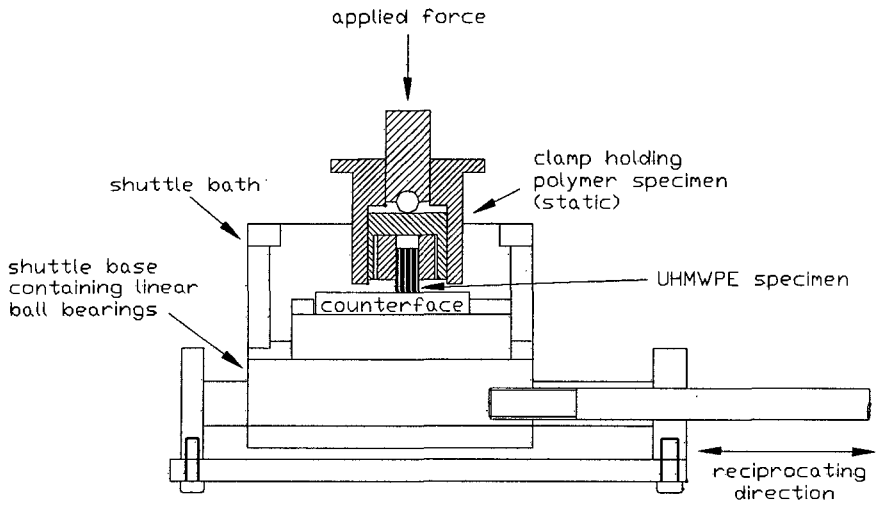

***Figure 4.10** A drawing of the reciprocating shuttle bath and base with counterface specimen mounted inside, as well as the wear pin and its clamping mechanism.*

4.4.4 The Wear Pin Clamping Mechanisms

The stationary wear pins (5) are held in a vertical position by specimen chucks consisting of two jaws each, one being fixed and the other being adjustable. The jaws are located inside square recesses milled into the specimen holder. While the fixed jaws are screwed onto the inner faces, the opposing jaws can be adjusted by turning grub screws and the wear specimens can thus be clamped tight.

The specimen holders are free to slide along the vertical axis inside the clamp housings (4). The clamp housings are hinged onto brackets bolted onto the vertical backing plate and thus the entire stationary wear specimen assembly's may be hinged through 90^0 to facilitate wear pin and counterface access. For operation, bolts connecting the bracket to the clamp housing plates keep the wear pin firmly in the vertical position.

4.4.5 The Loading Mechanism

A lever arm/dead weight loading technique was chosen for the new reciprocating wear apparatus because of its simplicity and consequent reliability. Whereas spring loading mechanisms usually do not cater for the reduction in applied force

as the spring becomes extended with the wearing down of the specimen, the lever arm/dead weight applied load remains constant even for extensive wear of the specimen pin.

The lever arms are hinged onto brackets bolted onto the crankshaft side of the vertical backing disc (14). The force transmission pins (3) exerting the force onto specimen holders are situated at a distance of 170 mm from the hinges, whereas the dead weights (1) are located 595 mm away from the hinges. The pin load is thus approximately 3.5 times higher than the applied mass. The exact load exerted onto the wear specimen was calculated by also taking into account the mass of the lever arm itself as well as the counterweight suspension system, force transmission pin and wear specimen holder:

$$F_{wear\ pin\ interface} = 34.16 * M_{dead\ weight} + 64.26,$$

where F is in Newtons and M in kilograms. The desired load can thus be achieved by selecting the appropriate weights.

Push button type load cells (Biomer Systems cc.) were used to ensure that the load exerted onto the force transmission pins (3) was effectively transmitted to the wear specimen/counterface interface.

4.4.6 The Lubricant/Coolant Recirculation System

The lubricant reservoir is situated some distance beneath the base plate (10). Lubricant is pumped up to the level of the reciprocating bath by a variable flow pump. A T-piece separates the flow into two flexible hoses which are connected to the Perspex sides of the bath. Lubricant drainage is achieved by single gravity drainage holes situated at the optimum lubricant level of the bath. The lubricant flows back to the reservoir in flexible hoses.

4.4.7 Friction Force Measurement

Each of the two reciprocating shafts (11) are split into two in order to accommodate the tension/compression diaphragm type load cells (12) used to measure friction. Both sides of the load cells (Biomer Systems cc.) feature tapped protrusions so that the shafts can simply be screwed onto the load cells. Lock nuts secure the load cells in position.

The signal from the load cells is amplified and led to an IWATSU DS-8631 digital storage oscilloscope and chart recorder. During friction force measurements, the reciprocating speed is briefly lowered to 0.1 $m.s^{-1}$ (average) so as to negate the secondary load effects generated by shuttle acceleration. A typical output curve is shown in figure 4.11. The load cells were calibrated before installation, so that the voltage readout could be translated into frictional force according to

$$F_{friction} = 14.442*Output + 0.14083 \quad \text{- load cell no.1}$$

$$F_{friction} = 15.178*Output + 0.08901 \quad \text{- load cell no.2}$$

where the force is given in Newtons and the output in Volts.

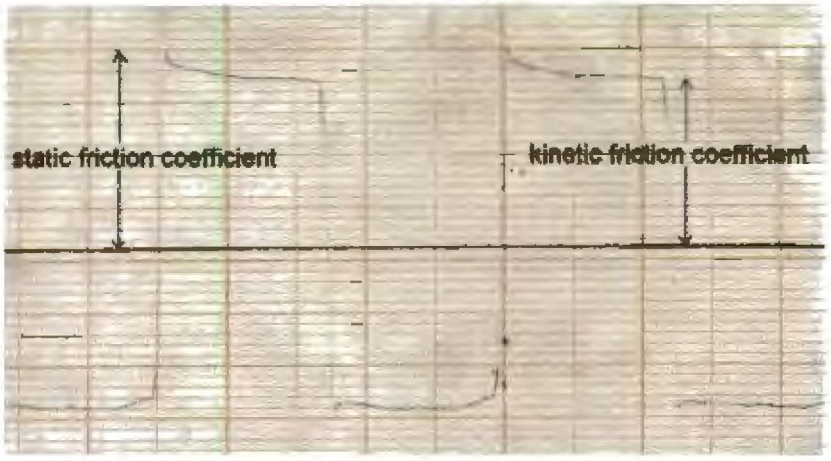

***Figure 4.11** A typical load cell output vs. time curve.*

4.4.8 The Electric Motor, Speed Controller and Cycle Counter

A Renold Crofts 1.5 kW electric motor is used as the primary drive for the new reciprocating wear testing apparatus. An integral gearbox reduces the output speed by a ratio of 7.52:1. The speed controller allows the speed of the motor to be varied by selecting different input frequencies. This is however not the final crankshaft speed because of the gearbox and timing belt power transmission and slightly inaccurate motor output speed/input frequency correlation. The exact ratio of final reciprocating speed to input frequency was calculated by setting the input at various frequencies and measuring the final drive speed with a digital hand held revolution counter:

*final reciprocating speed (rev/min) = 4.81929*input frequency (Hz) – 0.89286.*

The input select frequency must thus be set accordingly. Also note that the crankshaft velocity (rev/min) may be divided by 600 to obtain the shuttle average sliding speed ($m.s^{-1}$).

A revolution counter sensing the revolutions of the crankshaft was linked to the speed controller so that the number of revolutions could be counted. The device also allows the operator to select the number of revolutions he/she wishes to complete, the counter signalling the speed controller to stop after the programmed number of revolutions is reached.

4.4.9 Test Rig Operating Procedure

This section presents a basic guide to beginning and ending a test. Starting from the assumption that the wear pin clamping mechanism is in the testing position (as shown on the drawing):

1. Swing weight/lever arm (1) through 90^0 into the holding position.
2. Loosen the retaining bolt on the clamping mechanism bracket.
3. Swing the clamping mechanism through 90^0 to the holding position.
4. Loosen locating crews of counterface locating block.
5. Insert counterface (6) into the recess.
6. Tighten locating screws.
7. Slide the specimen holder out of the clamp housing (4).
8. Insert the wear pin in between the two jaws and tighten the grub screw to secure the specimen in place.
9. Insert the specimen holder back into the clamp housing.
10. Swing the clamping mechanism through 90^o to the testing position.
11. Fasten retaining bolts.
12. Lower lever arm.
13. Level the lever arm by adjusting the force transmission pin (3) nuts.
14. Suspend appropriate weights from the lever arm end.
15. Switch on lubricant flow (if desired) and wait until stabilised.
16. Select the number of cycles to be completed on revolution counter.
17. Set desired speed on the speed controller.
18. Start motor.

To end a test:

1. The revolution counter will have automatically stopped the motor after set cycles have elapsed.

2. Turn off the coolant.
3. Swing weight/lever arm (1) through 90^0 into the holding position.
4. Loosen the retaining bolt on the clamping mechanism bracket.
5. Swing the clamping mechanism through 90^0 to the holding position.
6. Loosen locating screws of counterface locating block.
7. Remove counterface (6) from the recess.
8. Slide the specimen holder out of the clamp housing (4).
9. Loosen the adjusting jaw grub screw and remove wear pin.

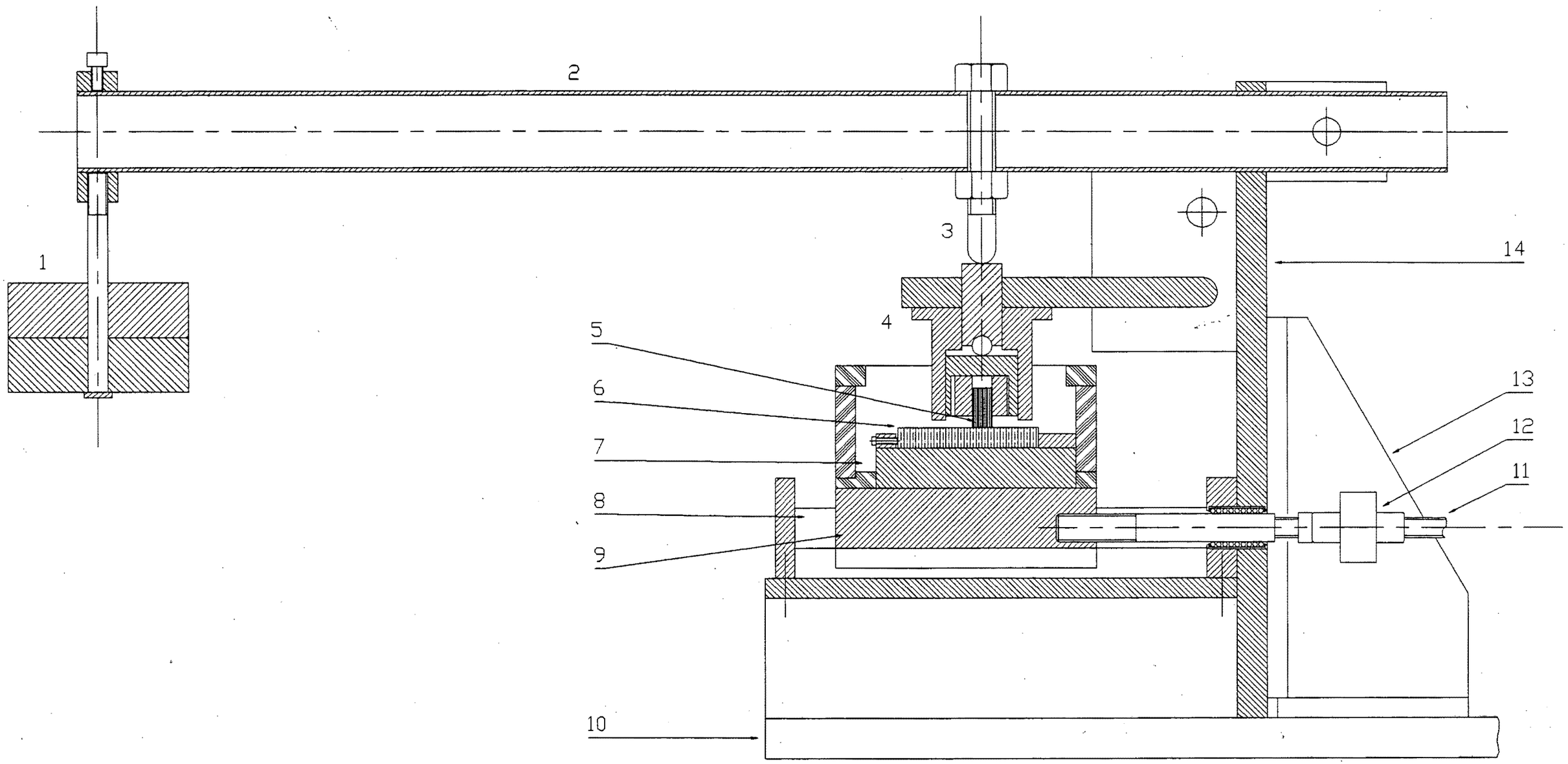

1	weights	9	shuttle base (housing linear bearings)
2	weight/lever arm	10	base plate
3	force transmission pin	11	shaft to connecting rod and crank shaft
4	wear pin clamping mechanism	12	friction measuring load cell
5	wear pin	13	gusset stand
6	counterface	14	backing plate
7	lubricant bath/environment		
8	linear bearing guide shafts		

UNIVERSITY OF CAPE TOWN
DEPARTMENT OF MATERIALS ENGINEERING

SUBASSEMBLY DWG OF RECIPROCATING WEAR APPARATUS

SCALE: 1:2	DRAWN BY: M. HOHL
DATE: 29/03/98	

4.5 Evaluation of the New Reciprocating Wear Testing Apparatus

The results of three tests wearing UHMWPE pins against similarly prepared, polished stainless steel counterfaces under identical test conditions were carried out to assess the correct functioning of the new design and the reproducibility of the test results. The wear of UHMWPE against smooth polished stainless steel specimens of counterface roughness $R_a = 0.02$ μm under distilled water lubrication and 10 MPa applied load represents a particularly stringent condition as the mass loss recorded is extremely low.

4.5.1 Test Results

material couple used:	UHMWPE/AISI 431 stainless steel (hardened)
reciprocating speed:	0.2 $m.s^{-1}$ average
counterface roughness:	$R_a = 0.02$ μm, polished
load:	1000 N
sliding distance covered:	20 km
lubricant/coolant:	distilled water
specimen dimensions:	refer to Chapter 4.2

Figure 4.12 shows the results obtained for the reproducibility tests. Deviation from the average of 0.179 mm^3 volume loss after 20 km of sliding is an average of ± 14 %, a very credible result. Additionally, the initial surface match between the wear pin and counterface will differ for each of the three tests and thus account for some of the discrepancy.

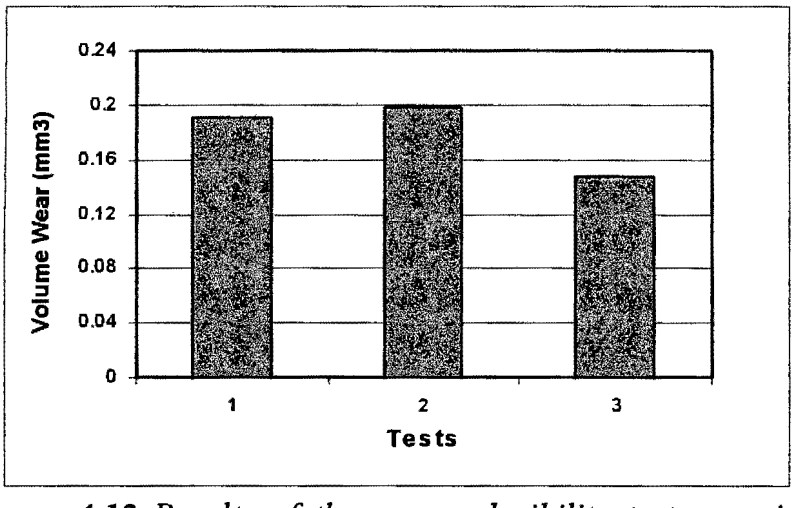

Figure 4.12 Results of three reproducibility tests wearing UHMWPE against polished stainless steel counterfaces for 20 km.

For tests wearing UHMWPE against a parallel ground counterface of R_a = 0.3 μm under distilled water lubrication, the volume wear recorded after 40 km of sliding corresponded very well to that recorded by Marcus [19] under similar test conditions using a different rig as shown in figure 4.3, at 6.06 mm^3 compared to 5.9 mm^3.

Repeated tests wearing UHMWPE against polished stainless steel counterfaces showed the new apparatus's friction measurements to be very consistent, with virtually zero discrepancy between repeated readings. They thus offer an excellent basis for comparing the friction of UHMWPE against different counterfaces. Friction force readings taken for an UHMWPE wear pin sliding against a parallel ground counterface of R_a = 0.33 μm in distilled water under a load of 11 MPa interface environment produced friction coefficient measurements of μ = 0.052, taken after 10 km. This is slightly higher than the 0.047 measured by Marcus under similar water lubricated reciprocating sliding conditions [19]. However, for an equivalent test, Lloyd *et al.* registered a friction coefficient of μ = 0.1 [63]. The comparison of friction coefficient values to other workers results is thus clearly problematic.

4.5.2 Test Rig

The design of the new reciprocating wear tester has proven to be highly successful. All of the requirements, constraints and criteria were met and in many instances exceeded. Specimen turnarounds require minimal time and noise levels generated are acceptable. The vibrations caused by the secondary imbalances are very low.

The rig has completed over 4000 km of testing (equivalent to 40 million revolutions) without major incident. The only parts of the apparatus subjected to wear are the shuttle base linear bearings, which require replacement every 1500 km.

A series of photographs given on the following pages show various details of the test rig in operating and holding positions.

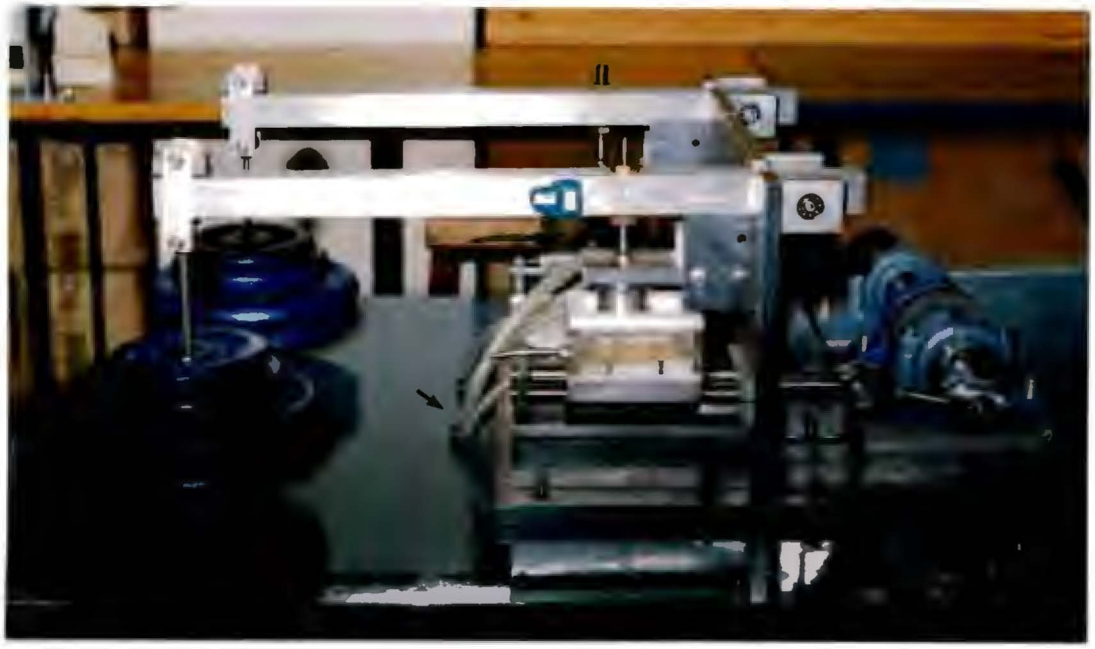

A view of most of the mechanical assembly showing the dead weights, lever arm, wear pin holding mechanism, reciprocating shuttle, as well as the backing plate and crankshaft, with direction of rotation as indicated. Also notice the lubricant recirculation tubes leading from underneath the table to the shuttle, as pointed out by the arrow.

Inverter/speed controller (1), cycle counter and set (2), chart recorder (3), digital storage oscilloscope (4).

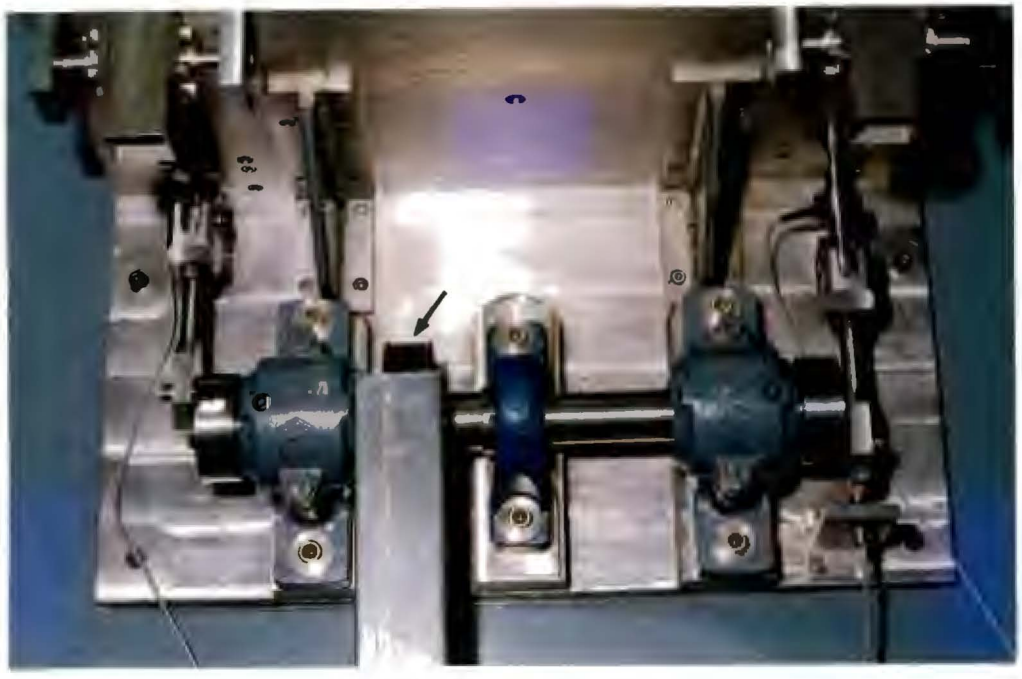

A view of the crankshaft arrangement showing the timing belt/pulley drive (as indicated by the arrow) and the three plumber blocks used to locate the shaft. The connecting pin holders, connecting pins and connecting rods can also be seen. Load cell No.1 forms part of the connecting shaft shown on the left hand side of the photograph, whereas load cell No.2 forms part of the connecting shaft to the right hand side of the photograph.

One of the friction measurement load cells, mounted as an integral part of the connecting shaft.

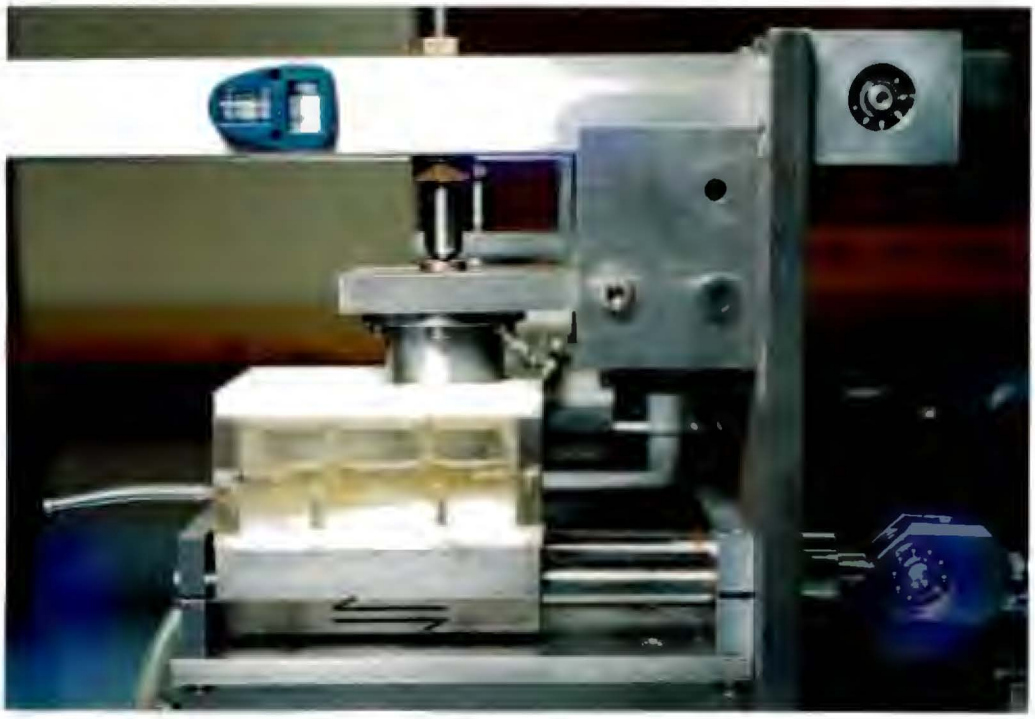

The reciprocating shuttle filled with water, with the wear pin holder secured in the operational position. The force transmission pin is also visible. The arrows indicate the direction of shuttle reciprocation.

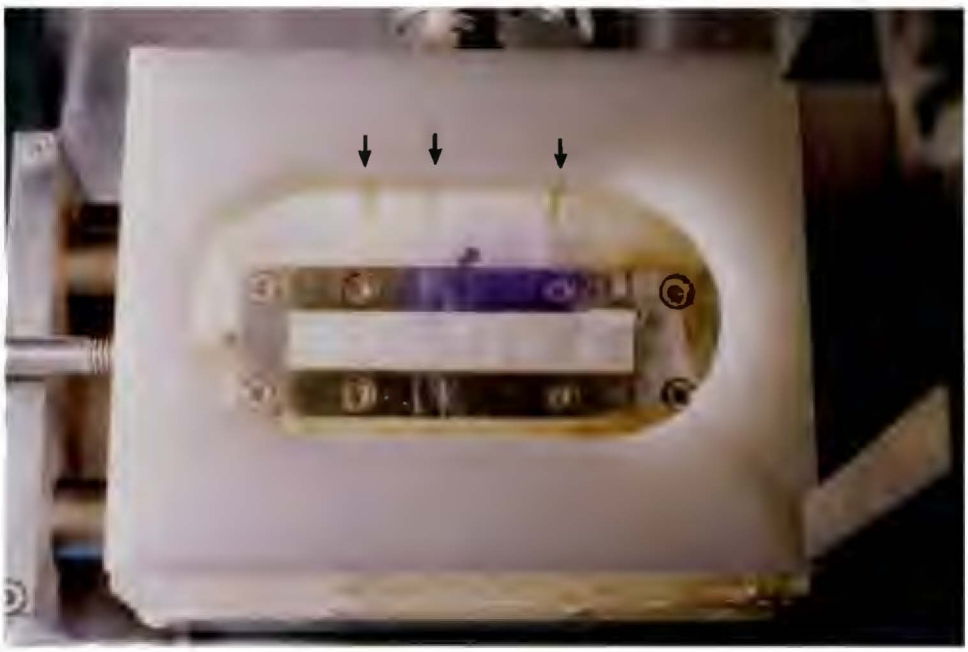

The shuttle bath with the stainless steel counterface holding mechanism inside. Locating screws fasten the counterface specimen (in this case Yttria Partially Stabilised Zirconia) into place. Also note water entering the bath via one of the perspex sides and the small bulkheads (as indicated by the arrows) installed to prevent excessive oscillation and consequent overflowing of the lubricant.

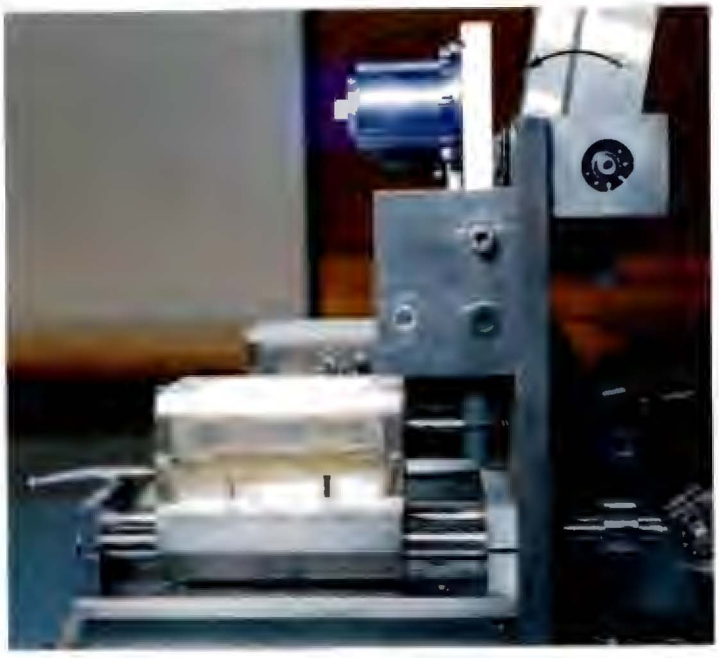

A view of the wear pin clamping mechanism in the holding position. The arrows indicate the rotating action of lever arm and wear pin holding mechanism to the operational position.

A different view of the wear pin clamping mechanism in the holding position. The protrusions from the side of the shuttle bath are the lubricant entry pipe (1) and lubricant drainage pipe (2). The usual lubricant drainage (2) is located at the water level required for sufficient wear specimen submergence. To enable complete drainage of the lubricant bath, an additional drainage pipe is located at the bottom level of the bath (3). The photograph on the right is a closer view of the wear pin clamping and holding mechanism with UHMWPE specimen mounted inside. The clamping mechanism (1) is free to slide inside the clamp holder (2).

CHAPTER 5

EXPERIMENTAL METHODS

5.1 Test Materials

5.1.1 The Polymer Wear Pins

The polymer wear pins used in this study were cut from the bulk ultra high molecular weight polyethylene (UHMWPE) material in the square form as shown in figure 5.1. The surface to be worn was machined to a surface roughness of 0.3 μm R_a. A small 45^0 chamfer was introduced along the leading and trailing edges of the wear surface to minimise possible rocking of the polymer pins during reciprocating sliding (see Chapter 4.2).

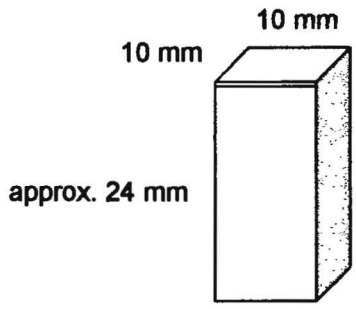

Figure 5.1 The geometry of the UHMWPE wear pins.

The UHMWPE used for this investigation is of medical grade (*Chirulen*, supplied by Solidur Poly-Hi Meditek) and is thus purer than the conventional industrial product. Special processing and production precautions ensure that the ash content is very low and that the titanium and aluminium concentrations are below 20 and 40 ppm respectively. Physical, thermal and electrical properties of the UHMWPE used, as supplied by the manufacturer, are listed in appendix A.

5.1.2 UHMWPE Ion Implantation

The UHMWPE wear pins were ion implanted in a nitrogen atmosphere (N^+ and N_2^+ species) under an accelerating voltage of 80 keV to a dose of 10^{15} ions/cm^2 by NITRUVID (Fraisses, France). Only the chamfered end was treated.

Comparison of the ion implanted pins with the unimplanted pins under a light microscope revealed no changes in appearance of the implanted surfaces. The surface roughness values also remained the same.

5.1.3 The Stainless Steel Counterfaces

The stainless steel counterfaces were machined from grade AISI 431 material to rectangular bars 70 mm in length, 12 mm wide and approximately 10 mm deep (the counterface height not being critical, see figure 5.2). They were then subjected to a heat treatment schedule resulting in a hardness of 500HV30 as measured on an ESEWAY hardness tester.

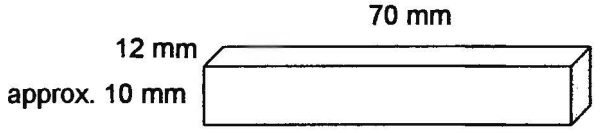

***Figure 5.2** The geometry of the counterface wear pins.*

Three different techniques were used to achieve the final surface finish of the steel counterfaces:

5.1.3.1 Surface "Parallel" Grinding

The stainless steel counterfaces were surface ground in a direction perpendicular to that of sliding motion. This resulted in a single scratch direction distribution (normal to the direction of sliding), as shown in figure 5.3. The surface roughness values achieved by this technique ranged from R_a = 0.15 to 0.66 μm.

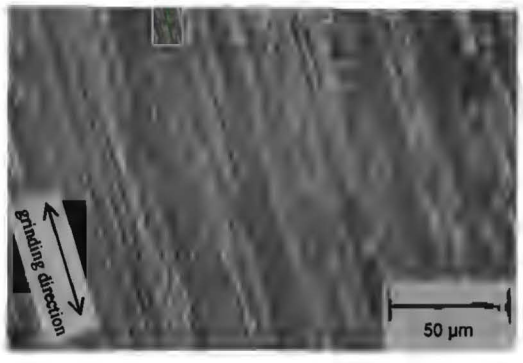

***Figure 5.3** Scanning Electron Microscope (SEM) image of unworn surface ground stainless steel surface showing single scratch direction. Surface R_a = 0.29 µm.*

5.1.3.2 Random Grinding

After the specimen wear surfaces were surface ground to an R_a of approximately 0.4 µm, they were further ground in a Struers Roto Module automatic polisher, using a special adapter which allows simultaneous preparation of three stainless steel bars. Different surface roughnesses of 0.46 to 0.05 µm R_a were achieved by wet grinding with different Struers silicon carbide grinding pads with grit sizes from 60-65 µm to 5-8 µm. This technique resulted in a random distribution of scratch directions (see figure 5.4).

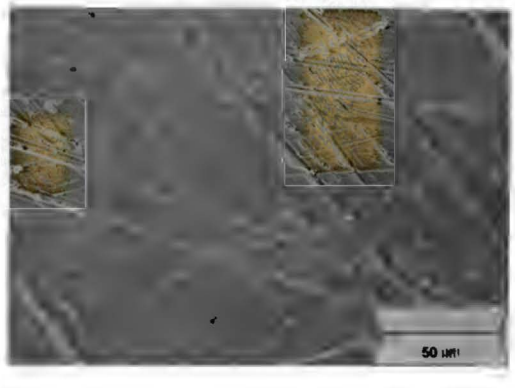

***Figure 5.4** SEM image of unworn ground stainless steel surface showing the random scratch direction. Surface R_a = 0.17 µm.*

5.1.3.3 Polishing

Surfaces to be polished were first ground wet in the automatic polisher using Struers grinding pads with grit sizes ranging from 60-65 μm to 5-8 μm. Using the same Struers Roto Module Automatic Polisher and adapter, they were then polished using a 0.25 μm diameter silicon oxide particle suspension.

5.1.3.4 Polishing/Grinding

Some of the polished counterfaces were only polished fairly briefly, resulting in some of the grinding scratches remaining. An intermediate polishing/grinding surface of surface roughness R_a = 0.04 μm was thus obtained.

5.1.4 The Yttria Partially Stabilised Zirconia Ceramic Counterfaces

The YPSZ bars were supplied by Astro Met Inc. (Ohio, USA) in a polished condition to an R_a value of 0.02 to 0.04 μm (R_a measurements taken by the author using a Taylor-Hobson Surtronic 3P surface profilometer indicated an average R_a value of 0.02 μm). Some comparative mechanical properties of Zirconia ceramics are listed in Appendix B.

5.2 Test Parameters

5.2.1 Sliding Velocity

The sliding velocity is sinusoidal with an average speed of 0.2 $m.s^{-1}$, the corresponding maximum speed thus being 0.32 $m.s^{-1}$. The speed was chosen as it allowed fairly rapid progression of the tests without significant frictional heating and also corresponded to the speed used by previous authors, thus allowing direct comparisons to their test results. As a precaution, the sliding speed was however lowered to 0.1 $m.s^{-1}$ during friction force measurements to negate the possible effects of acceleration and deceleration of the shuttle assembly on the friction measurement (see Chapter 4.4.7).

5.2.2 Pressure

The applied interface pressure used for all the tests was 11 MPa. This corresponds to a 1000 N force being exerted onto the wear pin contact area of 90 mm^2. This value lies within the physiological range of total hip replacements and similar values are thus used in many UHMWPE wear studies, allowing direct comparisons to previous studies to be made.

5.2.3 Counterface Roughness

Counterface roughnesses of both random ground and parallel surface ground metallic specimens were varied in order to allow the counterface surface roughness–wear behaviour of UHMWPE to be investigated. The counterface roughness value for both the polished stainless steel and YPSZ specimens was recorded as being 0.02 μm R_a.

5.2.4 Lubricant

Distilled water was used as a lubricant. The water temperature was prevented from rising, due to frictional heating, by recirculation through a large storage tank. The temperature thus remained constant between 25 to 27 ^{0}C. Distilled water has been used in many previous tests thus allowing direct comparisons of wear performance to be made.

5.2.5 Sliding Distance

The total sliding distance covered was usually 100 km. This distance is sufficient to cover any bedding in effects and the formation of any stable transfer layer (usually after a maximum of 20 km). The stabilised wear after transfer layer formation can thus be well studied. Sufficient distance is also covered to reveal any effect of fatigue wear, should any occur. Tests against very rough counterfaces were at times prematurely halted due to exceedingly high wear. Conversely, tests against YPSZ counterfaces lasted up to 200 km due to the extremely small UHMWPE mass loss encountered for this couple.

Tests were usually stopped at 20 km intervals to allow mass loss measurements to be made. However, at the beginning of each cycle of tests, mass loss measurements were at times made at shorter intervals.

5.3 Experimental Measurements

Prior to testing, all the test materials were subjected to a similar cleaning procedure. They were rinsed in water and then ultrasonically cleaned in absolute alcohol. The UHMWPE pins were cleaned in the same way during each of the test intervals, prior to the mass loss measurements. The stainless steel counterfaces were also demagnetised and solvent cleaned prior to the above procedure.

5.3.1 Measurement of Specific Wear Rate

The UHMWPE mass-loss was measured using a Mettler HR 54 R research balance with an accuracy of 0.01 mg. A soak control UHMWPE piece was weighed along with the wear specimens to ensure that no significant amount of water or alcohol (from the ultrasonic cleaning procedure) was absorbed and to check that the balance readings remained consistent.

Polymer mass-loss was converted to volume loss V which was plotted against the sliding distance S. This technique is preferred to measuring the dimensional change as the latter may also be influenced by creep. The specific wear rate K_0 was calculated for both the initial transfer layer forming period of wear (taken as the first 20 km of sliding) and the following more stable wear period (measured from 40 to 100 km) as these often differed greatly. K_0 was obtained by dividing the slope of the graph by the normal load P i.e.,

$$K_0 = V/PS \ (mm^3/N.m)$$

5.3.2 Measurement of Surface Roughness

A description of the R_a surface roughness classification method is given in Appendix C.

Surface roughness tests were conducted using a Taylor-Hobson Surtronic 3P talysurf and taken in the direction of sliding. Measurements were taken at the start of each test and at regular intervals coinciding with the mass loss measurements. However, for smoothly polished counterfaces, light microscopy revealed that the needle introduced a significant scratch onto the surface. A third polished sample (see Chapter 5.1.2.3), which was not used for any wear testing but subjected to identical polishing, was used in these instances to measure the initial surface roughness.

5.3.3 Measurement of Frictional Forces

A detailed account of the friction force measuring test apparatus subsystem is given in Chapter 4.4.7.

5.4 Polymer Characterisation

5.4.1 Optical Microscopy

A Reichart projection microscope was used to study the worn UHMWPE surfaces during test intervals.

5.4.2 Scanning Electron Microscopy

After completion of each test, the UHMWPE wear pins were ultrasonically cleaned in absolute alcohol and mounted on aluminium stubs using carbon dag, after which they were gold-palladium coated in a Polaron E 5100 Series II "cool" sputter coater. Conductive paint was applied from the sides of the specimen to the stub to create a conductive path. The sputter coating and painting procedure are undertaken so as to render the UHMWPE surface electrically conductive and to prevent charging. The samples were then viewed in a Cambridge S200 Stereoscan scanning electron microscope (SEM). A fairly low accelerating voltage of 10 kV was used to minimise radiation damage.

5.5 Counterface Characterisation

5.5.1 Optical Microscopy

Optical photographs of the counterface surfaces were taken at some stages of the wear process using a Reichart projection microscope.

5.5.2 Scanning Electron Microscopy

Scanning electron Microscopy was used to examine the counterfaces before and after the completion of a test. When examined before testing, no sputter coating was necessary except for the YPSZ specimens, in which case a single sample was sacrificed for this purpose (no testing can be done after the specimen is coated).

After the completion of a test, the bars were gold-palladium coated as described in Chapter 5.4.2. This was deemed necessary as the polymer transfer layer was sufficiently thick to hinder adequate electrical conductivity of the surface. An accelerating voltage of 10 kV was used.

5.5.3 Three Dimensional Laser Surface Profilometry

The unworn stainless steel counterfaces were further characterised by three dimensional laser surface profilometry (performed at the Atomic Energy Corporation, Pretoria, South Africa) so as to gain a better appreciation of the differences in surface topography achieved by the different surface preparation methods. Only one specimen of each different preparation method was chosen, the R_a values of the two differently ground counterfaces were similar which allowed a meaningful comparison to be made.

5.5.4 Wear Debris Analysis

The wear debris tended to collect at the sides of the polymer pin and bath and was easily recovered and deposited onto an aluminium stub. The debris was then Au-Pd coated using a Polaron E1500 Series II "cool" sputter coater, after which it was viewed in the Cambridge S200 Stereoscan SEM under an accelerating voltage of 10 kV.

CHAPTER 6

RESULTS: UHMWPE FRICTION AND WEAR AGAINST STAINLESS STEEL AND CERAMIC COUNTERFACES

6.1 Introduction

This chapter presents an analysis of the wear behaviour of ultra high molecular weight polyethylene (UHMWPE) sliding against stainless steel counterfaces of different surface roughnesses and topographies, as well as polished Yttria Partially Stabilised Zirconia (YPSZ) counterfaces, under water lubricated reciprocating sliding.

6.2 The Friction and Wear Behaviour of UHMWPE Sliding Against Stainless Steel Counterfaces

The results of tests conducted against stainless steel counterfaces are presented in this section. The tests were conducted in a distilled water environment at an average sliding speed of 0.2 $m.s^{-1}$ under an interface pressure of 11 MPa. The experimental results are divided into several parts as follows:

(i) Initial Counterface Characterisation

(ii) Wear Studies

(iii) Friction Studies

(iv) The Transfer Layer

(v) Polymer Behaviour

(vi) Wear Debris Analysis

6.2.1 Stainless Steel Counterface Characterisation

The basic technique used to characterise the stainless steel counterfaces was that of simple surface roughness (R_a) measurement, taken in the direction of sliding motion (as discussed in Chapter 5.3.2). However, the different preparation methods of either "random" grinding or surface "parallel" grinding in the direction perpendicular to that of sliding motion resulted in the topographies of two differently prepared counterfaces of equal surface roughness to be very different as well.

In order to gain a better appreciation of the topographical difference achieved by the different surface preparation methods, one specimen of each different preparation method (two ground and one polished) was three dimensionally (3-D) laser profiled, the R_a values of the two differently ground counterfaces being similar so as to allow a meaningful comparison.

6.2.1.1 "Parallel Ground" Counterface Characterisation

The results of the laser surface characterisation of the "parallel ground" stainless steel counterfaces are shown in figures 6.1 to 6.4. Figure 6.1 is an optical photograph of the area scanned. Figure 6.2 is a plan view of the scanning result, with colour coded center-line average displacements. Figure 6.3 and 6.4 are oblique and 3-D views. The parallel direction of the valleys and peaks is clearly evident. The asperity heights and valley depths are of similar magnitude throughout the area. The surface roughness of this counterface was confirmed to be 0.16 μm R_a.

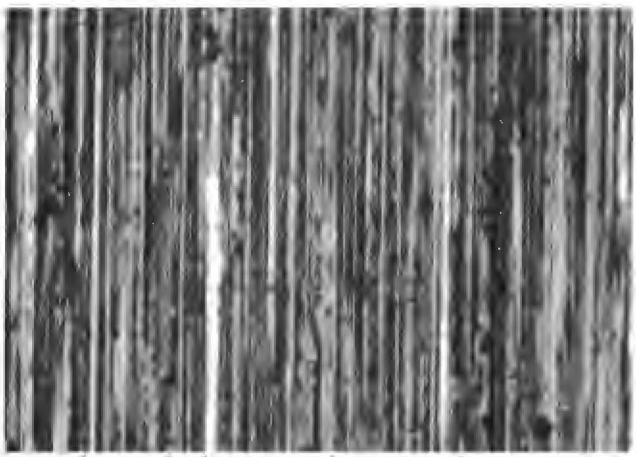

***Figure 6.1** Optical photograph of the characterisation area.*

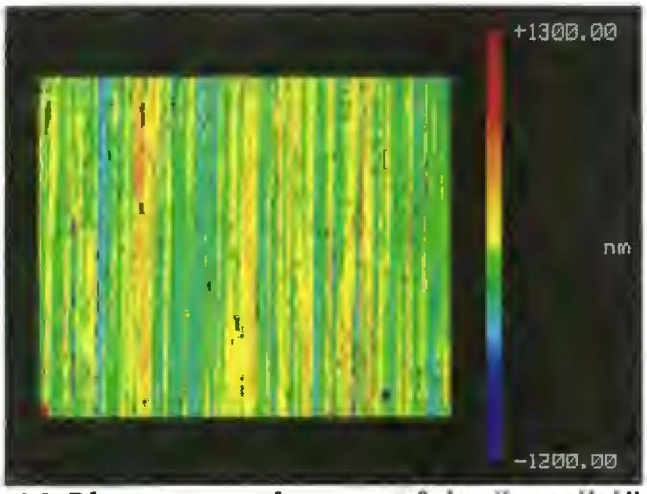

***Figure 6.2** Plan topography scan of the "parallel" ground stainless steel counterface.*

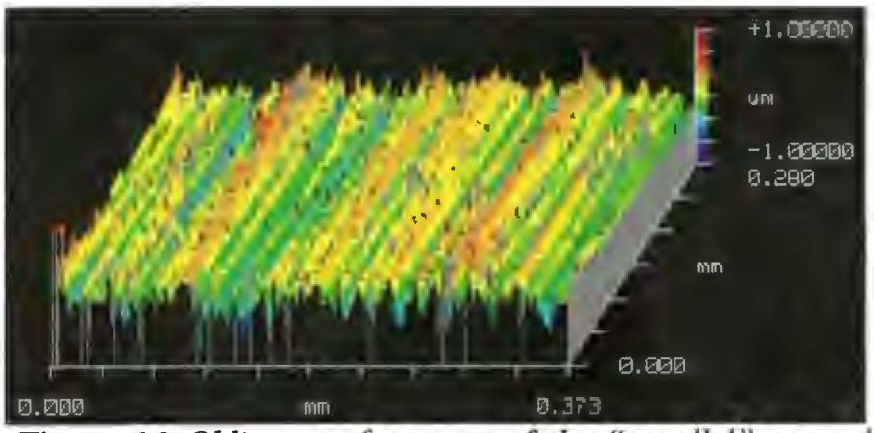

***Figure 6.3** Oblique surface map of the "parallel" ground stainless steel counterface.*

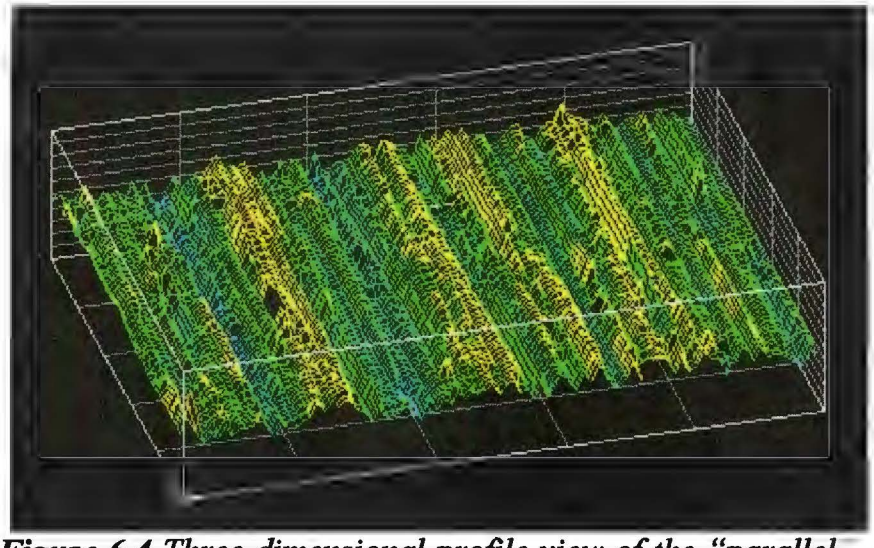

***Figure 6.4** Three dimensional profile view of the "parallel ground stainless steel counterface.*

6.2.1.2 Random Ground Counterface Characterisation

The results of the laser surface characterisation of the "random ground" stainless steel counterfaces are shown in figures 6.5 to 6.8. Figure 6.5 is the optical photograph of the area scanned and figure 6.6 is a plan view of the scanning result, with colour coded center-line average displacements. Figure 6.7 and 6.8 are oblique and 3-D views. The difference in surface topography to the "parallel ground" counterfaces is very clear. The "random grinding" preparation technique results in a random distribution of scratch direction and depth. The surface roughness of this counterface was confirmed to be 0.16 μm, the same as that of the "parallel ground" counterface.

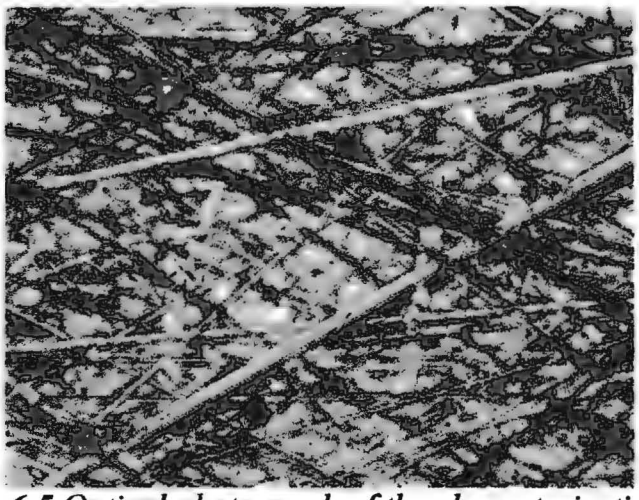

Figure 6.5 *Optical photograph of the characterisation area.*

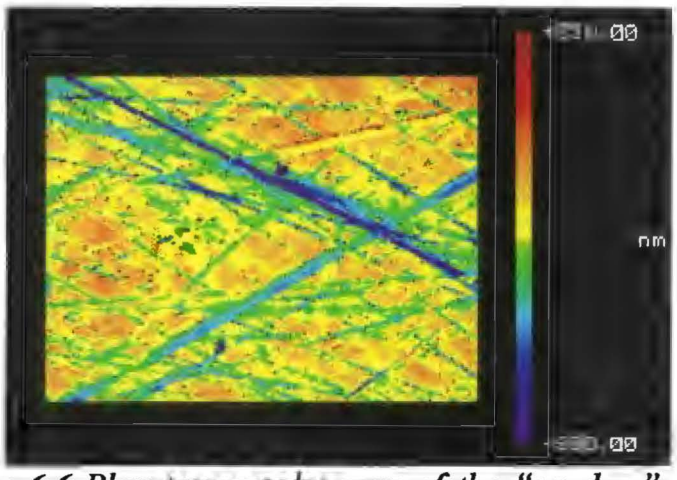

Figure 6.6 *Plan topography scan of the "random" ground stainless steel counterface*

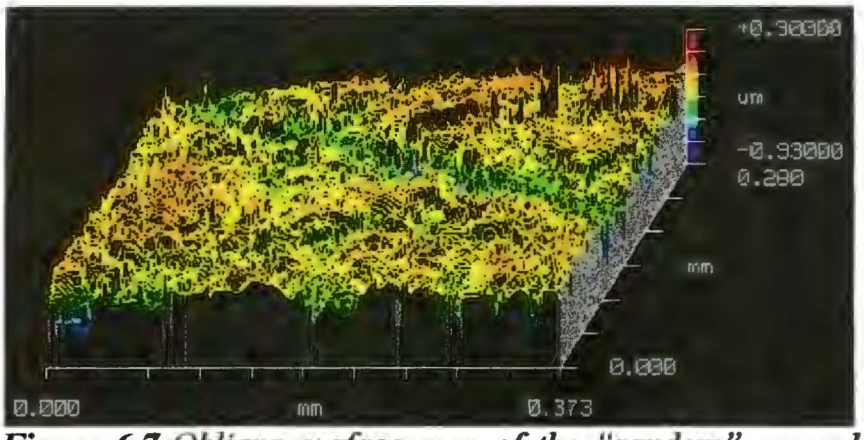

***Figure 6.7** Oblique surface map of the "random" ground stainless steel counterface.*

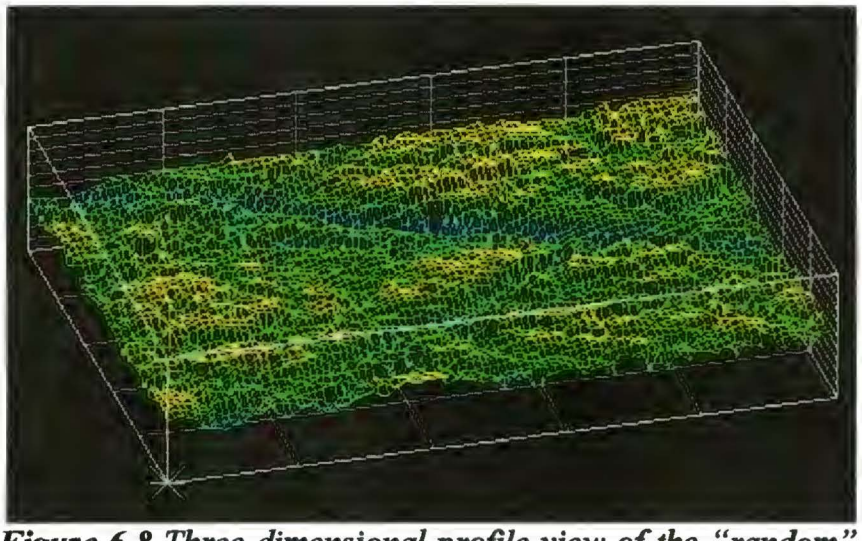

***Figure 6.8** Three dimensional profile view of the "random" ground stainless steel counterface, showing two deep scratches in an otherwise fairly smooth surrounding area.*

6.2.1.3 Polished Counterface Characterisation

The polished counterfaces (R_a = 0.02 μm) proved fairly difficult to characterise due to the very smooth topography. A profile map was thus unattainable. The oblique view, figure 6.11, does however highlight the many imperfections present.

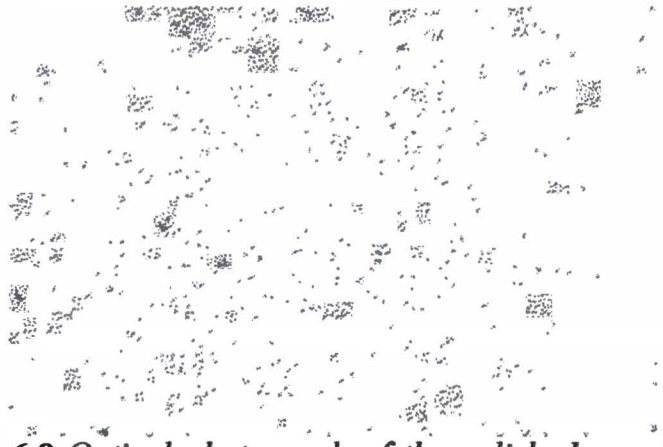

Figure 6.9 *Optical photograph of the polished counterface characterisation area.*

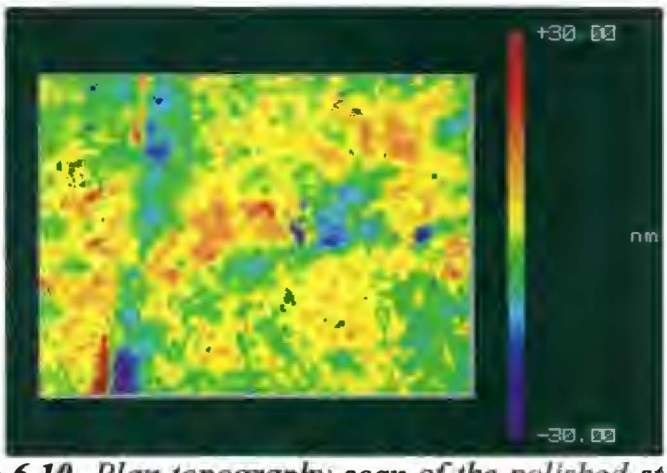

Figure 6.10 *Plan topography scan of the polished stainless steel counterface*

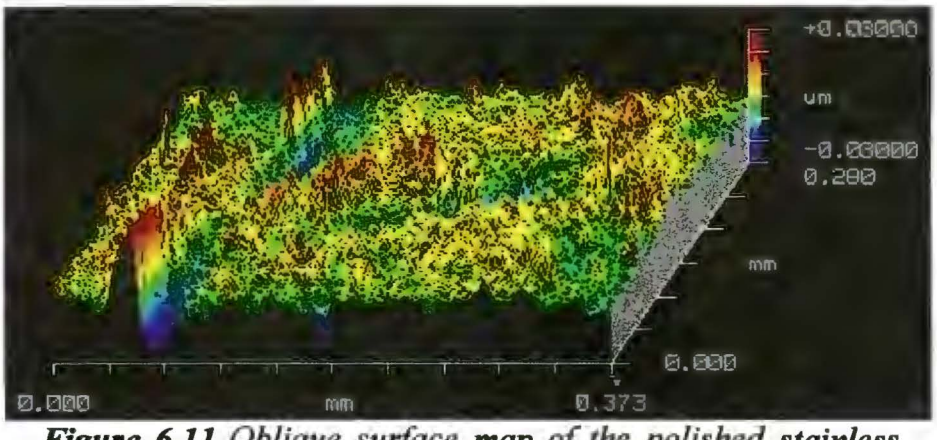

Figure 6.11 *Oblique surface map of the polished stainless steel counterface.*

6.2.2 UHMWPE-Stainless Steel Wear Behaviour

Wear against the differently prepared stainless steel counterfaces resulted in three distinctly different types of displacement-wear behaviour. Figures 6.12 to 6.14 are examples of typical displacement-wear curves for each of the three different wear regimes.

Figure 6.12 shows the curve normally obtained against counterface roughnesses ranging from 0.05 to 0.45 μm R_a (both "random" and "parallel" ground), where the wear rate falls with increasing sliding distance. Eventually, the wear rate becomes linear with distance. Two regions of differing wear can be clearly distinguished.

The *"bedding-in"* wear rate, lasting over the initial 20 km, is usually about 10 times greater than that of the more stable, *"steady-state"* wear rate for UHMWPE sliding against "random" ground counterfaces. Even greater differences between the *"bedding-in"* and *"steady-state"* wear rates were registered with wear against "parallel" ground counterfaces, where for instance the wear rate recorded against a "parallel" ground counterface of R_a = 0.15 μm was initially as high as K = 268.72 x 10^{-9} mm^3/N.m but then fell to K = 11.17 x 10^{-9} mm^3/N.m after some 40 km of sliding.

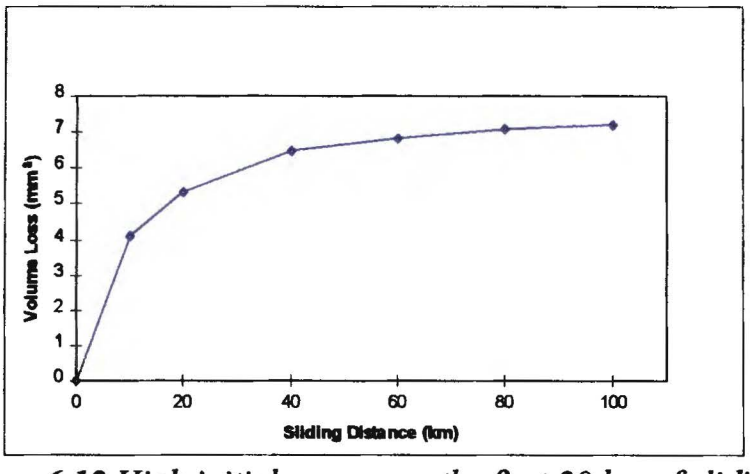

Figure 6.12 High initial wear over the first 20 km of sliding, followed by much reduced, linear, stable wear was typical for UHMWPE worn against counterfaces of moderate surface roughness between 0.05 and 0.45 μm R_a

This well documented behaviour of high initial wear followed by much reduced, stable wear is ascribable to two effects:

1. General *"bedding-in"* effects arising from initial polymer surface/counterface mismatch. The two interacting surfaces may not be perfectly parallel initially, resulting in localised areas of very high pressure and consequently accelerated wear.

2. Transfer Layer Formation

Whereas general *"bedding-in"* effects are encountered in most contact machinery, the formation of a stable polymer film onto stainless steel counterfaces has proven to be vital for obtaining low wear rates in the polymer/steel sliding couple. The transfer layer is formed by the polymer debris adhering to the metal counterface and being worked into the valleys thereof. Eventually, the polymer deposit not only fills the valleys of the counterface, but covers the entire counterface surface, including the hard, abrasive asperities. The transfer layer thus offers better load support and effectively shields the polymer surface from the abrasive action of the counterface asperities, thus reducing wear.

Figure 6.13 demonstrates the type of wear curve obtained for UHMWPE wearing against rougher counterfaces. The UHMWPE wear rate remained very high throughout the entire testing distance covered. The onset of this type of high wear rate behaviour corresponded with the counterfaces of such surface roughnesses allowing the easy removal of polymer wear debris and thus preventing the formation of a stable transfer layer. The polymer wear pin is thus not shielded from the hard asperities of the metal counterface and is consequently susceptible to much increased, abrasive wear.

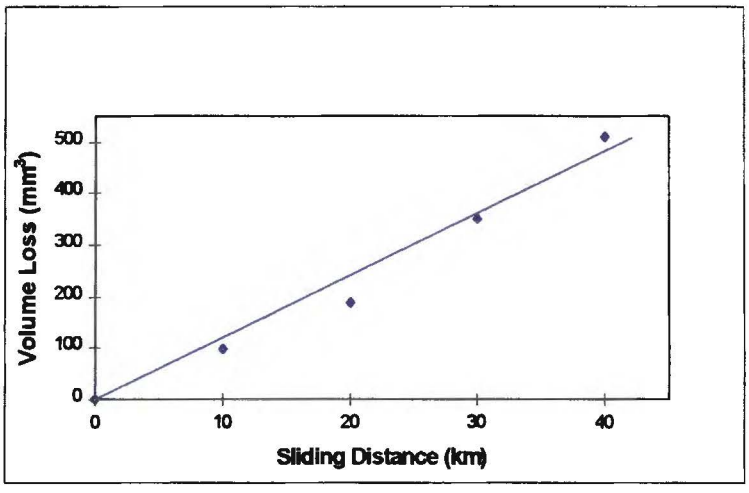

***Figure 6.13** Very high, constant wear of UHMWPE resulted when UHMWPE was worn against rough stainless steel counterfaces.*

For UHMWPE wearing against very smooth, polished stainless steel counterfaces (R_a = 0.02 μm), no high, *"bedding-in"* wear was encountered. Instead, the initial wear was extremely low at an average of K = 8.92 x 10^{-9} mm^3/N.m. A 5.7 times increase in wear rate to K = 51.02 x 10^{-9} mm^3/N.m (average) was however registered after approximately 50 km of sliding. The onset of this period of higher wear was very marked, with the displacement–wear curve both before and after the transition being approximately linear (see figure 6.14).

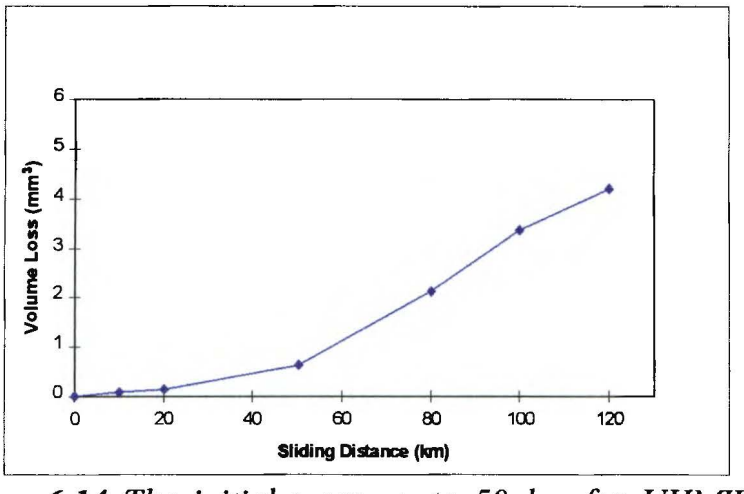

Figure 6.14 *The initial wear up to 50 km for UHMWPE sliding against smooth polished stainless steel counterfaces was extremely low, after which the wear rate increased.*

Table 6.1 shows the "initial" and "stable" wear coefficients calculated for UHMWPE sliding against the different stainless steel counterfaces. The "initial" wear was taken as being the wear over the first 20 km of sliding, whereas the wear from 40 to 100 km was used to calculate the "stable" wear coefficients.

Counterface R_a (μm)	Counterface Preparation Method		$K_{initial}$ ($mm^3/N.m \times 10^{-9}$)	K_{stable} ($mm^3/N.m \times 10^{-9}$)
0.66	stainless steel	parallel ground	27458.00	
0.64	stainless steel	parallel ground	18590.00	
0.60	stainless steel	parallel ground	8602.00	
0.54	stainless steel	parallel ground	477.00	60.00
0.52	stainless steel	parallel ground	447.80	28.83
0.51	stainless steel	parallel ground	9461.00	
0.45	stainless steel	parallel ground	1647.00	196.28
0.44	stainless steel	parallel ground	175.60	129.40
0.30	stainless steel	parallel ground	200.00	37.50
0.29	stainless steel	parallel ground	270.50	15.29
0.27	stainless steel	parallel ground	259.00	11.59
0.15	stainless steel	parallel ground	265.80	12.36
0.15	stainless steel	parallel ground	268.72	11.17
0.53	stainless steel	random ground	8726.00	
0.46	stainless steel	random ground	1920.00	223.90
0.45	stainless steel	random ground	222.00	26.69
0.36	stainless steel	random ground	160.75	17.21
0.27	stainless steel	random ground	130.27	16.85
0.17	stainless steel	random ground	45.00	54.04
0.13	stainless steel	random ground	104.54	17.16
0.05	stainless steel	random ground	109.40	
0.05	stainless steel	random ground	92.41	11.83
0.04	stainless steel	Polished/ground	12.00	42.86
0.02	stainless steel	polished	7.32	54.71
0.02	stainless steel	polished	9.94	47.33
0.02	stainless steel	polished	9.52	

***Table 6.1** Results of wearing UHMWPE against stainless steels of various surface roughnesses and topographies.*

Figures 6.15 and 6.16 show the influence of counterface surface roughness on the initial and stable wear coefficients of UHMWPE. In figure 6.15, the initial wear rate is seen to increase dramatically at counterface values of above 0.45 μm R_a. However, the initial wear rate did not increase substantially when sliding against counterfaces of surface roughness between 0.05 μm and 0.45 μm R_a. The rate recorded against a "random" ground counterface of R_a = 0.05 μm being an average of $K_{initial}$ = 100.91 x 10^{-9} $mm^3/N.m$, whereas that recorded against a similarly prepared counterface of R_a = 0.45 μm being $K_{initial}$ = 222.00 x 10^{-9} $mm^3/N.m$. These values represent only an approximate doubling of wear rate over this broad range of counterface surface roughnesses.

It should also be noted that there was generally higher initial wear for equivalent surface roughnesses for UHMWPE wearing against the "parallel" ground as opposed to "random" ground counterfaces, for surface roughnesses between 0.15 μm and 0.45 μm R_a. Because of this difference in wear against "random" and

"parallel" ground counterfaces for "moderate" counterface roughnesses, two different line fits were adopted for the respective data.

The initial wear rates obtained when sliding UHMWPE against polished stainless steel counterfaces (R_a = 0.02) were substantially lower than those recorded against the rougher metal counterfaces. No effort was thus made to integrate these much reduced initial wear rates into the curves fitted to the other data in figure 6.15.

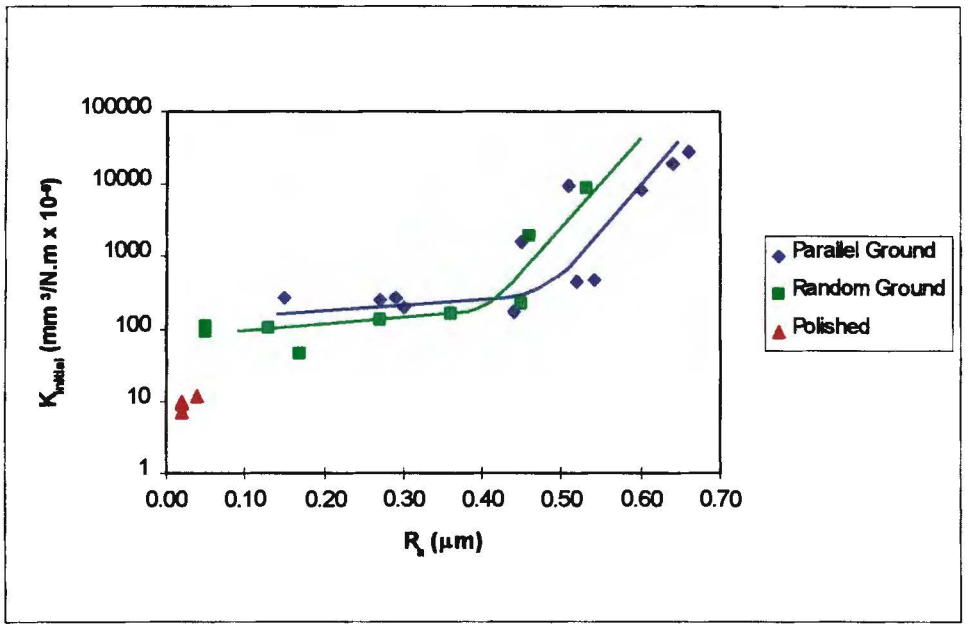

***Figure 6.15** Initial wear coefficient* vs. *counterface surface roughness. There is a dramatic increase in wear at an R_a of 0.45 μm.*

Figure 6.16 shows the relationship of stable wear coefficient of the polymer with counterface surface roughness. It can be seen that the stable wear coefficient does not increase greatly for wear against "moderate" counterfaces between R_a's of 0.05 μm and 0.45 μm, where 90% of the wear coefficients recorded were below K_{stable} = 38 x 10^{-9} mm^3/N.m.. Further, there was no significant difference in stable wear between UHMWPE sliding against "random" ground or "parallel" ground counterfaces of surface roughnesses between 0.05 μm and 0.45 μm R_a (unlike the initial wear behaviour observed when sliding against "intermediate" surface roughnesses).

However, there is a marked transition to higher values of stable wear at R_a values of approximately 0.45 μm, which corresponds to the transition observed for the very high initial wear rates discussed previously. The wear tests performed against much rougher counterfaces, where the initial wear was greater than K_{stable} = 1920.00 x 10^{-9} mm^3/N.m, were usually stopped before 100 km was covered to

prevent excessive amounts of wear debris clogging up the apparatus water recirculation system. Such very high wear rates are thus not plotted on the stable wear coefficient *vs.* R_a plot of figure 6.16.

As discussed earlier, the wear recorded for UHMWPE sliding against polished stainless steel counterfaces (R_a = 0.02 μm) increased after 50 km of sliding (see figure 6.14). The stable wear coefficient for this wear condition is thus higher than the initial wear coefficient and also significantly higher than the stable wear coefficient encountered for sliding against slightly rougher counterfaces ($R_a \geq 0.05$ μm) . The lowest stable wear coefficient recorded against a counterface of 0.05 μm R_a was $K_{stable} = 11.83 \times 10^{-9}$ mm^3/N.m, whereas the average wear coefficient recorded against the polished counterfaces of R_a = 0.02 μm was 4.31 times higher at $K_{stable} = 51.02 \times 10^{-9}$ mm^3/N.m.

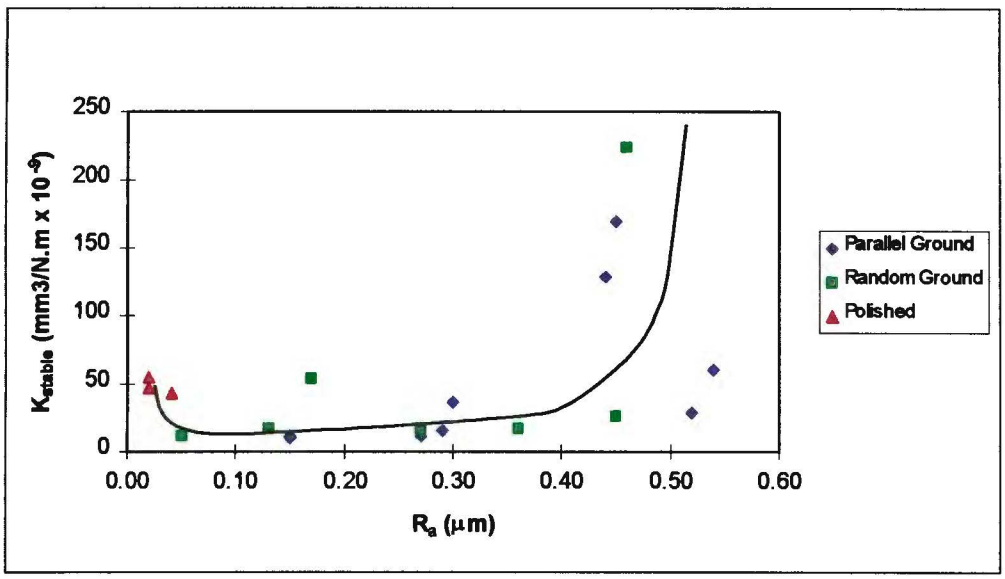

***Figure 6.16** Stable wear coefficient* vs. *counterface roughness.*

The variation of volume loss with counterface roughness and sliding distance is summarised in figures 6.17 (a) and 6.17 (b), where figure 6.17 (b) highlights the wear behaviour of UHMWPE against counterfaces of surface roughnesses between 0.02 μm and 0.54 μm. The results of some tests are deleted for greater clarity.

The three different types of wear behaviour can be clearly identified as:

- Very high wear at constant wear rate for UHMWPE sliding against rough ("random ground" and "parallel ground") stainless steel counterfaces of R_a greater than about 0.45 μm.

- High initial wear (over the first 20 km) followed by much reduced, stable wear, for UHMWPE sliding against smoother counterfaces ($0.05 \leq R_a \leq 0.45$ μm).

- Very low wear over the first 50 km followed by an increase in wear rate, for UHMWPE sliding against smooth polished (R_a = 0.02 μm) stainless steel counterfaces.

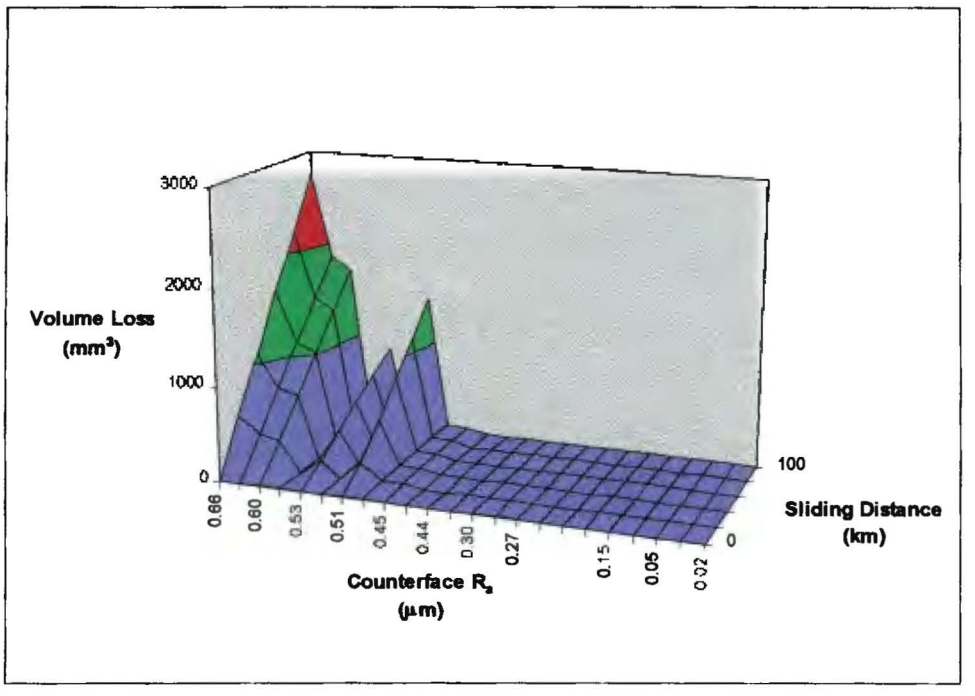

Figure 6.17 (a) *The variation of UHMWPE volume loss with sliding distance and counterface roughness. The sudden onset of very high wear for UHMWPE sliding against rougher counterfaces is clearly shown. Results to 100 km of sliding were extrapolated for UHMWPE wearing against the roughest counterfaces.*

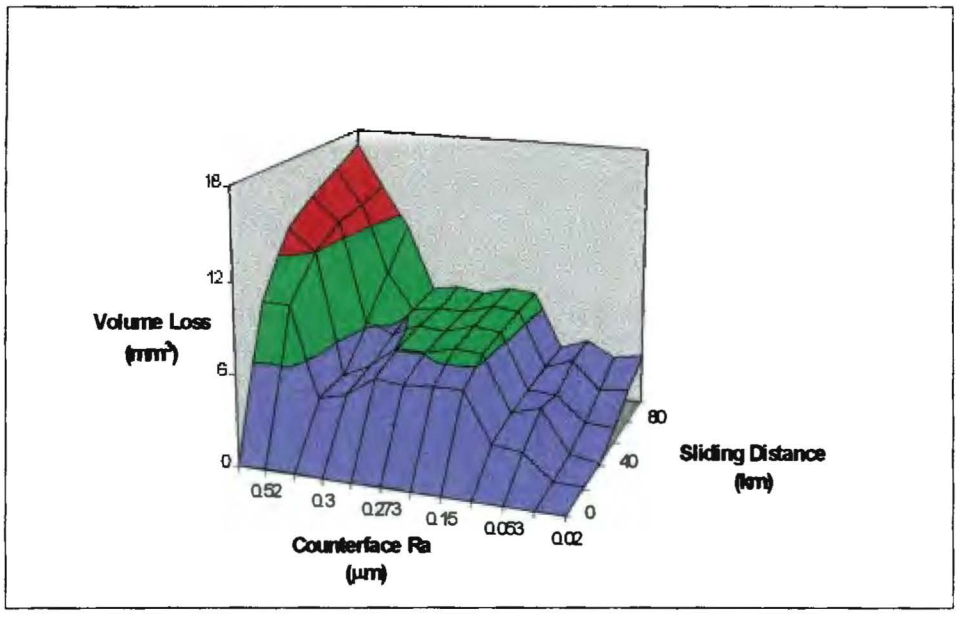

Figure 6.17 (b) *An enlarged view at the variation of UHMWPE volume loss with sliding distance for UHMWPE sliding against smoother counterfaces. For wear against polished counterfaces (R_a = 0.02μm), the initial wear was extremely low, but tended to increase after 40 km, whereas for all the other instances shown, the wear curve shows high initial wear followed by decreased, stable wear after 20 km. Note that some curves have not been shown so as to preserve clarity.*

6.2.3 UHMWPE-Stainless Steel Friction Behaviour

Figure 6.18 shows the relationship between the kinetic coefficient of friction and sliding distance for UHMWPE wearing against stainless steel counterfaces of different surface roughnesses and topographies. The variation of friction coefficient with sliding distance for the UHMWPE/YPSZ couple is also included as a comparison.

The friction coefficients were often highly unstable over the first 1 km of sliding. This may be attributed to *"bedding-in"* effects such as initial wear pin/counterface mismatch. Friction against "parallel" ground counterfaces usually decreased in a transitional period from 20 to 25 km. This "step" coincides with the transition from the initially "high" *"bedding-in"* wear to the reduced *"steady-state"* wear and may thus be ascribed to the completion of a stable transfer layer.

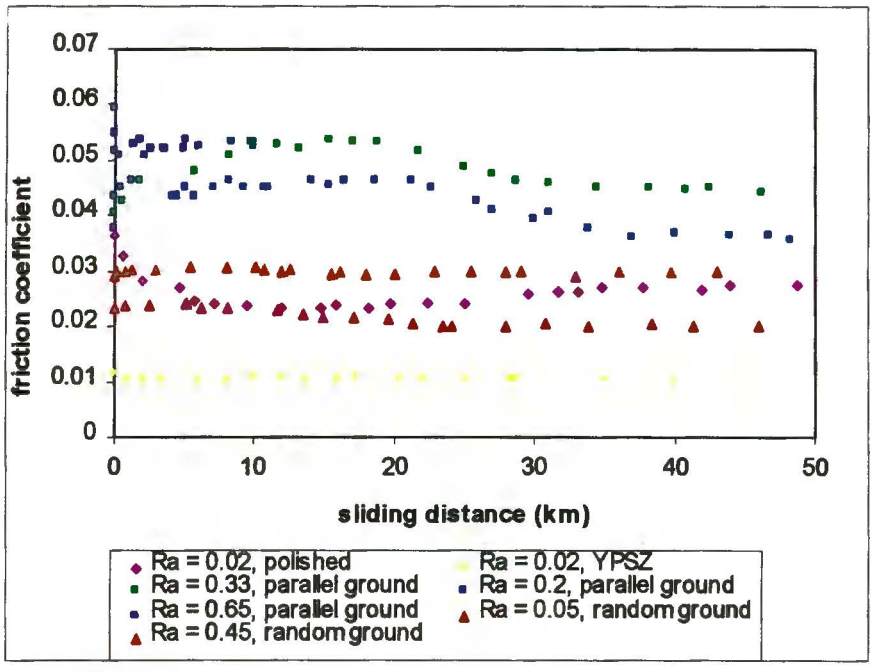

Figure 6.18 *The variation of the kinetic coefficient of friction with sliding distance for UHMWPE sliding against stainless steel counterfaces of different surface roughnesses and topographies. The friction coefficient of the UHMWPE/polished YPSZ couple with sliding distance is included for comparison.*

The friction coefficient of UHMWPE wearing against a rough, "parallel ground" (R_a = 0.65 μm) counterfaces was not significantly higher than that measured when wearing UHMWPE against a "moderate" "parallel" ground counterface of R_a = 0.33 μm, despite the wear being several orders of magnitude higher (the test was terminated after 9.9 km due to excessive wearing down of the polymer pin).

Friction coefficients measured for UHMWPE sliding against "random ground" counterfaces were generally lower for equivalent counterface surface roughnesses compared to the "parallel" ground surfaces. Furthermore, the "reduction step" evident when sliding the polymer against "parallel" ground counterfaces was not very apparent when wearing UHMWPE against the "random" ground stainless steel. Friction coefficients measured against smooth, "random" ground counterfaces (R_a = 0.05 μm) were lower than those measured when sliding the polymer against polished stainless steel counterfaces (R_a = 0.02 μm), at μ = 0.02. Tests conducted against counterface roughnesses of μ = 0.05 μm thus accounted for both friction and *"steady-state"* wear minima. The *"start-up"* friction when wearing against polished stainless steel counterfaces (R_a = 0.02 μm) was significantly higher when compared to the stable friction coefficient. This may be due to the much-increased real area of

contact A_r between polymer and counterface and consequent greater interfacial adhesion, prior to effective water lubrication. Note that the friction coefficients recorded for UHMWPE sliding against polished (R_a = 0.02 μm) YPSZ counterfaces are significantly lower than the friction coefficients measured against any of the stainless steel counterfaces.

6.2.4 The Transfer Layer

The formation of stable UHMWPE transfer layers or films is normally considered to be a prerequisite for achieving low wear rates against metal counterfaces. Marcus [19] provided a detailed investigation of transfer layer formation with sliding distance against parallel ground stainless steel counterfaces of R_a = 0.3 μm: The initial transfer process occurs at isolated ridges on the counterface, resulting from both abrasive and adhesive wear mechanisms. This polymer is then forced into the valleys between the ridges of the asperities and mechanically interlocks with the counterface topography. More and more polymer is built up in this way until the film gradually covers the entire metal surface.

However, the present author has shown that rough counterfaces are not able to support coherent transfer layers, which results in very high UHMWPE wear rates. Figure 6.19 shows a rough stainless steel counterface after prolonged reciprocating sliding against UHMWPE. No polymer transfer is evident. Figure 6.20 reveals some UHMWPE deposited onto the counterface and adhering to the asperity peaks. However, the counterface valleys are free of polymer.

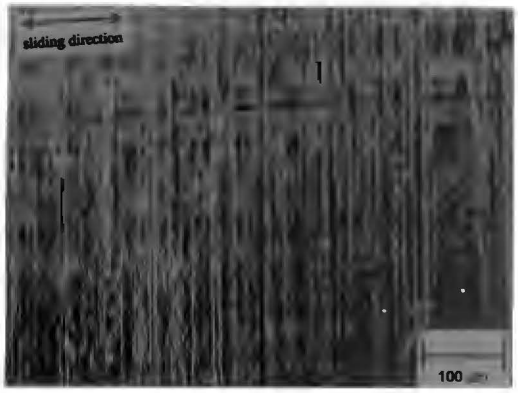

Figure 6.19 SEM micrograph of a rough stainless steel counterface after sliding against UHMWPE for 100 km. No transfer layer has been formed.

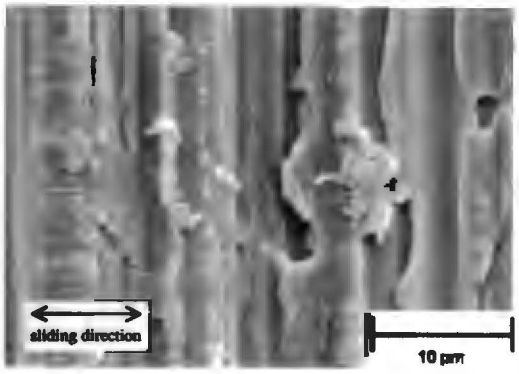

Figure 6.20 Polymer adhering to surface asperities of rough stainless steel counterface after 40 km of sliding.

As the counterface becomes smoother, the smaller valleys are able to retain the polymer, thus resulting in the build-up of a transfer layer. This is shown in figures 6.21 and 6.22, where polymer is shown covering most of the counterface except in regions of larger scratches.

Figure 6.23 shows the polymer layer in the region of a large scratch. The scratch "valley" is however too large, and the polymer cannot settle adequately. Although the polymer does not cover the counterface entirely, none of the counterface asperities protrude above the polymer layer and polymer abrasion by the metal is thus prevented. The wear rate thus falls as the transfer layer is built up. Against these rougher transfer layer supporting counterfaces, the polymer film suffers from a fatigue spallation process similar to that found by Marcus [19] for UHMWPE wearing against parallel ground stainless steel of R_a = 0.3 μm, where the delamination of UHMWPE flakes results from sub surface crack growth within the transfer layer.

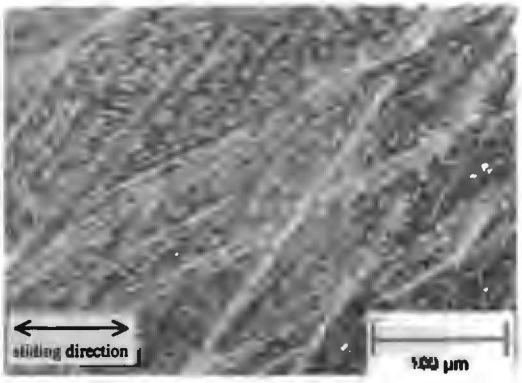

Figure 6.21 A SEM image of a "random" ground (R_a = 0.46 μm) stainless steel counterface after 100 km of sliding, showing polymer transfer over most of the surface. The large scratches are however not able to adequately retain the UHMWPE and thus remain exposed.

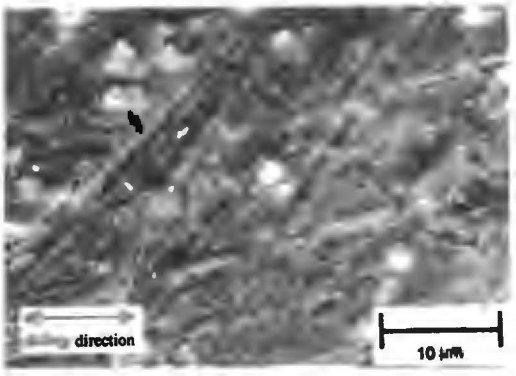

Figure 6.22 A higher resolution image of the previous micrograph. Note some of the polymer being removed off the surface, as indicated by the arrow.

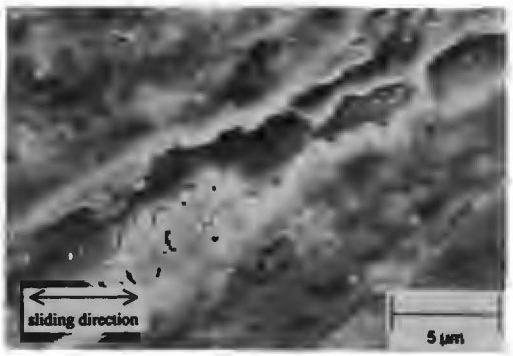

***Figure 6.23** A surface scratch surrounded by polymer layers. Note that despite the polymer not covering some of the scratch valleys, no counterface asperities protrude. Abrasion, and consequent high wear, is thus reduced.*

The smoother the initial counterface, the more coherent the transfer layer becomes. Figure 6.24 and 6.25 show transfer layers on "random" ground counterfaces (R_a = 0.05 µm) after 100 km of sliding. The micrograph of figure 6.26 shows some areas of transfer rupture, although these were actually quite rare. The counterface itself was not exposed by these rupture patterns, as only a surface section of the transfer film was removed (figure 6.26).

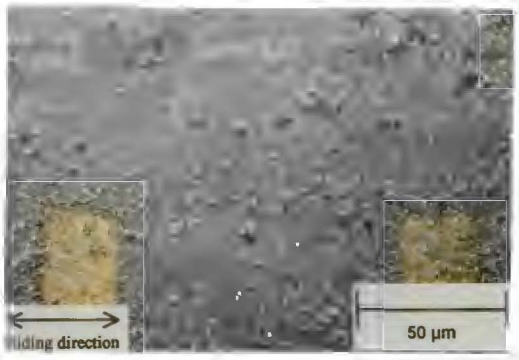

***Figure 6.24** A SEM image of the polymer transfer onto a stainless steel counterface of R_a = 0.05 µm initial surface roughness.*

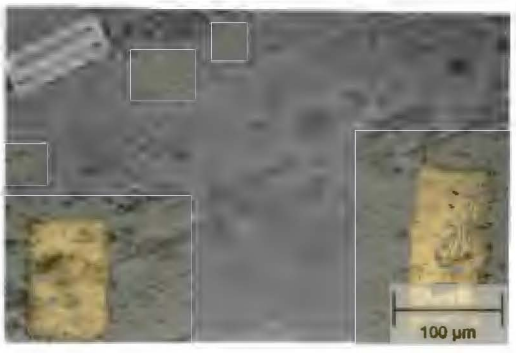

***Figure 6.25** A SEM image of an UHMWPE transfer layer on a stainless steel counterface. The micrograph shows some transfer layer rupture areas; most of the transfer layer was, however, uniform and featureless.*

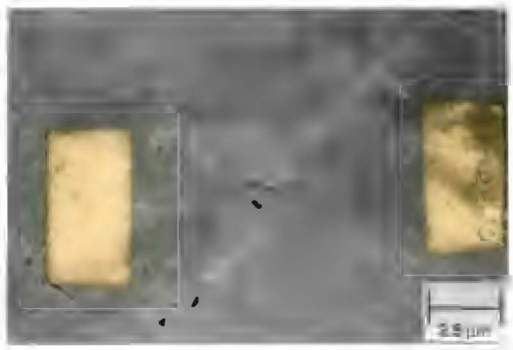

***Figure 6.26** A higher resolution view of the transfer layer rupture areas seen in figure 6.25. The counterface inside the transfer rupture areas remains covered by polymer.*

Figures 6.27 and 6.28 show the transfer layers formed on polished stainless steel counterfaces. Only very few rupture lines are evident, with most of the polymer transfer being exceptionally smooth.

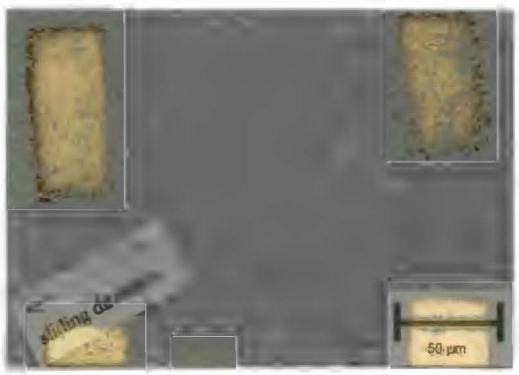

***Figure 6.27** The transfer layer formed on polished stainless steel counterfaces was very coherent and smooth.*

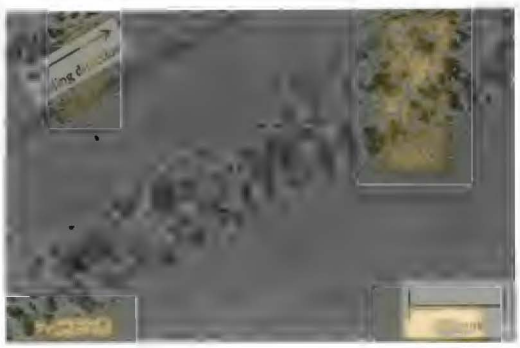

***Figure 6.28** A seldomly occuring transfer layer rupture in a transfer film formed on a polished stainless steel counterface after 100 km of sliding.*

6.2.5 UHMWPE Wear Surface Analysis

It was shown in the previous section that no coherent UHMWPE transfer layers could be formed on rough stainless steel counterfaces. This resulted in the counterface asperities continually ploughing through the polymer resulting in abrasive wear and consequently high wear rates. Figure 6.29 shows an UHMWPE

pin after 10 km of sliding against a 0.65 μm R_a stainless steel counterface. Abrasive tracks appear throughout the wear area. Large plastically deformed wave-like patterns, perpendicular to the direction of sliding motion, are also visible.

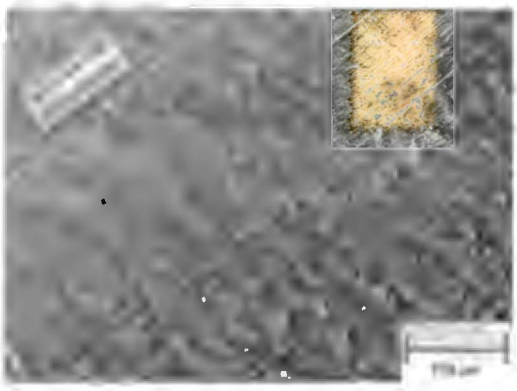

***Figure 6.29** SEM micrograph of UHMWPE wear surface after 10 km of sliding against a rough (R_a = 0.65 μm) counterface.*

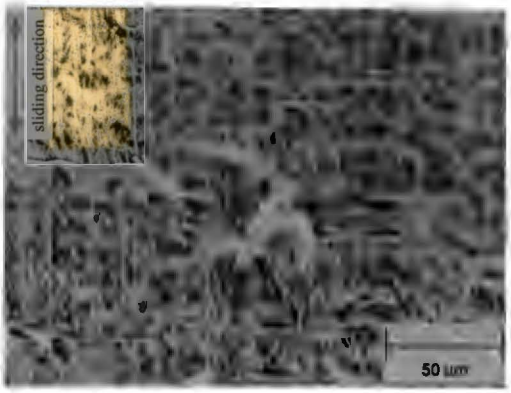

***Figure 6.30** A SEM image of an abraded UHMWPE surface after 40 km of wear against a stainless steel counterface of R_a = 0.45μm. Large cracks, normal to the direction of sliding, as well as some wear debris can be seen.*

Figures 6.30 and 6.31 show a polymer wear surface after 40 km of sliding against a stainless steel counterface of R_a = 0.45 μm. Surface cracking, normal to the direction of sliding, as well as polymer wear debris can be seen in figure 6.30. Figure 6.31 is a higher magnification image of the same wear pin surface showing the abrasive tracks caused by the metal asperities ploughing through the polymer surface.

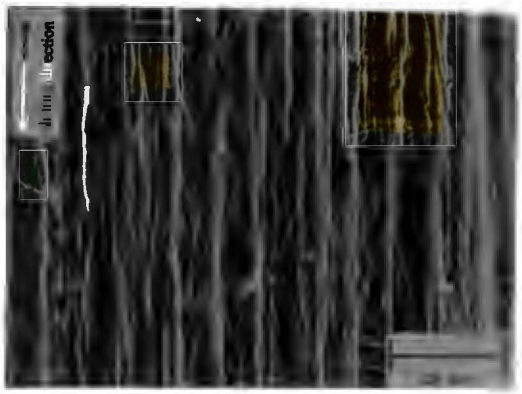

***Figure 6.31** A higher magnification image of the previously shown micrograph showing the abrasive tracks caused by the metal counterface asperities ploughing through the polymer surface.*

The wear mechanism changed from predominant abrasion to adhesion and/or fatigue when sliding against smoother counterfaces which supported the formation of stable polymer transfer films and thus prevented direct contact between the hard metal asperities and the softer polymer wear surface.

Figures 6.32 to 6.39 show SEM images of the surfaces of worn polymer pins presented in order of decreasing counterface surface roughnesses. During wear against rougher counterfaces supporting transfer films, large plastic deformation and surface cracks running in the direction of sliding motion was evident (figure 6.32). The strong adhesive forces between polymer and counterface (or transfer layer) resulted in a thin surface layer of the UHMWPE a few microns in thickness becoming highly orientated. The resultant acute change in polymer properties between oriented and bulk properties allows the easy shear at the subsurface interface [19]. The resultant shearing off of a polymer layer is shown in figure 6.33.

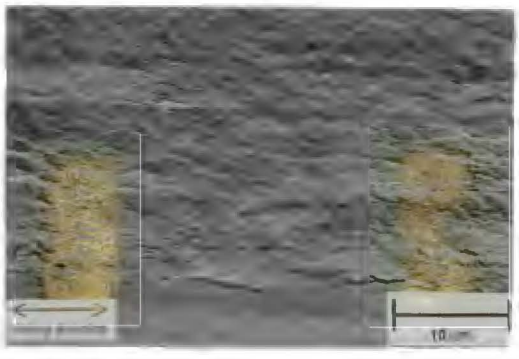

Figure 6.32 *SEM image of UHMWPE wear surface after sliding against a random ground counterface of 0.36 μm R_a for 100 km, showing plastic deformation and surface cracks in the direction of sliding.*

Figure 6.33 *UHMWPE layer being sheared off the surface.*

Figure 6.34 shows the more regular features usually evident when wearing against smoother counterfaces ($R_a \leq 0.3$ μm). The UHMWPE surfaces worn against fairly smooth, "random" ground counterfaces were mostly plastically deformed and similarly to those wearing against "parallel" ground, transfer layer forming counterfaces. At times, however, the wear surface morphology was rather mixed, as can be seen in figure 6.35, with some areas showing typical plastic deformation morphology and others lines of ripples, the lines being parallel to and the ripples perpendicular to the direction of sliding.

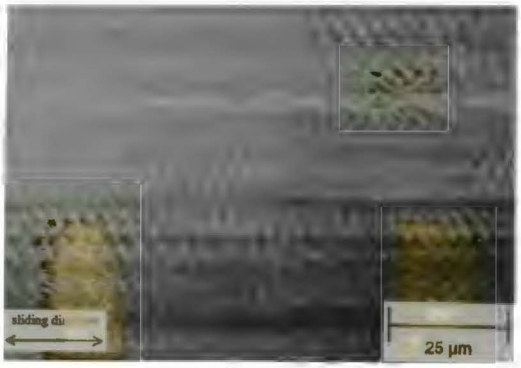

Figure 6.34 *Regular features of UHMWPE wearing against a parallel ground counterface of R_a = 0.3 µm.*

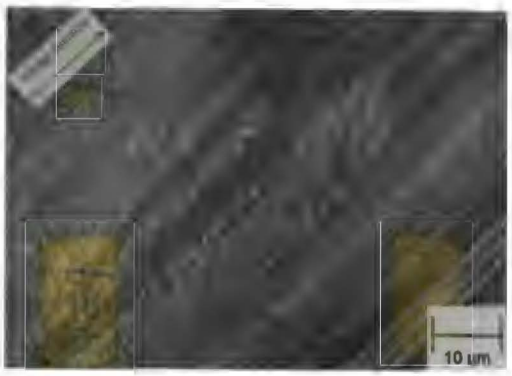

Figure 6.35 *Mixed surface morphology. The UHMWPE was sliding against a stainless steel counterface of R_a = 0.13 µm.*

Generally, the more regular or "patterned" the UHMWPE wear surfaces, the lower the corresponding wear rate would be. Figure 6.36 shows the "patterned" type of surface resulting from wear against a 0.05 µm R_a counterface. Figure 6.37 is a higher magnification image of the same wear pin, showing the plastically deformed UHMWPE wear surface.

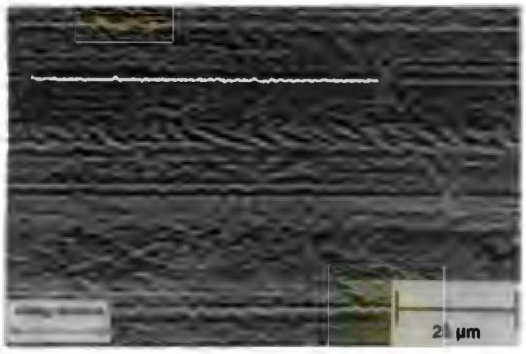

Figure 6.36 *Regular wear patterns generally occurred with reduced UHMWPE wear (counterface R_a = 0.05 µm).*

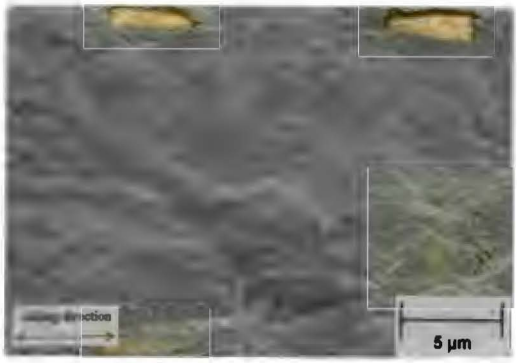

Figure 6.37 *UHMWPE wear surface morphology after sliding against "random ground" stainless steel counterfaces of R_a = 0.05 µm.*

UHMWPE sliding against polished stainless steel counterfaces resulted in extremely low wear over the first 50 km. The polymer wear surface in this case featured large surface rippled areas. The ripples, running perpendicular to the direction of sliding, are sometimes referred to as Schallamach waves and result

from polymer/counterface stick-slip behaviour. The Schallamach waves were always associated with very low wear rates (figures 6.36 and 6.39).

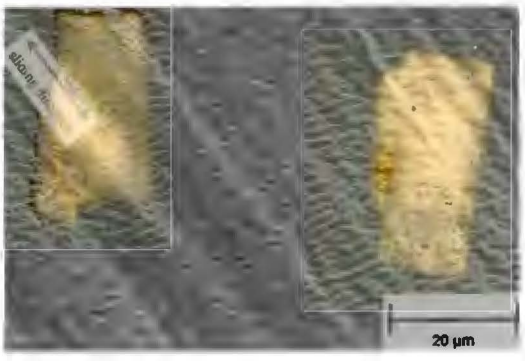

Figure 6.38 Schallamach waves on UHMWPE wear pins after sliding against polished counterfaces for 20 km.

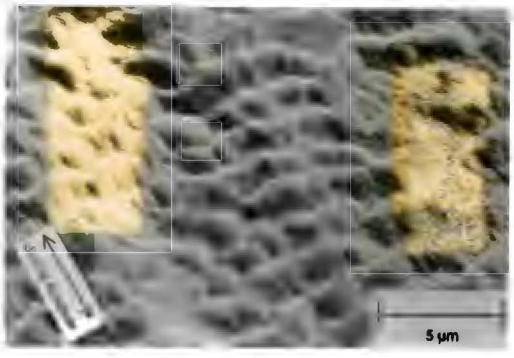

Figure 6.39 A higher magnification view of the Schallamach wave patterns associated with very low UHMWPE wear.

6.2.6 Wear Debris Analysis

The appearance of the UHMWPE wear product differed markedly according to the different wear mechanisms encountered. Very high wear rates, due to the abrasive action resulting from sliding against rough counterfaces, produced fine, powdery debris. This is due to the counterface asperities acting as micro cutting tools and effectively ploughing out small amounts of polymer with every reciprocating pass. Figures 6.40 and 6.41 show typical examples of this fine type of wear debris.

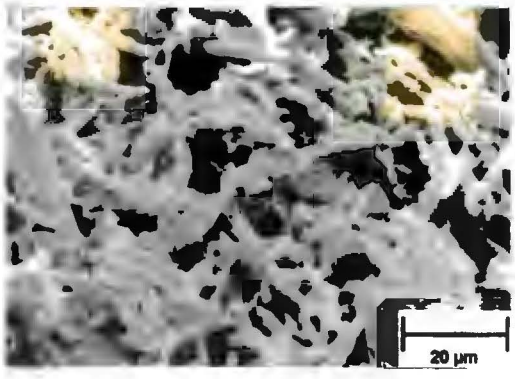

Figure 6.40 SEM image of the fine, powdery type wear debris produced when sliding against rough stainless steel counterfaces.

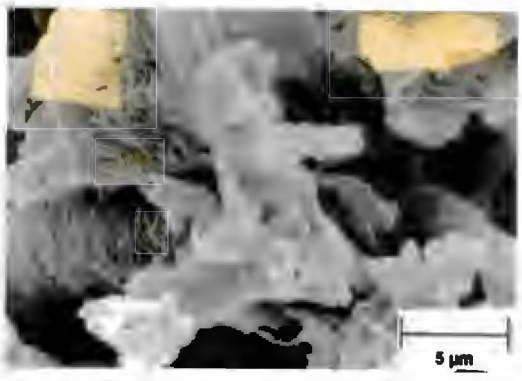

Figure 6.41 A higher resolution image of the previous micrograph. Counterface R_a = 0.51 µm, sliding distance covered = 40 km.

Figures 6.42 and 6.43 show the debris resulting from sliding against counterfaces which produced lower wear (counterface R_a's between 0.05 μm and 0.45 μm) detailed in Chapter 6.2.4. The actual debris is larger than the polymer detachments produced on the transfer layer seen in figure 6.22. Transfer layer breakdown resulting from the fatigue spallation process also resulted in the needle like wear debris shown in figure 6.44. The needle like appearance is a result of the debris becoming trapped in-between the two wearing surfaces and consequently being repeatedly rolled across the counterfaces/transfer layer by the UHMWPE wear pin.

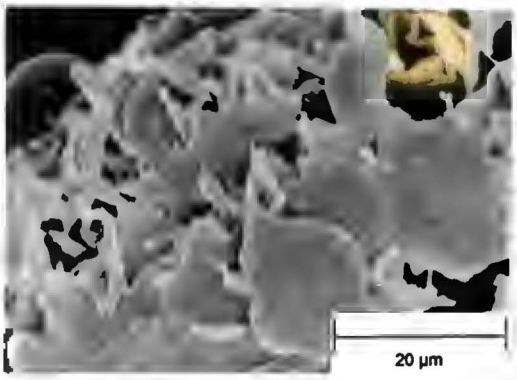

***Figure 6.42** Micrograph of UHMWPE wear debris formed by fatigue spallation of transfer film.*

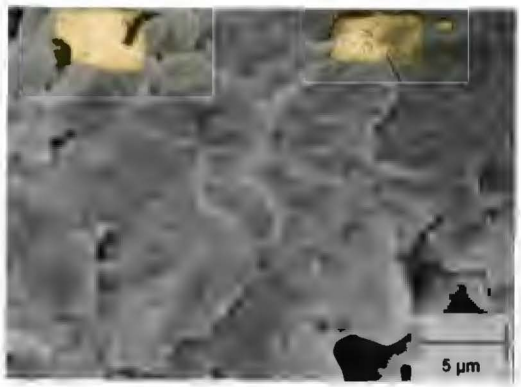

***Figure 6.43** A higher magnification image of the polymer debris produced by the above-described process.*

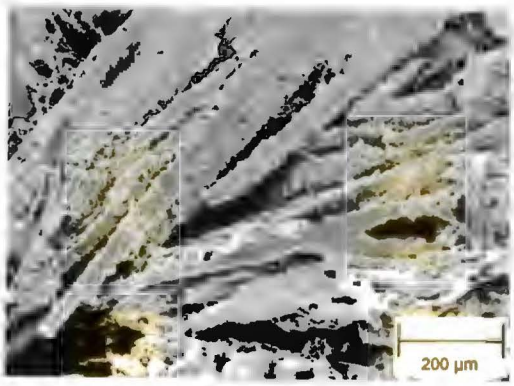

***Figure 6.44** Rolled, needle-shaped wear debris produced by UHMWPE wearing against a "random ground" stainless steel counterface of surface roughness R_a = 0.13 μm.*

Large wear sheets of polymer were produced after prolonged sliding against polished (R_a = 0.02 μm) stainless steel counterfaces (figures 6.45 to 6.48). In contrast to the debris produced against the smoother ground counterfaces ($0.05 \leq R_a \leq 0.45$), the debris produced against the polished counterfaces resulted not from the breakdown of the transfer film, but rather from the tearing off of a thin surface

layer of the polymer pin itself. The transfer layers formed against polished counterfaces usually remained mostly rupture free and very stable, certainly no rupture areas the size of the generated wear debris could be seen. Wear sheet thickness was estimated to be about 2 μm (see figures 6.47 and 6.48). Thus even at the higher rate of 1 mm^3 wear for every 20 km encountered after 40 km of sliding, only 4.5 wear sheets (covering the entire wear pin surface) could be produced every 20 km. Evidence of the tearing off of such a wear sheet from the polymer surface was never found on examining the worn UHMWPE pin. This is however hardly surprising, since actual detachment of a wear sheet only occurs at long time intervals (if a sheet were the size of the actual wear pin area, one would be produced every 45000 reciprocating cycles or 2.25 km of sliding).

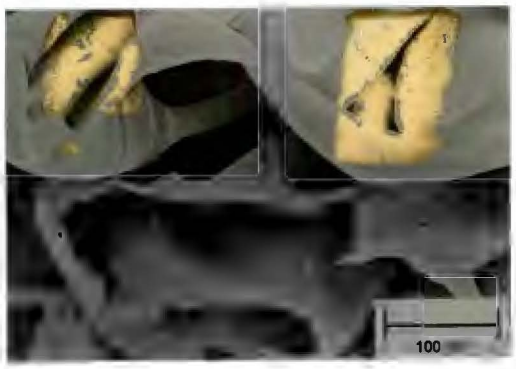

***Figure 6.45** SEM image of the corrugated sheets produced when sliding UHMWPE against polished stainless steel surfaces. Counterface R_a = 0.02 μm, total sliding distance covered was 120 km.*

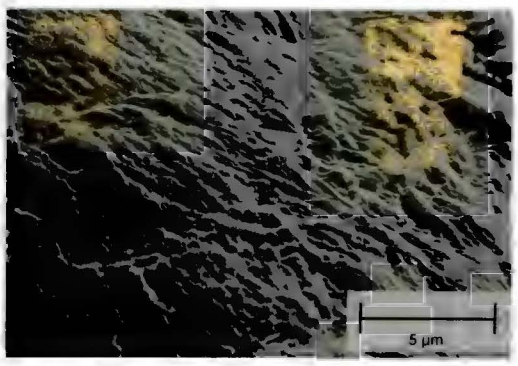

***Figure 6.46** Surface morphology of the UHMWPE wear sheets.*

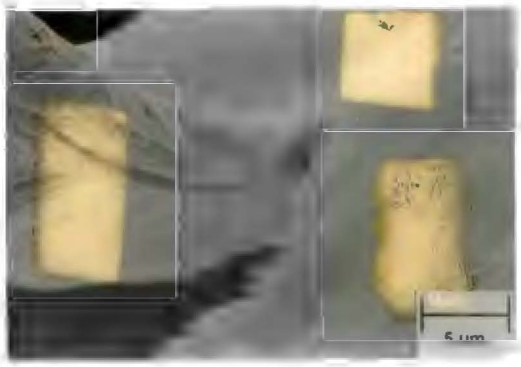

***Figure 6.47** A surface tear in the UHMWPE wear sheet produced when wearing against a polished (R_a = 0.02 μm) counterface, allowing an estimation of the thickness of the sheet.*

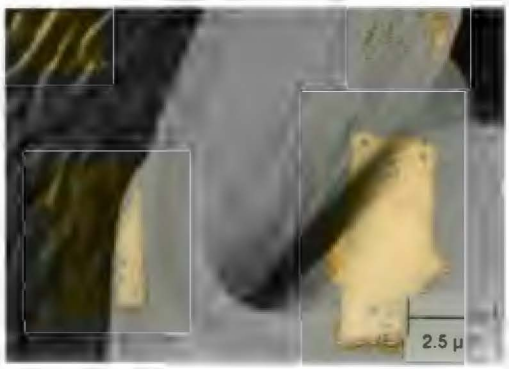

***Figure 6.48** A side view of an UHMWPE wear sheet. The sheet thickness was estimated to be approximately 2μm.*

6.3 The Friction and Wear Behaviour of UHMWPE Sliding Against Polished Yttria Partially Stabilised Zirconia Counterfaces

The results of tests conducted against polished Yttria Partially Stabilised Zirconia (YPSZ) counterfaces are presented in this section. The ceramic specimens were supplied in the polished condition (R_a = 0.02 μm) by Astro Met Inc., U.S.A. Tests were conducted in a distilled water environment at an average sliding speed of 0.2 $m.s^{-1}$ under an interface pressure of 11 MPa.

6.3.1 UHMWPE-YPSZ Wear Behaviour

UHMWPE wear against the polished YPSZ counterfaces proved to be so low as to make accurate measurement of the UHMWPE mass loss impossible, even after 100 km of sliding. Two tests were performed to 200 km of sliding, without any appreciable wear occurring. Figures 6.49 and 6.50 are optical photographs of UHMWPE wear pin surfaces after 0 km and 10 km of sliding against a YPSZ counterface. Throughout most of the wear surface, machine tracks (original wear pin R_a = 0.3 μm) can still be seen, thus giving an indication of how low the UHMWPE-YPSZ wear rate actually was. The SEM image of figure 6.51 shows the UHMWPE wear surface after 100 km of sliding. Most of the area is flat and featureless with only minimal plastic deformation occurring, in contrast to the plastic deformation and Schallamach patterns evident after wear against polished stainless steel counterfaces of similar surface roughnesses (refer to figures 6.38 and 6.39). Some ripple lines (lines in the direction of sliding) perpendicular to the direction of sliding are visible.

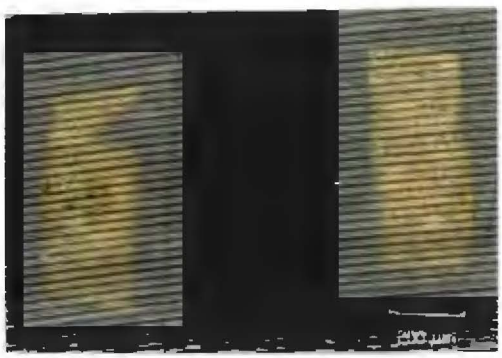

***Figure 6.49** Optical photograph of the unworn UHMWPE wear pin surface showing the machine tracks resulting from the polymer pin manufacturing. The unworn wear pin surface roughness was 0.3 μm R_a*

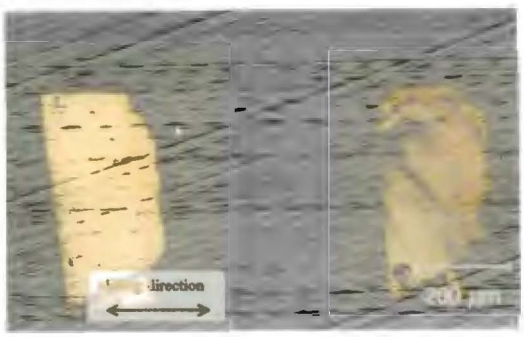

***Figure 6.50** Optical photograph of UHMWPE wear surface after 10 km of sliding against polished YPSZ. The wear pin machining tracks are still visible, thus giving an indication as to how low the wear was.*

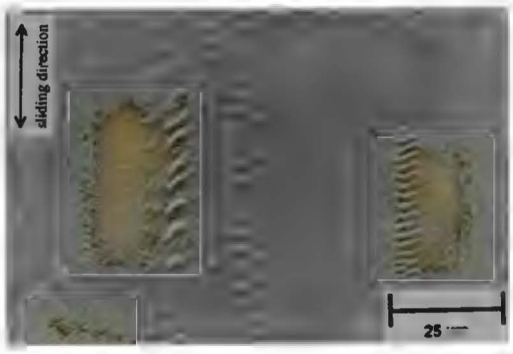

***Figure 6.51** SEM image of UHMWPE wear surface after 100 km of wear. Very little deformation is visible, apart from a few ripple lines traversing the surface in the direction of sliding.*

No transfer layers or polymer deposits were formed on the YPSZ counterfaces. Virtually no UHMWPE mass loss occurred, so hardly any UHMWPE could have been transferred. Figure 6.53 shows the nearly featureless YPSZ counterface after 100 km of sliding against a UHMWPE pin. There is no apparent difference to the unworn YPSZ counterface shown in figure 6.52.

***Figure 6.52** A unworn YPSZ counterface. Talysurf tests indicated the unworn ceramic counterface roughness to be 0.02 μm R_a*

***Figure 6.53** SEM image of a YPSZ counterface after 100 km of UHMWPE wear.*

6.3.2 UHMWPE-YPSZ Friction Behaviour

Figure 6.54 shows the friction coefficient of the UHMWPE-polished YPSZ couple plotted against reciprocating sliding distance covered; the friction behaviour of UHMWPE against polished stainless steel is included for comparison. Throughout the entire testing period, the coefficient remained stable at around 0.0103 to 0.0105, which represents about a half to a third of the frictional force measured for UHMWPE wearing against a polished stainless steel counterface of similar surface roughness (R_a = 0.02 μm) . Furthermore, the friction at start-up remained low, as opposed to the high start-up coefficients experienced when wearing UHMWPE against polished stainless steel.

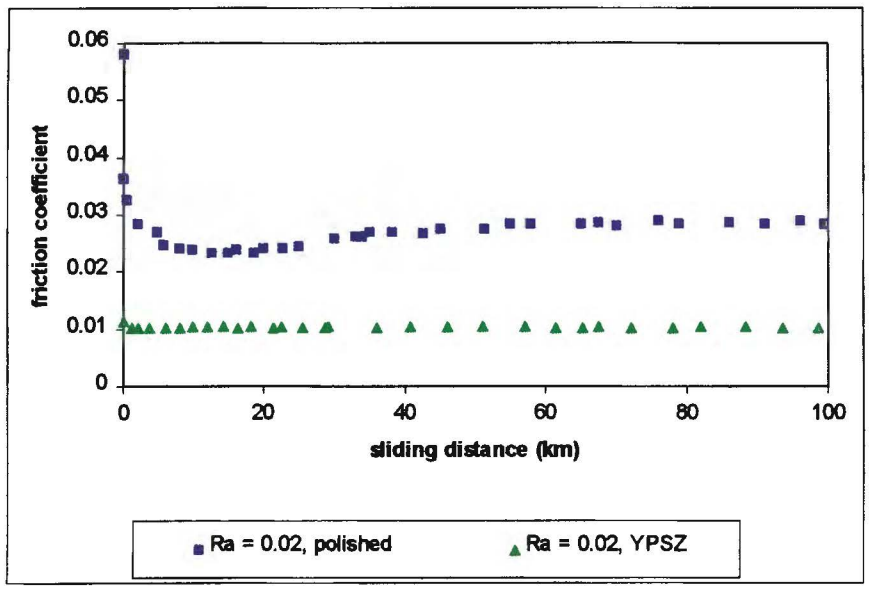

Figure 6.54 *Friction coefficient* vs. *sliding distance for UHMWPE wearing against YPSZ counterfaces and polished stainless steel counterfaces. The friction coefficients measured for the UHMWPE/YPSZ couple correspond well to those found by Kernick [77].*

CHAPTER 7

RESULTS:
A COMPARITIVE EVALUATION OF THE FRICTION AND WEAR PERFORMANCE OF ION IMLANTED UHMWPE

7.1 Introduction

This chapter presents the test results comparing the friction and wear behaviour of ion implanted ultra high molecular weight polyethylene (UHMWPE) to that of untreated UHMWPE. All the UHMWPE used, both ion implanted and normal, were from the same medical grade stock. Tests were performed against both polished stainless steel as well as Yttria Partially Stabilised Zirconia counterfaces. The tests were conducted in a distilled water environment at an average reciprocating speed of 0.2 $m.s^{-1}$. The experimental results are divided into two sections:

(i) Comparative Wear Studies

(ii) Comparative Friction Studies

7.2 Ion Implanted UHMWPE Wear Evaluation

7.2.1 Wear Against Stainless Steel Counterfaces

The results of Chapter 6 show that the initial wear of UHMWPE against all but the polished stainless steel counterfaces (R_a = 0.02 μm) is high. Since the affected and hardened implanted layer is approximately 0.5 μm thick, it is considered that this would be worn off very rapidly in the initial stages of wear against all but the smoothest counterfaces. The average initial wear coefficient recorded against smooth, polished counterfaces of surface roughness 0.02 μm R_a was $K_{initial}$ = 8.92 x 10^{-9} $mm^3/N.m$ i.e. 0.1784 mm^3 of polymer is worn off the wear pin after 20 km of sliding (under an applied load of 1000N). Assuming a wear pin surface area of 90 mm^2, the depth of wear after 20 km will therefore be nearly 2 μm. The surface treated layer is thus expected to be worn off after 20 km, even for a quadrupling in the ion implanted UHMWPE wear performance. Tests comparing the wear performance of ion implanted UHMWPE to that of the untreated polymer when

sliding against metal counterfaces were thus limited to a sliding distance of 20 km against polished (R_a = 0.02 μm) stainless steel counterfaces.

7.2.1.1 Wear Rate Comparisons

Figure 7.1 is a graphic depiction of the respective wear rates of UHMWPE and ion implanted UHMWPE taken over 20 km of sliding against polished stainless steel counterfaces. The wear rates were calculated as an average of three tests. The average wear rate of the surface modified UHMWPE is 6.01 x 10^{-9} mm^3/N.m, a 32.6 % decrease compared to the 8.92 mm^3/N.m x 10^{-9} average recorded for the as-received UHMWPE.

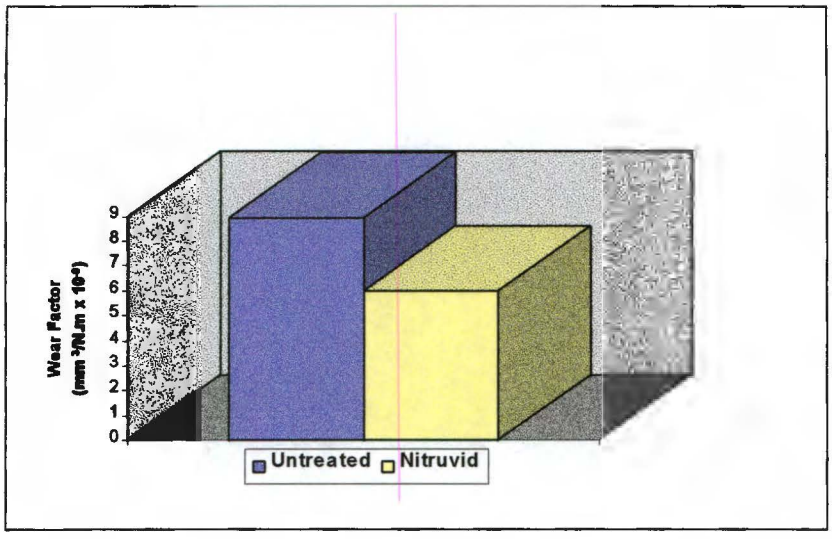

***Figure 7.1** Graphical illustration of the comparative wear rates of as-received and NITRUVID surface modified UHMWPE.*

7.2.1.2 Wear Surface Comparison

Both untreated and surface modified UHMWPE rely on the formation of stable transfer layers to achieve very low wear rates against polished stainless steel counterfaces (see Chapter 6.2.4). Although the transfer layers formed were of a very similar nature, some differences in the UHMWPE wear surface were evident. Whereas the untreated UHMWPE wear surface was "patterned" and featured Schallamach waves (figure 7.2), the surface hardened UHMWPE pin showed abrasive tracks and some polymer cracking (figure 7.3). No wear debris analysis was performed due to the difficulty of collecting the extremely small amount of debris produced.

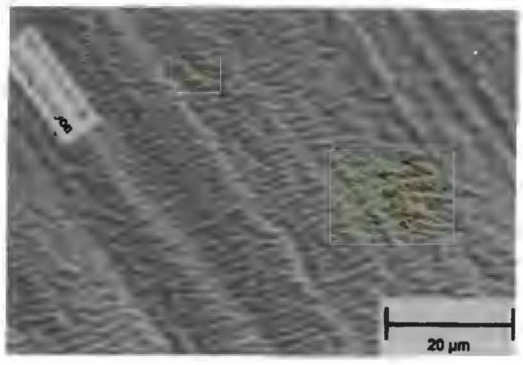

Figure 7.2 SEM image of typical untreated UHMWPE wear pin morphology after 20 km of sliding against a polished (R_a = 0.02 µm) stainless steel counterface.

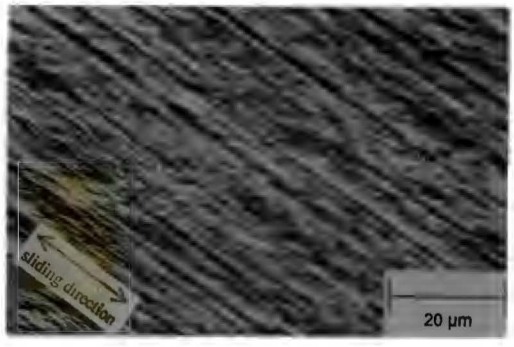

Figure 7.3 The ion implanted wear surfaces showed less plastic deformation, and instead were covered by small tracks and cracks.

7.2.2 Wear Against Polished YPSZ Counterfaces

The wear of UHMWPE and ion implanted UHMWPE against YPSZ counterfaces (R_a = 0.02 µm) was too low to measure with any degree of accuracy. Even after 100 km of sliding, no mass loss for either untreated or surface hardened UHMWPE could be recorded. Optical examination of the two different wear surfaces showed them to be much the same, machine tracks from the original pin manufacturing process still being present after 10 km of sliding (figures 7.4 and 7.5). The wear rates are thus expected to be of similar magnitudes as well.

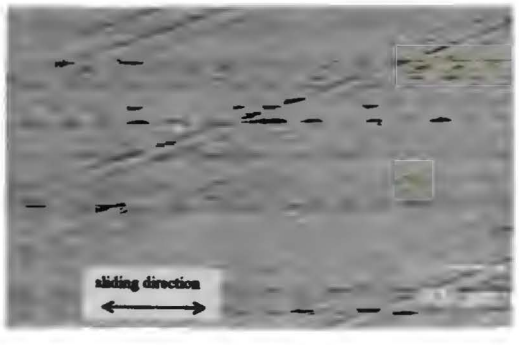

Figure 7.4 Optical image of untreated polymer surface after 10 km of sliding against a YPSZ counterface (R_a = 0.02 µm).

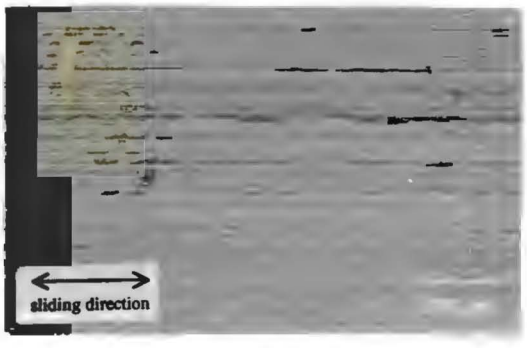

Figure 7.5 The rate of machine track removal is much the same for the ion implanted UHMWPE as it is for the untreated polymer.

7.3 Ion Implanted UHMWPE Friction Evaluation

The comparative friction behaviour of the ion implanted UHMWPE was evaluated over 20 km against both polished stainless steel and YPSZ counterfaces. The friction behaviour of the ion implanted UHMWPE was found to be no different to that of the untreated polymer, both against polished stainless steel and YPSZ counterfaces (figure 7.6).

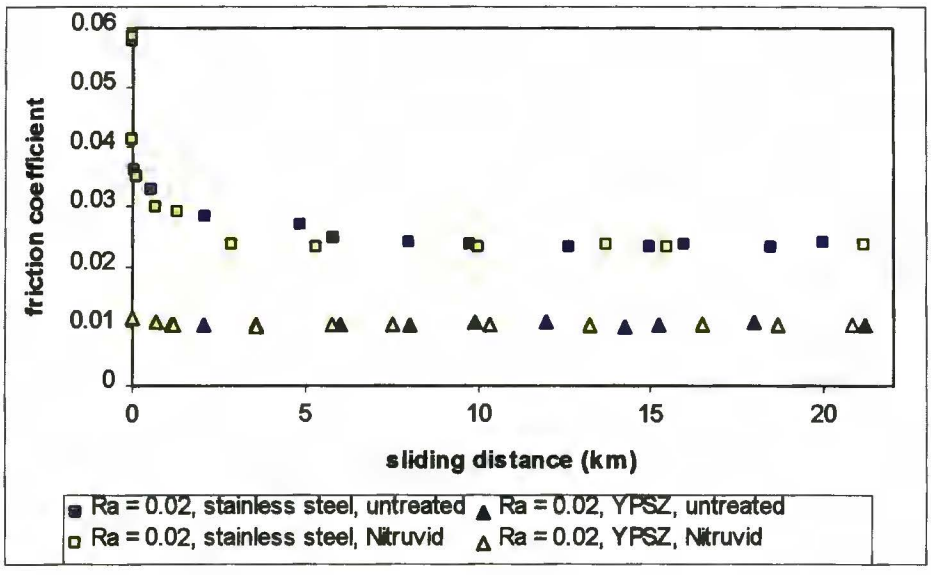

***Figure 7.6** Comparative friction coefficients of untreated and ion implanted UHMWPE against polished stainless steel and YPSZ counterfaces.*

CHAPTER 8

DISCUSSION

8.1 Introduction

The friction and wear behaviour of ultra high molecular weight polyethylene (UHMWPE) is, like any other tribological system, critically dependent on a multitude of parameters. An understanding of the relative effect of these can thus help in finding an optimal UHMWPE sliding couple/environment solution and hence reduce bearing wear and broaden the applicability of UHMWPE as a bearing material.

One of the parameters principally defining the wear of UHMWPE is that of counterface character and type: Counterface surface roughness, topography and material type can dictate the wear mechanism in operation and thus the wear performance itself. The following discussion describes how counterface surface roughness and topography influence the tribological behaviour of an UHMWPE/stainless steel sliding couple. A comparison to an alternative material type, Yttria Partially Stabilised Zirconia, is also included.

Clearly, however, it is the actual wear performance improvement of the polymer itself which would ultimately be of greatest benefit. The second part of this discussion evaluates an attempt to increase the wear resistance of UHMWPE by a surface hardening technique, namely ion implantation.

8.2 The Effect of Counterface Surface Roughness, Topography and Material Type on the Friction and Wear of UHMWPE

Although counterface surface roughness, topography and material type are certainly all interrelated parameters affecting the friction and wear behaviour of UHMWPE, they are discussed separately to preserve clarity.

8.2.1 The Effect of Counterface Surface Roughness on the Polymer Wear Mechanism

Variation in the stainless steel counterface surface roughness from very smooth, polished surfaces (R_a = 0.02 μm) to rough random and parallel ground surfaces (R_a up to 0.66 μm), resulted in three distinct wear patterns:

1. Wear Against Rough Counterfaces

   The displacement-wear curves obtained when wearing UHMWPE against rough (R_a > 0.45 μm) stainless steel counterfaces show this type of wear to be consistently very high, with no decrease in wear rate with sliding distance (see figure 6.14). Scanning electron microscopy (SEM) of the worn counterfaces revealed no evidence of transfer layer formation; all of the polymer wear debris was eventually ejected from the sliding interface (figures 6.19 to 6.20).

   Polymer abrasion by the hard counterface asperities was identified as the dominant wear mechanism for UHMWPE sliding against rougher counterfaces, as evidenced by abrasive tracks on the polymer and the powdery, forked fibrillar debris (figures 6.40 and 6.41) typical of abrasive wear [61]. Large striation marks (about 10 μm in width) running perpendicular to the direction of sliding, as well as surface cracks (perpendicular to the direction of sliding) were also evident (figure 6.29). Tanaka *et al.* have attributed such features to frictional traction large enough to rupture the polymer surface following multiple passes, and have consequently classified it as evidence of fatigue wear [67]. However, the current author believes this fatigue wear to be of lesser importance in this instance, as the high rate of polymer removal by abrasion is very much greater than the loss of material through fatigue cracking and spallation.

2. Wear Against Counterfaces of Moderate Surface Roughnesses

   The displacement-wear curves obtained for UHMWPE sliding against stainless steel counterfaces of moderate surface roughnesses (0.05 μm ≤ R_a ≤ 0.45) showed an initial high *"bedding-in"* wear rate, lasting about 20 km. This was followed by much reduced, stable, *"steady-state"* wear, where the stable wear coefficient was about a tenth of that of the initial wear coefficient at K_{stable} = 15 x 10^{-9} mm^3/N.m to 45 x 10^{-9} mm^3/N.m for counterface R_a's ranging from 0.05 μm to 0.45 μm (see figure 6.12). This type of wear curve has been found by many previous workers against similar counterfaces [19,67,78], and

is attributable to general "bedding-in" effects such as initial wear pin/counterface mismatch (resulting in localised areas of very high pressure and consequently accelerated wear), and, more importantly, the formation of a polymer transfer layer.

During the initial wear stage, Marcus identified both abrasion and adhesion as the operative wear mechanisms, where the dominant wear mode was postulated as being adhesive [19]. However, the current author believes the initial abrasive component of polymer wear to be very significant, as the hard, initially unshielded metal asperities cut and plough through the softer UHMWPE surface. As the UHMWPE wear debris is pressed into the counterface valleys, the abrasive metal asperities are covered by polymer and the effectively smoothed counterface offers greater load support, resulting in a consequent reduction in wear. Eventually, a polymer film over most of the stainless steel counterface is thus built up, covering all the hard asperities and hence completely negating abrasion, or microcutting, of the polymer. Some areas of the transfer layer may, however, rupture with time, and it is partly the constant renewal and repair of the transfer layer which causes continued polymer wear, even in the *"steady-state"* region. The transfer layer "rupture sites" nonetheless still showed underlying polymer, so the sliding UHMWPE pin was not exposed to hard metal asperities at any time after coherent transfer layer formation.

SEM investigation of the worn (100 km) UHMWPE pins reveals some quite severe plastic deformation of these surfaces, which is evidence of the continuing presence of adhesive attraction between the polymer and counterface/transfer layer. Further evidence of the preservation of these adhesive forces is provided by measurement of continually high UHMWPE/counterface frictional forces. The shear stresses thus constantly induced along a single axis in the polymer surface will lead to the surface molecules becoming substantially oriented in the direction of sliding, resulting in a strain hardened surface layer approximately 5 to 10 μm thick [19,61]. The acute change in the polymer properties of this surface layer results in the easy shear at the interface with the undeformed bulk material, with the consequent loss of thin sheets of polymer (as seen in figure 6.33), some of which is transferred back onto the counterface and thus repairs the transfer layer ruptures, and consequently accounts for the continued wear of the polymer pin during the *"steady-state"* wear regime.

3. Wear Against Smooth, Polished Counterfaces

Results from tests sliding UHMWPE against very smooth, polished stainless steel counterfaces (R_a = 0.02 μm), showed no high, *"bedding-in"* wear. Instead, the initial wear rate was extremely low at $K_{initial}$ = 8.92 x 10^{-9} $mm^3/N.m$ average. However, an increase in wear rate was registered after about 50 km of sliding to K = 51.02 x 10^{-9} $mm^3/N.m$ (figure 6.14).

Such a transition from very low wear to increased wear rates against smooth counterfaces after lengthy periods of sliding has been found by other authors. Dowson *et al.* noted a sudden, threefold increase in UHMWPE wear after 25 km of sliding against smooth stainless steel counterfaces [62] using a pin-on-disc testing apparatus. Anderson showed the sliding distance to wear transition to have a strong dependence on the applied load and thus postulated that the increased wear rate is a consequence of fatigue effects [47].

Cooper *et al.* have proposed a subsurface fatigue mechanism, or *"macroscopic asperity wear"*, for this type of UHMWPE wear behaviour against such very smooth stainless steel counterfaces [79]. A further prerequisite for this wear mechanism is a fairly rough polymer surface: The relatively large polymer peaks are deformed under applied load, producing surface and subsurface stress concentrations as shown schematically in figure 8.1. The deformation is then gradually built up until plastic failure strain is reached and a polymer sheet is removed from the surface.

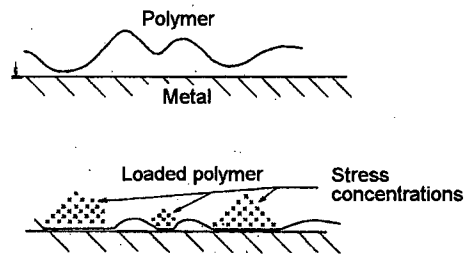

Figure 8.1 *Schematic showing Coopers' "macroscopic asperity wear" mechanism [after ref. 79].*

Coopers' theory is well supported by the current evidence of large wear sheet debris production after extensive polymer sliding against a very smooth, stainless steel counterface. Furthermore, prolonged sliding against the counterface/transfer layer resulted in macroscopic plastic deformations, caused by strong adhesive interfacial forces, which could in turn result in the large subsurface stress concentrations shown in figure 8.1. Figure 8.2 shows these plastic deformations to be large enough in length and height to compare to the size of the wear debris.

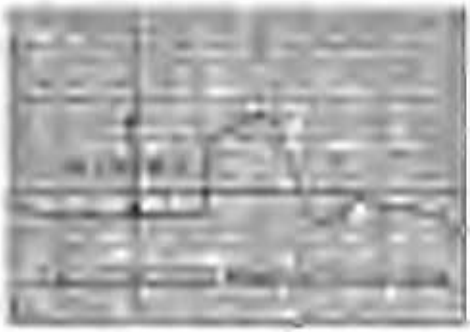

Figure 8.2 Talysurf trace across the polymer wear pin in the direction of sliding. The trace shows the macroscopic deformation as being approximately 2 mm in length and 2 μm in elevation, thus corresponding well to the size of the wear debris produced.

8.2.2 The Relationship of UHMWPE Wear Rate to Counterface Surface Roughness

The slight increase in *"steady-state"* wear rate with increasing counterface surface roughness, for R_a values between about 0.05 μm and 0.45 μm, followed by much higher wear rates at higher surface roughnesses, is a well established trend for UHMWPE sliding against stainless steel counterfaces. Lloyd *et al.* described the relationship of stable wear rate to counterface surface roughness as being exponential [4]:

$$K_{stable} = 1.1 \times 10^{-8} \exp(7.7 R_a)$$

Figure 8.3 shows the exponential "best fit" to the present authors' data as corresponding very well to that found by Lloyd *et al.* Such curves are however of limited value, since the rapid transition from moderate to very high wear experienced at an R_a of around 0.45 μm is not adequately shown. The sudden transition is clearly due to the polymer debris' ability to mechanically interlock with the smaller valleys and asperities of the counterfaces with R_a values of 0.02 μm to 0.45 μm and thus form a stable transfer layer, whereas the large valleys of the rougher counterfaces of R_a above 0.45 μm are not able to adequately restrain the polymer wear debris. Therefore, as soon as transfer layer formation becomes possible, the wear rate decreases dramatically.

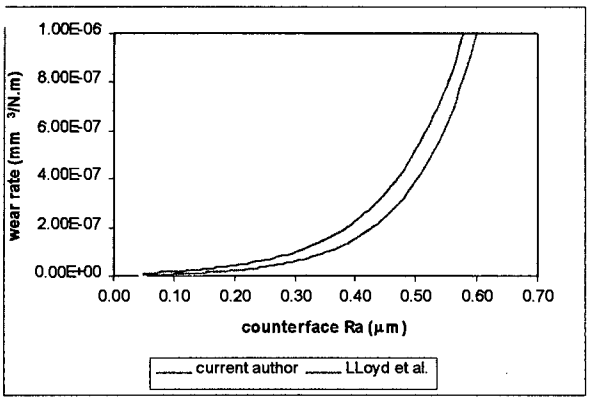

Figure 8.3 *A comparison of Lloyd's exponential fit wear curve to the curve obtained for the present authors data, for R_a's between 0.05 and 0.60 μm.*

The *"steady-state"* wear rate of UHMWPE sliding against counterfaces of surface roughnesses in the range from 0.05 μm to 0.45 μm increases only slightly with increasing counterface surface roughnesses. SEM investigation of worn stainless steel counterfaces of different initial surface roughnesses show the smoother counterfaces supporting more coherent transfer layers, with less areas of rupture. Less polymer film renewal is thus required, leading to the slightly lower rates of wear.

At surface roughnesses below R_a = 0.05 μm, a sudden, dramatic, increase in *"steady-state"* wear rate together with a slight yet significant rise in friction coefficient was registered. The consequent minimum wear condition, at a counterface surface roughness of about 0.05 μm R_a, has also been found by previous workers wearing UHMWPE against stainless steel under conditions of reciprocating sliding, and is often associated with the onset of "lumpy" transfer [62,47]. However, the present authors' examination showed exceptionally smooth, rupture-free transfer films on the polished stainless steel counterfaces, and the increase in wear can thus certainly not be ascribed to a lack of stable transfer layer formation. Rather, the onset of *"macroscopic asperity wear"*, whereby large surface and subsurface stress concentrations induced in the polymer pin lead to subsurface fatigue and consequent polymer surface sheet removal, offers a more feasible explanation. The "microscopic" wear encountered across the entire polymer wear surface when sliding against rougher ($R_a \geq$ 0.05 μm) counterfaces (by surface layer shearing or other mechanisms) effectively prevents the formation of the large subsurface strains required for the development of the subsurface fatigue stress and the mechanism does hence not operate when sliding against slightly rougher counterfaces. The onset of *"macroscopic asperity wear"* is aided by greater interfacial adhesion, as evidenced by the measurement of increased

frictional forces compared to those of UHMWPE sliding against stainless steel of R_a = 0.05 μm. However, since interfacial forces of adhesion are known to operate below 0.1 nm (see Chapter 3.2.4.1), it is not the increase in real area of contact A_r between the stainless steel counterface and polymer which causes the increased adhesion, since the actual counterface is well shielded by the polymer transfer layer. Instead, it is the exceptionally smooth transfer films which build up on the polished counterfaces which cause an increase in A_r and may thus eventually lead to increased wear rates.

8.2.3 Topographical Effects

The different counterface preparation techniques of "random" grinding and "parallel" surface grinding (perpendicular to the direction of sliding) had no significant effect on the UHMWPE/stainless steel *"steady state"* wear rate for equivalent surface roughnesses. The topography of randomly directed valleys and asperity ridges is thus able to support the formation of transfer layers just as well as that of the "parallel" ground counterfaces. This might seem somewhat surprising, since the polymer debris has been shown to experience difficulty in interlocking with corrugations running in the direction of sliding [19], and, since some of the randomly ground counterfaces' scratches are bound to run roughly in the direction of sliding, it could be expected to lead to slightly higher wear. There are, however, two likely reasons for this not being the case:

1. Polymer debris can interlock with surface corrugations running at a slight angle to the sliding direction. Thus, there are too few scratches which do not support the formation of a transfer film to have any significant impact on the rate of UHMWPE wear.

2. There is adequate transfer layer build-up surrounding such non-supportive corrugations to adequately "shield" the polymer wear surface, as is evidenced in figure 6.23.

Likewise, both the "random" ground and "parallel" ground counterfaces experienced the sudden onset of rapid wear at surface roughness values above 0.45 μm R_a, caused by the polymers' inability to form transfer layers against these rougher counterfaces.

Differences in topography did however result in differences in the coefficients of friction and the initial wear rate of UHMWPE against stainless steel for equivalent surface roughnesses. The "parallel" ground counterfaces usually lead to increased

friction and the initial wear of UHMWPE sliding against such counterfaces was approximately double that of the polymer wearing against "random" ground counterfaces. The greater initial wear against the "parallel ground" counterfaces is believed to be caused by the sharper asperity ridges associated with this surface preparation technique (see figures 6.3 and 6.4) resulting in high initial abrasion, or *microcutting*, of the polymer. The "random" ground counterface asperities, on the other hand, are less pronounced (see figures 6.7 and 6.8) and are consequently less abrasive. Furthermore, the "random" ground counterfaces are likely to offer greater load support and thus lead to decreased adhesive friction and initial wear.

8.2.4 Counterface Material Effects

The kinetic friction coefficient for UHMWPE wearing against a polished (R_a = 0.02 μm) Yttria Partially Stabilised Zirconia counterface under conditions of water lubricated reciprocating sliding remained virtually unchanged throughout the entire test distance covered at μ = 0.0103 to 0.0105, whereas high "start-up" friction (μ = 0.036) followed by reduced, "stable" friction of about μ = 0.025 was registered for the UHMWPE – polished stainless steel (R_a = 0.02 μm) couple.

No measurable UHMWPE mass loss could be recorded when sliding against the ceramic material, even after 200 km of testing. Additional evidence of the very low wear encountered when sliding against this ceramic was provided by optical microscopy. The polymer pin manufacturing machine tracks (initial R_a = 0.3 μm) had not been worn away after some 10 km of reciprocation. Furthermore, SEM images of the "worn" polymer surfaces, taken after 100 km of sliding, showed hardly any surface deformation occurring. There were no signs of any abrasive wear mechanism taking place.

Such low rates of wear against ceramic materials, especially Zirconia, have also been found by other authors, both in water lubricated reciprocating pin-on-flat and hip-joint simulator tests [80,81,82]. As was the case in the current study, no changes such as transfer layer formation or polymer deposit could be detected on the counterfaces themselves. The extremely low wear encountered when sliding UHMWPE against polished YPSZ compared to stainless steel counterfaces are thus ascribable to two factors:

1. Reduced adhesive attraction between the polymer and YPSZ counterface i.e. the interfacial bonds formed between the stable ceramic counterface and the polymer pin are weaker than those formed between the metal/metal oxide and polymer pin (see Chapter 3.2.4.1). Surface activity (i.e. the abiliy to create

interfacial bonding) is inversely related to the degree of ionic character of the surface material, where high ionic character will indicate a passive surface. The ionic character, in turn, is directly related to the electronegativity between the elemental constituents of the counterface material type (passive oxide for metals) and it thus follows that, since the electronegativity of the ceramic counterface is much higher than that of the stainless steel oxide film, the interfacial adhesion of the UHMWPE – YPSZ couple will be far less [82].

Dry friction tests performed by the author showed the initial kinetic friction coefficient of a YPSZ - UHMWPE couple to be $\mu = 0.023$, whereas that of a polished stainless steel – UHMWPE couple was recorded as $\mu = 0.036$. Since the respective surface roughnesses of the counterfaces were the same and no lubricant was present, the real area of contact is presumed to be similar, and the difference in dry, initial friction between the two couples is thus taken as evidence of the stronger interfacial bonding of the metal – polymer couple.

Less interfacial adhesion between polymer and wear pin will thus lead to a general decrease in adhesive wear phenomena. The UHMWPE wear surface will not be subjected to the high shear forces experienced against stainless steel counterfaces, and consequently the oriented surface layers leading to surface delamination, and macroscopic surface deformations leading to macroscopic asperity wear, are less likely to occur.

2. Far greater wettability of the YPSZ counterfaces leading to better water lubrication and a consequent reduction in adhesive wear [82]. Comparative surface wettability studies are usually performed by measuring the contact angle between the lubricants and surfaces. High contact angles denote low surface wettability, whereas lower contact angles indicate greater wettability. Typical contact angles obtained for water on YPSZ surfaces are in the range of 40° to 50°, while those obtained for water on stainless steel and Co-Cr-Mo surfaces are above 70° [11]. Furthermore, the wettability of the actual metals below their protective oxide layers is even less, and as these oxide layers may well be disturbed during reciprocating sliding, the surface wettability of these materials could effectively become even less compared to that of YPSZ.

   A comparison of the wet to the dry friction coefficients recorded with the UHMWPE – YPSZ and UHMWPE – stainless steel couples shows the vastly superior wettability and hence lubrication ability of the ceramic counterfaces. Whereas there is no significant difference between the wet and the dry initial coefficient of friction recorded for the UHMWPE – stainless steel couple, the dry friction coefficient of the UHMWPE – YPSZ couple is twice that of the water lubricated UHMWPE – YPSZ couple ($\mu_{dry} = 0.023$, $\mu_{wet} = 0.011$).

8.3 A Comparative Evaluation of the Friction and Wear Performance of Ion Implanted UHMWPE

In an attempt to increase the wear performance of the actual polymer material itself, UHMWPE wear pins were subjected to a surface hardening technique, namely ion implantation. The structural modifications induced by this method are however confined to within a thin, 0.5 μm surface layer. This layer would be rapidly removed by the initial high wear regime encountered when sliding UHMWPE against all but smooth polished counterfaces, and thus quantitative analysis was only conducted against the smooth polished (R_a = 0.02 μm) stainless steel counterfaces. Some tests were also performed against polished YPSZ counterfaces, but since the mass loss recorded by wearing even untreated UHMWPE against such counterfaces was not reliably measurable, these tests only yielded qualitative results in the form of optical comparisons of the rate of machine track removal on the wear pin surfaces.

Wear tests performed against polished stainless steel counterfaces showed a 32.6 % decrease in the wear of the surface modified UHMWPE. It was calculated that at the average wear coefficient of 6.01 x 10^{-9} $mm^3/N.m$ obtained for the ion implanted UHMWPE, all of the surface hardened polymer would have been removed after 20 km of sliding. This was confirmed by the wear rate of the modified polymer becoming similar to that of the "standard" UHMWPE after further sliding. Wear tests performed against polished YPSZ counterfaces resulted in similarly low (unmeasurable) wear rates for ion implanted as for untreated UHMWPE. Optical microscopy of the respective polymer wear surfaces showed no significant difference in the rate of machine track removal, and it is thus presumed that the wear rate, if measurable, would be similar for both ion implanted and untreated UHMWPE against such ceramic counterfaces.

Throughout the test duration of 20 km, the kinetic friction coefficients recorded for the ion implanted UHMWPE sliding against polished stainless steel (R_a = 0.02 μm) and YPSZ counterfaces remained akin to those recorded for untreated UHMWPE sliding against similar counterfaces. This is somewhat surprising, since the harder, ion implanted surface was expected to result in higher friction. Tests wearing cross-linked phenol formaldehyde against polished stainless steel (R_a = 0.02 μm) counterfaces yielded much higher initial kinetic friction coefficients compared to those of UHMWPE sliding against similar counterfaces (μ = 0.055 compared to μ = 0.036). A similar trend was observed when these two polymers were slid against YPSZ counterfaces of R_a = 0.02 μm (μ = 0.055 compared to μ = 0.036), thus supporting the premise that wearing a harder polymer against a metal or ceramic should result in increased friction. Other workers, however, have also

reported some difficulty in relating the effect of ion implantation to the friction behaviour of the surface treated polymers. Rao *et al.* conducted both standard friction and friction microbe tests on standard and ion implanted poly (ether ether ketone) (PEEK) and polystyrene (PS) and found their friction behaviour to vary with the implantation fluence, with lower PEEK implantation fluence gradually leading to increased friction and higher PEEK implantation fluence gradually leading to decreased friction as compared to the untreated polymer. These fluency – friction coefficient trends were reversed for the PS tests [21]. The large fluctuations in friction coefficient with implantation fluency recorded by Rao *et al.* are however in contrast with the results of the current author, where the ion implantation had no significant effect on the friction behaviour of UHMWPE, both against polished stainless steel (R_a = 0.02 μm) and YPSZ counterfaces.

Despite the transfer layer formed on the stainless steel counterfaces by the ion implanted polymer being no different to that of the untreated UHMWPE, some difference in wear pin morphology were detected after 10 km of sliding, with the surface treated UHMWPE showing less signs of plastic deformation. Considering the proven increases in nanohardness of the modified surface layer (table 2.1 and 2.2), this was to be expected. However, small surface cracks and tracks were evident on the ion implanted polymer wear surface, probably due to the increased brittleness of the modified material. This nevertheless had no deleterious effect on the wear performance of the implanted polymer, the possible consummation of surface cracking and consequent polymer surface delamination possibly being prevented by low, continued wear of the UHMWPE surface. However, no increase in wear rate of the ion implanted polymer sliding against Zirconia counterfaces was registered, even after prolonged sliding. It may thus be assumed that the observed features of polymer pin "cracking" will not lead to an increase in wear, even after prolonged sliding against "low wear" counterfaces.

Although significant when wearing against polished stainless steel counterfaces, the improvement in the wear performance of the ion implanted polymer is not as great as has been found by previous authors against surface treated titanium counterfaces [83] in pin-on-disc and stainless steel femural heads in hip-joint simulation tests [20]. The relatively greater effectiveness of the ion implantation treatment is to be expected during the multi-axial hip-joint simulation tests. This is because crosslinking the UHMWPE should prevent the orientation softening, and hence increased wear, of the linear polymer when subjected to multi-axial motion [34] (see Chapter 3.6.2).

However, for the instance of single axis reciprocating motion, the present authors results show the current ion implantation treatment as yielding only limited benefits over moderate sliding distances against optimal counterfaces.

CHAPTER 9

CONCLUSIONS

A new reciprocating wear testing apparatus has been designed, built, and commissioned. All of the requirements, constraints and criteria initially set for the design were fully met. A series of three tests wearing ultra high molecular weight polyethylene (UHMWPE) pins against similarly prepared, polished stainless steel counterfaces yielded an average ±14 % deviation from the mean recorded volume loss after 20 km of sliding. Furthermore, the friction and wear measurements recorded with the new apparatus generally coincided well with those reported by previous workers.

The new wear testing apparatus was then used to study the water-lubricated sliding wear of UHMWPE and ion implanted UHMWPE. The work carried out during the course of this investigation has led to the following noteworthy conclusions about the water-lubricated reciprocating sliding wear of untreated and surface modified UHMWPE:

1. The Effect of Counterface Roughness

Variations in stainless steel counterface roughness resulted in three distinct wear regimes:

(a) Very high wear for UHMWPE sliding against counterface surface roughnesses above R_a = 0.45 μm. This was caused by the inability of such surfaces to support stable transfer layers.

(b) High initial *"bedding-in"* wear followed by much reduced *"steady-state"* wear for UHMWPE sliding against counterfaces of "moderate" surface roughnesses in the range 0.05 μm ≤ R_a ≤ 0.45 μm. The reduction in wear was attributed to the formation of a stable transfer film during the initial *"bedding-in"* wear, thus effectively shielding the polymer pin from the harder counterface.

(c) Very low initial wear followed by increased wear after 50 km of sliding for UHMWPE wearing against polished stainless steel counterfaces of R_a = 0.02 μm. The increased wear was attributed to a subsurface fatigue mechanism known as *"macroscopic asperity wear"*.

A minimum in UHMWPE/stainless steel friction and wear was observed when sliding against counterfaces of $R_a = 0.05$ μm.

2. The Effect of Counterface Topography

The different stainless steel counterface topographies achieved by either "random" grinding or "parallel" grinding did not have any significant effect on the *"steady-state"* wear performance of UHMWPE. However, the *"bedding-in"* wear encountered against the "random ground" counterfaces was generally lower.

3. The Effect of Counterface Material Type

Tests performed against polished (R_a = 0.02 μm) Yttria Partially Stabilised Zirconia (YPSZ) counterfaces resulted in no measurable UHMWPE wear. Furthermore, the friction coefficients measured for the UHMWPE/ceramic couple were less than a half of those measured against similarly prepared stainless steel counterfaces.

4. The Comparative Friction and Wear Performance of Ion Implanted UHMWPE

The ion implantation surface treatment resulted in a 32.6% decrease in UHMWPE wear against polished stainless steel counterfaces over sliding distances of 20 km. It was however predicted that the surface hardened layer would be quickly worn away by the high initial wear regime encountered when sliding against "moderate" counterface surface roughnesses (0.05 μm $\leq R_a \leq$ 0.45 μm). Furthermore, the modified polymer layer will be worn off after 20 km even when sliding against polished stainless steel counterfaces.

The current ion implantation treatment will thus yield only limited benefits over moderate sliding distances against optimal counterfaces.

REFERENCES

[1] Maloney J., Jasty M. Harris W.H., Galante J.O., Callaghan J.J., *"Endosteal Erosion in Association with Stable Uncemented Femoral Components"*, **J. Bone and Joint Surgery**, No. 72-A, 1990, pp. 1025-1034.

[2] Liao J.D., Rieu J., Corre Y., Rabbe L. -M., Boudoukha L., Paletto S., *"Mechanical and Chemical Modifications of Polyethylene Surfaces by Ion Implantation"*, **Proc. World Ceramics Congress**, Int. Ceramics Fed., Florence, 1994.

[3] Davidson J.A., *"Characteristics of Metal and Ceramic Total Hip Bearing Surfaces and their Effect on Long-Term Ultra High Molecular Weight Polyethylene Wear"*, **Clinical Orthopaedics and Related Research**, No. 294, 1993, pp. 361-378.

[4] Lloyd A.I.G., **The Sliding Wear of UHMWPE Against Stainless Steel**, MSc Thesis, University of Cape Town, 1986.

[5] Tanaka K., Nagai T., *"Effect of Counterface Roughness on the Friction and Wear of Polytetrafluoroethylene and Polyethylene"*, **Proc. Conf. Wear of Materials**, Ludema K.C. (ed.), ASME Trans., 1985, pp. 394-404.

[6] McCrum N.G., Buckely C.P., Bucknall C.B., **Principles of Polymer Engineering,** Oxford Sci. Publ., 1988.

[7] Osswald T., Menge G., **Materials Science of Polymers for Engineers**, Hanser/Gardner Publications Inc., 1995.

[8] Crow J.M.G., **Polymers: Chemistry and Physics of Modern Materials,** 2nd edn., Blackie & Son Ltd., Chapman and Hall Inc., N Y, 1991.

[9] Nicholson J. W., **The Chemistry of Polymers,** Royal Society of Chemistry, 1991.

[10] Mears P., **Polymers: Structure and Bulk Properties,** D Van Nostrand Company Ltd., London, 1965.

[11] Allcock H.R., Lampe F.W., **Contemporary Polymer Chemistry,** Prentice-Hall Inc., New Jersey, 1981.

[12] Hall C., **Polymer Materials: An Introduction for Technologists and Scientists**, Macmillan Publishers Inc., 1981.

[13] Rodriguez F., **Principal of Polymer Systems,** Mcgraw-Hill Book Company, N.Y., 1970.

[14] Peterlin A., *"Molecular Model of Drawing Polyethylene and Polypropylene"* **J. Materials Science**, Vol. 6, 1971, pp.470-508.

[15] Suehiro K., Terashima T., Takayanagi M., *"Change of Mosaic Block Size of Bulk Polyethylene in Drawing Process"*, **J. Materials Science**, Vol. 9, 1974, pp. 1563-1568.

[16] Peterlin A., *"Structure of Drawn Polymers"*, **Technical Report AFML-TR-67-6**, U.S. Air Force Materials Lab., Wright-Patterson AFB., Ohio, 1966.

[17] Zum Gahr K. H., **Microstructure and Wear of Materials**, Tribology Series, Vol. 10, Elsevier, Amsterdam, 1987.
[18] Solidur Pamphlet, Pty. Ltd., S.A.
[19] Marcus K., **Micromechanisms of Polymer Sliding Wear**, PhD Thesis, University of Cape Town, 1992.
[20] Rieu J., Pichat A., Rabbe L.-M., Rambert A., Chabrol C., Robelet M., *"Structural Modifications Induced by Ion Implantation in Metals and Polymers Used for Orthopaedic Prosthesis"*, **J. Materials Science and Technology**, Vol. 8, 1992, pp. 589-593.
[21] Rao G.P., Blau P.J., Lee E.H., *"Friction Microbe Studies of Ion Implanted Polymer Surfaces"*, **Wear**, 184, 1995, pp. 213-222.
[22] Allen N.S. (editor), **Degradation and Stabilisation of Polyolefins**, App. Sci. Pub. Inc., 1983.
[23] Charlesby A., *Molecular Weight Changes and Network Formation by Scission and Crosslinking"*, **Crosslinking and Scission in Polymers**, edited by O. Gueven, Kluwer Acedemic Publishers, 1990.
[24] Briscoe B.J., *"Fundamentals of Friction and Wear"*, Paper 2, **Non-Metallic Bearings in Engineering**, NCT Notes, 1989, pp. 1-45.
[25] Briscoe B.J., Tabor D., *"Friction and Wear of Polymers: The Role of Mechanical Properties"*, **British Polymer Journal**, Vol. 10, 1978, pp. 74-78.
[26] Halling J., **Introduction to Tribology**, Wykenham Publ., London, 1976.
[27] Moore D.F., **The Friction and Lubrication of Elastomers**, Pergamon Press Ltd., 1972.
[28] Moore D.F, **Principles and Applications of Tribology**, Pergamon Press Ltd., 1975.
[29] Tabor D., *"The Wear of Non-Metallic Materials: A Brief Review"*, **Wear of Non-Metallic Materials**, Proceedings of the 3rd Leeds-Lyon Symposium on Tribology, Mechanical Engineering Publications Limited, 1976.
[30] Pooley C.M., Tabor D., *"Friction and Molecular Structure: The Behaviour of Some Thermoplastics"*, **Proc. Royal Society**, London, Series A, Vol. 329, 1972, pp. 251-274.
[31] Briscoe B.J., *"Wear of Polymers: An Essay of Fundamental Aspects"*, **Tribology International**, Vol. 14, No. 4, August 1981, pp. 231-243.
[32] Briscoe B.J., *"Interfacial Friction of Polymer Composites, General Fundamental Principles"*, **Friction and Wear of Polymer Composites**, Friedrich K. (ed.), Vol. 1, Ch. 2, Composite Materials Series, Vol. 1, Amsterdam, Elsevier, 1986, pp. 25-59.
[33] Briscoe B.J., Scruton B., Willis F.R., *"The Shear Strength of Thin Lubricant Films"*, **Proc. Royal Society**, London, Series A, Vol. 333, 1973, pp. 99-114.
[34] Wang A., Polineni V.K., Essner A., Sokol M., Sun D.C., Stark C., Dumbleton J.H., *"The Significance of Non-Linear Motion in the Wear Screening of*

Orthopaedic Implant Materials", **J. Testing & Evaluation**, Vol. 25, No. 2, 1997, pp. 239-245.

[35] Halling J., (ed.), **Principles of Tribology**, Macmillan Press Ltd., 2nd edn., London, 1983.

[36] Hutchings I.M., **Tribology: Friction and Wear of Engineering Materials**, Hodder and Stoughton Ltd., 1992.

[37] Evans D.G., Lancaster J.K., *"The Wear of Polymers"*, **Treatise on Materials Science and Technology**, Scott D. (ed.), Vol. 13, Academic Press Inc., 1979, pp. 85-140.

[38] Buckely D.H., **Surface Effects in Adhesion, Friction, Wear and Lubrication**, Tribology Series 5, Elsevier, N.Y., 1981.

[39] Lancaster J.K., *"Abrasive Wear of Polymers"*, **Wear**, Vol. 14, 1969, pp. 223-239.

[40] Lancaster J.K., *"Friction and Wear"*, **Polymer Science**, Jenkins A.D. (ed.), A Materials Science Handbook, Ch. 14, North-Holland Publ. Co., Elsevier, N.Y., 1972.

[41] Ratner S.B., Farbevora I.I., Radyukevich O.V., Lure E.G., *"Connection Between the Wear Resistance of Plastics and Other Mechanical Properties"*, **Soviet Plastics**, 1964, Vol. 7, pp. 37-45.

[42] Giltrow J.P., *"A Relationship Between Abrasive Wear and the Cohesive Energy of Materials"*, **Wear**, Vol. 15, 1970, pp. 71-78.

[43] Belyi V.A., Sviridyonok A.I., Savkin V.G., Smurugov V.A., *"Friction Transfer of Polymers and it's Effect on Wear"*, **Proc. Wear of Materials**, Rhee S.K., Ruff A.W., Ludema K.C. (eds.), 1981, pp. 167-170.

[44] Lloyd A.I.G., **The Sliding Wear of UHMWPE Against Stainless Steel**, MSc Thesis, University of Cape Town, 1986.

[45] Dowson D., El-Hady Diab M.M., Gillis B.J., Atkinson J.R., *"The Influence of Counterface Topography Upon the Wear of Ultra High Molecular Weight Polyethylene Under Wet or Dry Conditions"*, **Polymer Wear and it's Control**, Lee L.H. (ed.), ACS Series 287, Ch. 12, 1985, pp. 171-187.

[46] Clarke C.G., **The Sliding Wear of Polymers Against Steel**, MSc Thesis, University of Cape Town, 1988.

[47] Anderson J.C., *"High Density and Ultra High Molecular Weight Polyethylenes: Their Wear Properties and Bearing Applications"*, **Tribology International**, Vol. 15, No. 1, 1982, pp. 43-47.

[48] Tanaka K., *"Friction and Wear of Semicrystalline Polymers Sliding Against Steel Under Water Lubrication"*, **J. Lubrication Technology**, ASME Trans., Vol. 102, 1980, pp. 526-533.

[49] Anderson J.C., *"The Wear and Friction of Commercial Polymers and Composites"*, **Friction and Wear of Polymer Composites**, Friedrich K. (ed.),

Vol. 1, Ch. 10, Composite Materials Series, Amsterdam, Elsevier, 1986, pp. 329-362.

[50] Rhee S.K., Ludema K.C., *Mechanisms of Formation of Polymeric Transfer Films"*, **Wear**, Vol. 46, 1978, pp. 231-240.

[51] Tanaka K., *"Transfer of Semi-Crystalline Polymers Sliding Against Smooth Stainless Steel Surfaces"*, **Proc. Conf. of Materials**, Rhee S.K., Ruff A.W., Ludema K.C. (eds.), ASME Trans., N.Y., 1981, pp. 98-106.

[52] Evans V.R., Kennedy F.E., *The Effects of Tempereture on Friction and Wear in Oscillatory Motion of Polyethylene Against Stainless Steel"*, **Proc. Conf. Wear of Materials**, ASME Trans., Houston, Vol. 1, 1987, pp. 427-434.

[53] Tabor D., **The Role of Surface and Intermolecular Forces in Thin Film Lubrication. Microscopic Aspects of Adhesion and Lubrication**, Tribology Series, Georges J.M. (ed.), Elsevier, 1982.

[54] **Lubrication Theory and its Application**, BP Trading Ltd., London, 1969.

[55] Kapsa Ph., Martin J.M., *"Boundary Lubricant Films: A Review"*, **Tribology International**, Vol. 15, No. 1, 1982.

[56] Amuzu J.K.A., Briscoe B.J., Tabor D., *"Polymers as Bearings and Lubricants: Aspects of Fundamental Research"*, **Advances in Tribology**, Inst. Mech. Eng., London, 1978, pp. 59-62.

[57] Marcus K., Allen C., *"The Sliding Wear of Ultra High Molecular Weight Polyethylene in an Aqueous Environment"*, **Wear**, Vol. 187, 1994, pp. 17-28.

[58] Wang A., Essner A., Polineni V.K., Sun D.C., Stark C., Dumbleton J.H., *"Lubrication and Wear of Ultra High Molecular Weight Polyethylene in Total Joint Implants"*, **New Directions in Tribology**, Plenary and Invited Papers from the First World Tribology Congress, Mech. Eng. Publ., London, 1997, pp. 443-448.

[59] Wang A., Sun D.C., Stark C., Dumbleton J.H., *"Wear Testing Based on Unidirectional Motion: Fact or Artifact?"*, **Proc. 5th World Biomaterials Congress**, Toronto, 1996, p. 583.

[60] Bragdon C.R., O'Connor D.O., Lowenstein J.D., Syniuta J.R., Syniuta W.D., *"The Importance of Multidirectional Motion for the Wear of Polyethylene in the Hip"*, **Proc. World Trib. Congress**, Mech. Eng. Publ., 1997, p. 735.

[61] Wang A., Sun D.C., Yau S.S., Edwards B., Sokol M., Essner A., Polineni V.K., Stark C., Dumbleton J.H., *"Orientation Softening in the Deformation and Wear of Ultra High Molecular Weight Poyethylene"*, **Wear**, 203-204, 1997, pp. 230-241.

[62] Dowson D., Challen J.M., Holmes K., Atkinon J.R., *"The Influence of Counterface Roughness on the Wear Rate of Polyethylene"*, **The Wear of Non-Metallic Materials**, Dowson D., Godet M., Taylor C.M. (eds.), Proc. 3rd Leeds-Lyon Symp. on Tribology, MEP, London, 1976, Paper IV (iv), pp. 99-102.

[63] Lloyd A.I.G., Noel R.E.J., *"The Effect of Counterface Surface Roughness on the Wear of UHMWPE in Water and Oil-In-Water Emulsion"*, **Tribology International**, Vol. 21, No. 2, 1988, pp. 83-88.

[64] Hollander A.E., Lancaster J.K., *"An Application of Topographical Analysis to the Wear of Polymers"*, **Wear**, Vol. 25, No. 2, 1973, pp. 155-170.

[65] Evans D.C., *"Polymer-Fluid Interactions in Relation to Wear"*, **The Wear of Non-Metallic Materials**, Paper III, Proc. of the 3rd Leeds-Lyon Symp. on Trib., Dowson D., Godet M., Taylor C.M. (eds.), 1976, MEP, pp. 47-55.

[66] Cohen S.C., Tabor D., *"The Friction and Lubrication of Polymers"*, **Proc. Royal Society**, London, Series A, Vol. 291, No. 1425, 1966, pp. 186-207.

[67] Tanaka K., *"Friction and Wear of Semicrystalline Polymers Sliding Against Steel Under Water Lubrication"*, **J. Lubrication Technology.**, ASME Trans., Vol. 102, 1980, pp. 526-533.

[68] Anderson J.C., *"Wear of Commercially Available Plastic Materials"*, **Tribology International**, Vol. 15, No. 5, 1982, pp. 255-263.

[69] Dumbleton J.H., Shen C., *"The Wear Behaviour of Ultra High Molecular Weight Polyethylene"*, **Wear**, Vol. 37, 1976, pp. 279-289.

[70] Challen J.M., Dowson D., *"The Calculation of Interfacial Temperatures in a Pin-On-Disc Machine"*, **The Wear of Non-Metallic Materials**, Proc. 3rd Leeds-Lyon Symp. on Tribology, Dowson D., Godet M., Taylor C.M. (eds.), Paper (iv), MEP, London, 1976, pp. 87-93.

[71] Kar M.K., Bahadur S., *"An Investigation of the Temperature Rise in Polymer-Metal Sliding"*, **Wear**, Vol. 82, 1982, pp. 81-92.

[72] Rhee S.H., Ludema K.C., *"Transfer Films and Severe Wear of Polymers"*, **The Wear of Non- Metallic Materials**, Proc. 3rd Leeds-Lyon Symp. on Tribology, Dowson D., Godet M., Taylor C.M. (eds.), MEP, London, 1976, pp. 11-17.

[73] Lancaster J.K., *"Estimation of the Limiting PV Relationships for Thermoplastic Bearing Materials"*, **Tribology**, Vol. 4, No. 2, 1971, pp. 82-86.

[74] Shen C., Dumbleton J.H., *"The Friction and Wear Behaviour of Irradiated Very High Molecular Weight Polyethylene"*, **Wear**, Vol. 30, 1974, pp. 349-364.

[75] Dowson D., Atkinson J.R., Brown K., *"The Wear of High Molecular Weight Polyethylene with Particular Reference to it's use in Human Joints"*, **Preprints of Am. Chem. Soc. Meeting on Friction and Wear of Polymers**, Los Angeles, 1974, pp. 354-363.

[76] Kienle U.F.B., **A Laboratory Simulation of Adhesive Wear of High Speed Reciprocating Components in Water Powered Mining Equipment**, MSc Thesis, University of Cape Town, 1988.

[77] Kernick M., **The Sliding Wear of UHMWPE Against Ceramics in Solutions Containing Proteins**, MSc Thesis, University of Cape Town, 1992.

[78] Lee K-Y, Pienkowski D., *"Reduction in the Initial Wear of Ultrahigh Molecular Weight Polyethylene after Compressive Creep Deformation"*, **Wear**, 203-204, 1997, pp. 375-397.

[79] Cooper J.R., Dowson D., Fisher J., *"Macroscopic and Microscopic Wear Mechanisms in Ultra-High Molecular Weight Polyethylene"*, **Wear**, 162-164, 1993, pp. 378-384.

[80] Kumar P., Oka M., Ikeuchi K., Shimizu K., Yamamuro T., Okumura H., Kotoura Y., *"Low Wear Rate of UHMWPE Against Zirconia Ceramic (Y-PSZ) in Comparison to Alumina Ceramic and SUS 316L alloy"*, **J. Biomed. Mater. Res.**, 25, 1991, pp. 813-828.

[81] Saikko V., *"Wear and Friction Properties of Prosthetic Joint Materials Evaluated on a Reciprocating Pin-On-Flat Apparatus"*, **Wear**, 166, 1993, pp. 169-178.

[82] Davidson J. A., *"Characteristics of Metal and Ceramic Total Hip Bearing Surfaces and their Effect on Long Term Ultra High Molecular Weight Polyethylene Wear"*, **Clinical Orthopaedics and Related Research**, No. 294, 1993, pp. 361-378.

[83] Allen C., Bloyce A., Bell T., *"Sliding Wear Behaviour of Ion Implanted Ultra High Molecular Weight Polyethylene Against a Surface Modified Titanium Alloy"*, **Tribology International**, Vol. 29, No. 6, 1996, pp. 527-534.

APPENDIX A

Properties of UHMWPE

MediTECH

®Chirulen

Surgery

Under the trade name ®Chirulen, a specially pure form of ultrahigh-molecular-weight polyethylene (PE-UHMW) has been used as a semi-finished product for joint replacement surgery (see standards DIN 58834 and 58836).

Physical properties

The data quoted were determined on test specimens prepared from compression moulded sheet and film. Depending on the conditions of specimen preparation, individual measurements may deviate from these average values.

Property	Unit	Test method	Test specimen	®Chirulen
Density (of the homogeneously pressed material)	g/cm3	DIN 53479 method A	sheet	0,93
Viscosity number	ml/g	DIN 53728 sheet 4	concentration in decahydronaphthalene 0,0003 g/cm3	2300
Intrinsic Viscosity	ml/g	-	-	1920
Average molecular wt.	g/mol	-	-	$4{,}4 \cdot 10^6$
Yield value (150/10)	N/mm²	DIN 53493	dumbbell bar	0,25±0.05
Mechanical properties		(measured under standard climatic conditions 23°C, 50% RH)		
Yield stress	N/mm²	DIN 53455 ISO 527 testing rate: 50 [mm/min]	no. 3	≥ 20
Elongation at yield	%			≤ 20
Elongation at break	%			> 50
Tensile modulus	N/mm²	DIN 53457	test specimen no.3 of DIN 53455	720
Tensile creep modulus 1 hour value	N/mm²	DIN 53444		460
1000 hour value	N/mm²	ISO 899		230
Ball indentation hardness (value test load 365N)	N/mm²	DIN 53456 30-s-Wert	sheet, 4mm	38
Shore hardness D	-	DIN 53505 3 sec value	sheet, 6mm	63
Notched impact strength	mJ/mm²	DIN 53453	small standard test bar	no failure
Notched impact strength (with 15° V-notch on both sides)	mJ/mm²	DIN 53453	120*15*10mm	≥ 200
Abrasion	-	Slurry method	sheet	100

APPENDIX A

Properties of UHMWPE (continued)

MediTECH

Property	Unit	Test method	Test specimen	®Chirulen
Thermal properties				
Heat deflection temperature	°C	DIN53461,ISO75 method A	≥ 110*10*4mm	42
Vicat softening point	°C	DIN ISO 306 method B	10 * 10 * 4mm	80
Crystalline melting range	°C	differential thermal analysis	powder	130 – 135
Coefficient of linear expansion between 23°C and 80°C	1/K	DIN 53752	25 * 4 * 4mm	ca. $2 \cdot 10^{-4}$
Thermal conductivity at 23°C	W/m*K	resistance wire method	sheet, 10mm	0,41
specific heat at 23°C	kJ/kg*K	adiabatic calorimeter	powder	1,84
Electrical properties		(mesured under standartd climatic conditions 23°C, 50% RH)		
Volume resistivity	Ohm*cm	DIN 53482 VDE 0303 part 3	sheet, 1mm	> 10^{14}
Surface resistance	Ohm	DIN 53482 VDE 0303 part 3	sheet, 1mm	> 10^{11}
Dielectric strenght	kV/mm	DIN 53481 VDE 0303 part 2	sheet, 1mm	45
Relative transmittivity at 50 Hz	-	DIN 53483 VDE 0303 part 4	sheet, 1mm	2,1
at 1 MHz	-			3,0
Dissipation factor at 50 Hz	-		sheet, 1mm	$3,9 \cdot 10^{-4}$
Tracking CTI	comparative	DIN IEC 112		600
CTIM	index	VDE 0303 part 1	15 * 15 * 4mm	600
Arc resistance	rating	DIN 53484 VDE 0303 part 5	120*120*10mm	L4

This information is based on our present state of knowledge and is intended to provide general information on our products and their uses.
Therefore, it should not be construed as guaranteeing specific properties of the products described on their suitability for a particular application.

03/1994

APPENDIX B

Some Comparative Properties of Yttria Partially Stabilised Zirconia

A comparison of several mechanical properties between surgical grade alumina (ISO requirements) and two commercially available yttrium-oxide-partially-stabilised zirconia (Prozyr, Ceramiques Techniques Desmarquest, France; Metroxid AG, Switzerland)

Property	Alumina (ISO/DIS 130/D13 requirements)	'Prozyr' YPSZ	'Metoxit' YPSZ
Density (kg.m^-3)	3900	6100	c. 6050
Average grain size (μm)	<7	<0.5	0.2
Vickers hardness (HV)	2000 - 3000	1000 - 1300	c. 1200
Youngs modulus (GPa)	380	200	150
Bending Strength (MPa)	400	1200	c. 800
Toughness (m.Nm^-3/2)	06-May	10-Sep	c. 7

APPENDIX C

The average roughness R_a is defined as the arithmetic mean deviation of the surface height from the mean line through the profile, or

$$R_a = 1/L \int_0^L |y(x)| dx$$

where y is the height of the surface above the mean line at a distance x from the origin, and L is the overall length of the profile under examination (see figure A below). The mean line is defined so that equal areas of the profile lie above and below it.

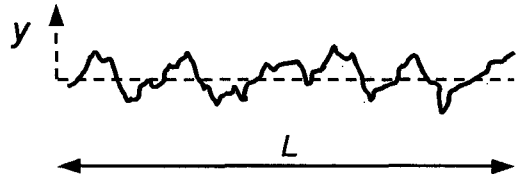

Figure A *A surface profile is a graph of surface height,* y, *relative to a mean line, plotted against distance. The overall length of the profile under examination is* L.

PUBLICATIONS

(1) Hohl M.W., Allen C., *"Ultrahigh molecular weight polyethylene sliding wear optimisation"*, **Proc. of the Microscopy Society of Southern Africa**, Vol. 27, 1997, pp. 31.

(2) Hohl M.W., Allen C., *"An investigation of the sliding wear behaviour of ultrahigh molecular weight polyethylene"*, **Proc. of the South African Institute of Tribology**, 1998.

ULTRAHIGH MOLECULAR WEIGHT POLYETHYLENE SLIDING WEAR OPTIMISATION

M W Hohl & C Allen

Department of Materials Engineering, University of Cape Town

Ultrahigh molecular weight polyethylene (UHMWPE) may be regarded as a high performance engineering thermoplastic exhibiting excellent low stress sliding wear characteristics. The current investigation focuses on wear performance improvement by means of optimising the counterface topography as well as surface modification of the UHMWPE by means of ion implantation.

A new reciprocating wear testing apparatus has been designed to facilitate this research. The counterface specimens are forced to reciprocate on a single axis with a sinusoidal velocity profile, while the wear specimens are clamped stationary and pressed onto the counterface.

UHMWPE pins were worn under an applied pressure of 10MPa at an average sliding velocity of 0.2m.s^{-1} in a distilled water environment. The total test distance covered was 100km. The apparatus was stopped at various intervals to allow the UHMWPE specimens to be weighed and the wear surfaces to be investigated using optical microscopy. After the entire test distance was covered, the specimens were gold-palladium coated and viewed in a scanning electron microscope.

Counterface roughness was shown to greatly influence polymer wear. When sliding against a fairly rough surface, the transfer of polymer fills up the valleys and thus decreases the effective roughness[1]. It follows that for this instance the initial wear is much higher than that encountered after coherent transfer layer formation; the author has found this initial wear to be 10 to 15 times higher than the steady state rate when UHMWPE was worn against a stainless steel surface ground perpendicular to the direction of sliding to an R_a = 0.3μm. Fig. 1 is a SEM image of the UHMWPE pin showing polymer being sheared off the surface. At very rough surfaces (R_a = 0.7μm) the abraded polymer failed to form a coherent transfer layer, possibly due to the valleys being too large to restrain the UHMWPE adequately. Consequently, the recorded wear rate was extremely high.

Very low wear was recorded against smooth zirconia counterfaces of R_a = 0.01 to 0.02μm. No coherent transfer layer was formed as even the initial wear was too low for significant polymer transfer. Fig. 2 shows UHMWPE worn against zirconia for 10km. Some microscratching is evident, but the machining tracks (initial pin R_a = 0.3μm) are still very visible in the background.

Surface hardening[2] of UHMWPE by ion implantation is expected to lead to a further decrease in wear against suitably prepared surfaces. Indeed, ion implanted poly (ether ether ketone) and polystyrene have already shown large improvements in their wear behaviour[3].

The financial support of the FRD and Eskom is gratefully acknowledged.

References

1. Lloyd, A. I. G. (1986) MSc thesis.

2. Liao, J. D., Rieu, J., Corre, Y., Rabbe, L. M., Boudoukha, L., Paletto, S. (1994) Proc. World Ceramics Congress, Int. Ceramic Fed., Florence, Italy.

3. Rao, G. R., Blau, P. J., Lee, E. H. (1995) Wear 184, 213

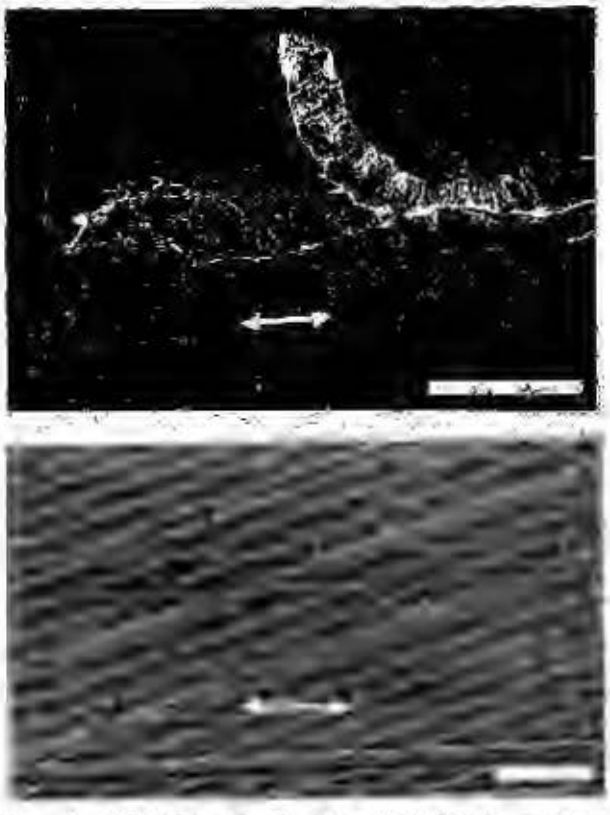

Fig. 1. SEM image of worn UHMWPE surface showing polymer being sheared off the surface. The arrow indicates the direction of sliding. Bar represents 50μm.

Fig. 2. Optical image of UHMWPE worn against zirconia of R_a = 0.01 to 0.02. The arrow indicates the direction of sliding. Bar represents 100μm.

AN INVESTIGATION OF THE SLIDING WEAR BEHAVIOUR OF ULTRA HIGH MOLECULAR WEIGHT POLYETHYLENE

M.W. Hohl, C. Allen

Department of Materials Engineering
University of Cape Town
South Africa

Abstract

A study has been made of the wear behaviour of ultra high molecular weight polyethylene (UHMWPE) and surface treated UHMWPE during water lubricated reciprocating sliding against differing stainless steel counterfaces. Counterface preparation method and surface roughness have been shown to determine the formation of a stable transfer layer, which in turn determines the wear performance of UHMWPE.
Ion implanted surface treated UHMWPE has demonstrated wear behaviour improvements when sliding against suitably smooth counterfaces.

1. Introduction

Ultrahigh molecular weight polyethylene (UHMWPE) is one of the most frequently used polymers for sliding wear applications due to its excellent and well proven tribological and mechanical properties. Uses range from control and foil bearings in the aerospace industry to replacement of degenerative human bearings such as hip, knee and shoulder joints.
Failure of these types of bearings does occur however due to the wear of the polymer surface. Further, even small amounts of wear debris formed by joint implants may lead to loosening of the implant, pain upon weight bearing and the need for revision joint surgery (Jasty, 1993).
Surface modifying the polymer by ion implantation offers the possibility of further improvement upon UHMWPE wear performance. The implantation process alters the near surface microstructure of the polymer by various means such as cross linking, resulting in large modulus of elasticity and hardness increases. Liao *et al.* have demonstrated nanohardness increases of 10 to 15 times and modulus of elasticity increases of 5 to 7 times (from 30 to 100 nm surface depth) using nitrogen ions to a dose of 1.4×10^{17} ions.cm^{-2} (Liao *et al*, 1994).
This work is an attempt to evaluate the wear performance of UHMWPE in the as received and ion implanted condition during water lubricated reciprocating sliding against stainless steel counterfaces and the effect of counterface roughness and topography on the wear behaviour of the polymer.

2. The wear testing apparatus

A new reciprocating type wear testing apparatus was designed and built to facilitate this research. The main features of this design include

- a lever arm/dead weight system to apply the load onto the test specimen (as opposed to a load cell or spring load system); the load is thus constant even if the specimen wears substantially
- an isolating chamber/bath surrounding the UHMWPE/counterface interface, containing liquid which is recirculated so as to keep this environment at a constant temperature
- duplication of the complete system so as to allow two tests to be performed simultaneously.

Figure 1 is a schematic of the rig showing the reciprocating shuttle bath, with counterface mounted inside, and the UHMWPE specimen clamped stationary and forced onto the counterface. The critical dimensional characteristics of the rig are:

Counterface accommodation size:	70mm x 12mm x 10mm (length x width x height)
Wear specimen accommodation size:	10mm x 10mm x approx. 25mm (length x width x height)
Sliding stroke:	50mm

The performance characteristics were chosen so as to cover the conditions which will be encountered in UHMWPE bearing applications. The applied force can thus be set up to 1000 N and the average sliding speed to a maximum of 0.5 m/s. The maximum frictional sliding couple catered for is 800N.

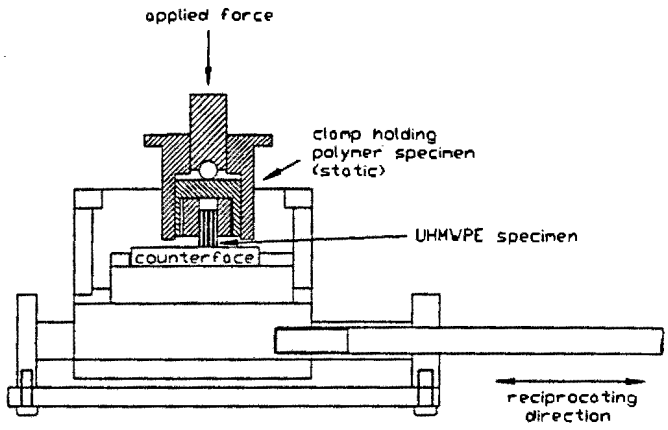

Fig. 1. A cross section of the reciprocating shuttle bath, with counterface mounted inside, and the UHMWPE specimen clamped stationary and forced onto the counterface. The shaft to the right is forced to reciprocate by means of a connecting rod/crank shaft arrangement (not shown).

3. Experimental details

3.1 Materials

3.1.1 UHMWPE wear pins

The UHMWPE used for testing was supplied by Solidur Poly-Hi Meditek under the commercial name Chirulen. This UHMWPE is processed to be purer than conventional grades. The ash content is very low and the titanium and aluminium contents are below 20 and 40 ppm respectively. The physical and mechanical properties are shown in table 1.

The wear pins were cut from the bulk material to a size of 10 mm x 10 mm x 24 mm in length (the wear pin length is not critical and varied slightly). A 45° chamfer was cut along the leading and trailing edges of the wear surface giving an initial cross-sectional area of 90 mm^2.

UHMWPE Properties	Unit	Value
Physical properties		
Density of homogenous material	$g.cm^{-3}$	0.93
Average molecular weight	$g.mol^{-1} \times 10^{-6}$	8
Mechanical properties (at 23°C, 50% RH)		
Tensile strength	MPa	20
UTS	MPa	40
Elongation to fracture	%	>350
Shore D hardness		57
Impact strength (notched)	$MJ.mm^{-2}$	>100
Elastic modulus	MPa	232
Thermal properties		
Melting point	°C	136
thermal conductivity	$W.m^{-1}.K^{-1}$	0.42
Coefficient of friction		
Wet	μ	0.05-0.08
Dry	μ	0.11-0.22

Data was obtained from Solidur Plastics S.A. (Pty.) Ltd and Chemplast Marc Etter (Pty.) Ltd.

Table 1. The physical and mechanical properties of UHMWPE.

The surface hardened UHMWPE wear pins were ion implanted in a nitrogen atmosphere (N+ and N++ species) under an accelerating voltage of 80 keV to a dose of 10^{15} ions.cm^{-2} by NITRUVID (Fraisses, France). Only the chamfered end was treated.

Comparison of the ion implanted pins with the unimplanted pins under a light microscope revealed no changes in appearance of the implanted surfaces. The surface roughness values also remained the same.

3.1.2 The stainless steel counterfaces

The stainless steel counterfaces were machined from grade AISI 431 material and subsequently hardened and tempered to give a final hardness of 460 HV30. Two different methods were used to finish grind the surfaces. The first was to grind the counterfaces in a direction perpendicular to the sliding motion using a mechanical surface grinder. This resulted in the scratch direction running purely perpendicular to that of the sliding motion.

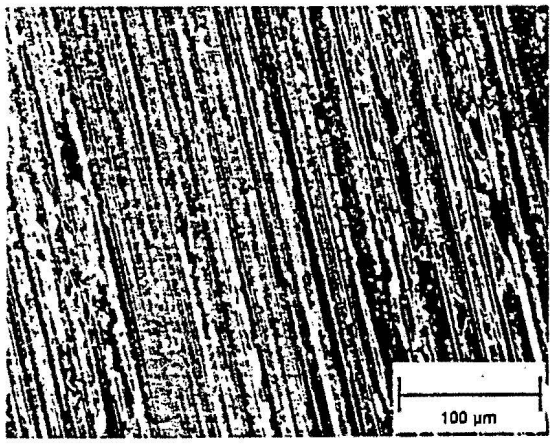

Fig 2. Scanning electron microscope (SEM) image of unworn ground stainless steel surface showing single scratch direction.

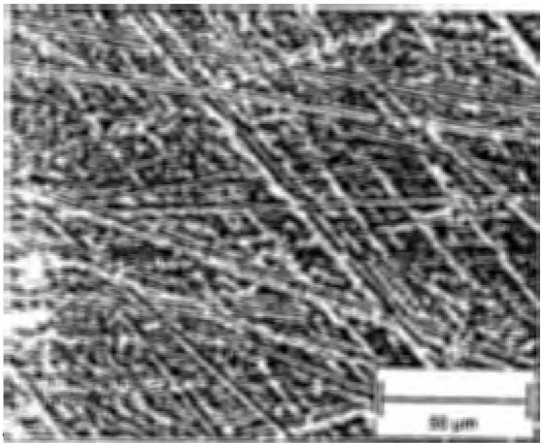

Fig. 3. SEM micrograph of unworn random ground stainless steel surface showing random distribution of scratch direction.

The second method results in a random scratch direction distribution on the counterface. This was achieved by grinding/polishing the specimen wet using a Struers Roto Module automatic polisher with a special adaptor allowing simultaneous polishing of three stainless steel bars. The silicon carbide grinding pads used varied from 200 to 4000 grade according to the surface roughness desired. Surfaces to be polished (R_a = 0.02µm) were further prepared using a silicon carbide suspension.

Following preparation, the surfaces were demagnetized and ultrasonically cleaned. A Taylor Hobson surface profilometer was used to measure the center-line average (R_a) surface roughness of the counterfaces in the direction parallel to that of sliding. Parallel ground specimens were prepared to surface roughnesses ranging from 0.15 to 0.66 µm R_a, while random ground surfaces were prepared to surface roughness values from 0.05 to 0.45 µm.

3.2 Test parameters

The sliding velocity is sinusoidal and reaches a maximum of 0.32 $m.s^{-1}$ at the center of the stroke with an average velocity of 0.2 $m.s^{-1}$. All testing was carried out in a distilled water environment at temperatures between 25 and 27 °C. The test parameters employed are given in Table 2.

Operating Variables	Unit	Value
Stroke	mm	50
Velocity	$m.s^{-1}$	0.2 (ave.)
		0.32 (max.)
Pressure	$N.mm^{-2}$	11
Sliding Distance	km	20-200km
Lubricant		distilled water

Table 2. Operating Variables

3.3 Mass loss and counterface roughness measurement

The UHMWPE mass loss was measured using a Mettler H 54 AR research balance with an accuracy of 0.01mg, taking the mean of three readings. A soak control UHMWPE piece was weighed along with the wear specimens to ensure that no significant amount of water or alcohol (from the ultrasonic cleaning procedure) was absorbed and to check that the balance readings remained consistent.

Polymer mass loss was converted to volume loss (V) which was plotted against the sliding distance (S). This technique is preferred to measuring the dimensional change as the latter may also be influenced by creep. The specific wear rate (K_0) was calculated for both the initial transfer layer forming period of wear (taken as the first 20 km) and the following more stable period (often referred to as the steady state period), as these usually differed greatly. K_0 was obtained by dividing the slope of the graph by the normal load P i.e. K_0 = V/PS ($mm^3/N.m$).

The counterface roughnesses were measured at the start of the test and, for the rougher counterfaces, at regular intervals coinciding with the mass loss measurements. The measurements taken during the sliding intervals were useful in revealing the formation of the transfer layer. However, for smoother counterfaces the recorded wear was extremely low and the scratching effect of the needle deemed insignificant for further surface roughness measurements. Indeed, for very smooth counterfaces the initial surface roughness was obtained by

measuring a third specimen which had been prepared in an identical way but was not used in the wear tests.

3.4 Characterization of the worn material

The worn polymer specimens, counterfaces and wear debris were examined using both optical and scanning electron microscopy. These surfaces were sputtered with an Au/Pd coating to render them electrically conducting, prior to examination in the scanning electron microscope. An accelerating voltage of 10 kV was used.

4. Results

4.1 Wear rate comparisons

4.1.1 Topographical comparisons

Figure 4 represents a typical wear curve of UHMWPE against a hardened stainless steel counterface ground perpendicular to the direction of sliding.

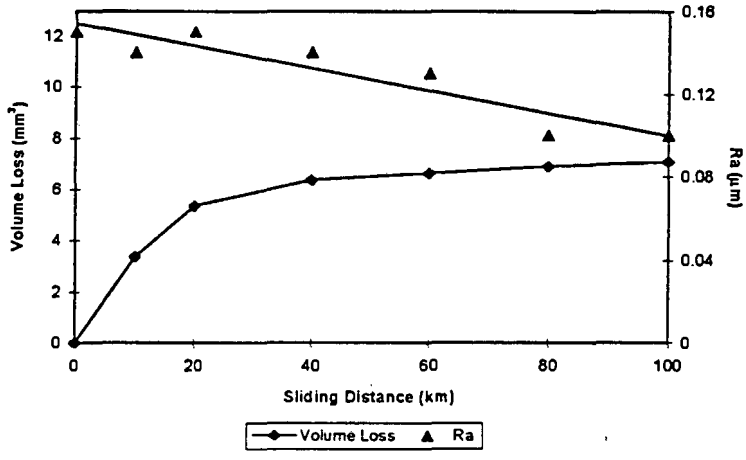

Fig. 4. A typical wear curve for UHMWPE sliding against a stainless steel counterface ground in the direction perpendicular to sliding.

The loss of material is seen to decrease with sliding distance particularly during the first 20 kilometers. Thereafter the volume loss with sliding distance, and hence the wear rate, remain approximately constant and much reduced.

It is also apparent that the surface roughness of the counterface decreases with sliding distance from approximately 0.16 to 0.11 µm, indicating the build up of a polymer transfer layer.

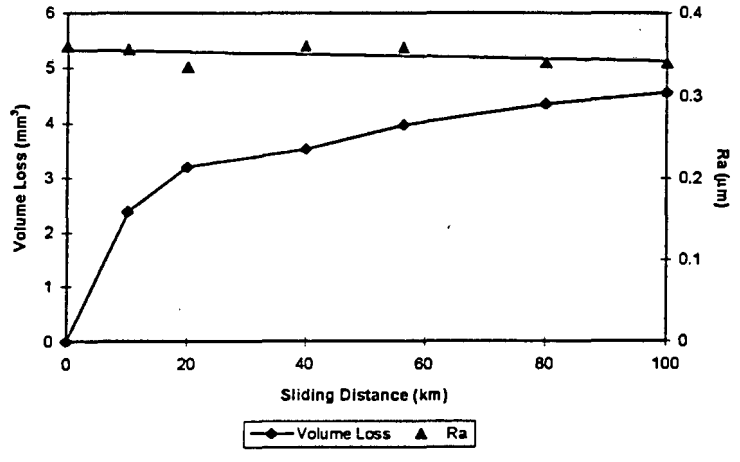

Fig 5. A typical wear curve for UHMWPE sliding against a random ground stainless steel counterface.

Figure 5 shows a typical result for UHMWPE sliding against a randomly ground stainless steel counterface. Again, the initial wear differs markedly from that after about 20 km of sliding. For each test therefore, both

against polished and ground surfaces, an initial wear coefficient K_i and stable wear coefficient K_s were calculated for the initial wear period (up to 20 km) and stable wear period (20 to 100 km) respectively. It is noticable that the counterface roughness value does not change significantly from the original value of 0.35 μm with sliding distance up to 100 km.

Figure 6 shows the relationship between initial UHMWPE wear (ie that of the first 20 km of sliding) and counterface R_a for parallel ground counterfaces of $R_a \leq 0.66$ μm. Increasing the R_a values up to 0.54 μm results in a slight increase in this initial wear rate. However, above an R_a value of about 0.54 μm the wear rate increases drastically.

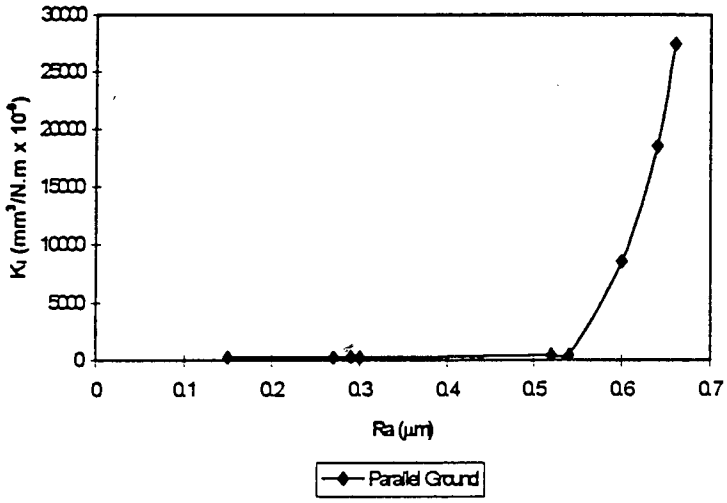

Fig. 6. Initial wear rate as a function of surface roughness for parallel ground counterfaces.

Figure 7 presents the dependency of the initial wear rate for UHMWPE wearing against random and parallel groung counterfaces (of $R_a \leq 0.54$ μm). Significantly, the initial wear factor K_i for wear against the randomly scratched counterface is much lower (about half) than that for parallel ground counterfaces, for similar values of surface roughness.

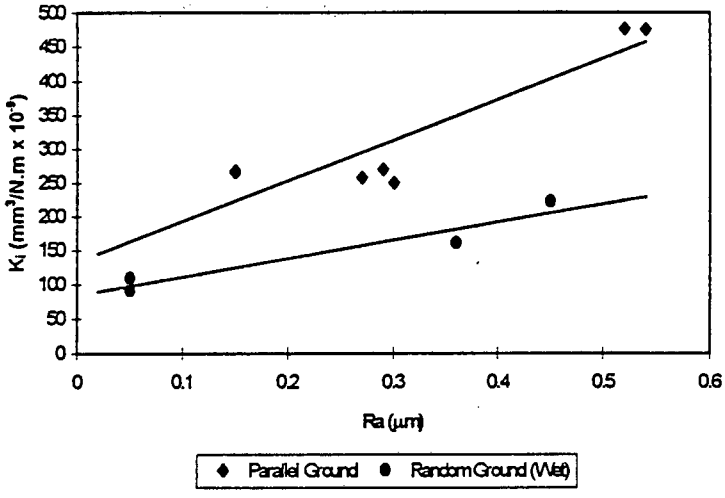

Fig. 7. Initial wear rate as a function of surface roughness for parallel ground and random ground counterfaces.

Figure 8 shows the stable UHMWPE wear dependancy on counterface roughness. The stable wear rate is

similar for both the parallel ground and the random ground counterfaces (for equivalent surface roughness values). This indicates that the ratio of initial wear to stable wear is greater for the parallel ground instance because of the higher initial abrasive action (prior to transfer layer formation) of the parallel ground counterface.

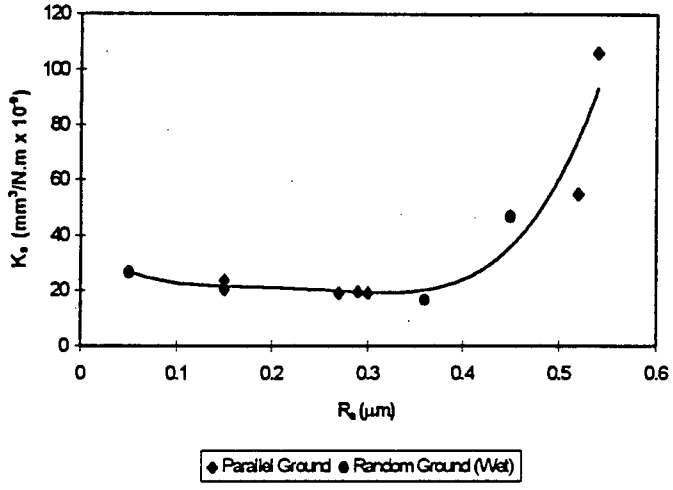

Fig. 8. Stable wear as a function of surface roughness for parallel ground and random ground counterfaces.

4.1.2 Comparative wear rate of ion implanted UHMWPE

Only tests against polished stainless steel counterfaces have yielded any difference in wear behaviour. This is because the surface treated layer is very thin and is thus easily worn away against rougher counterfaces. Liao *et al.* showed that for a dose of 1.0×10^{15} ions/cm^2 the hardness increase is significant only to 0.5 µm depth. Thus even for the very low wear rates achieved with surface treated UHMWPE wearing against polished stainless steel counterfaces, most of the hardened layer will be removed after less than 10 km of sliding and hence only initial wear rate improvements can be expected.

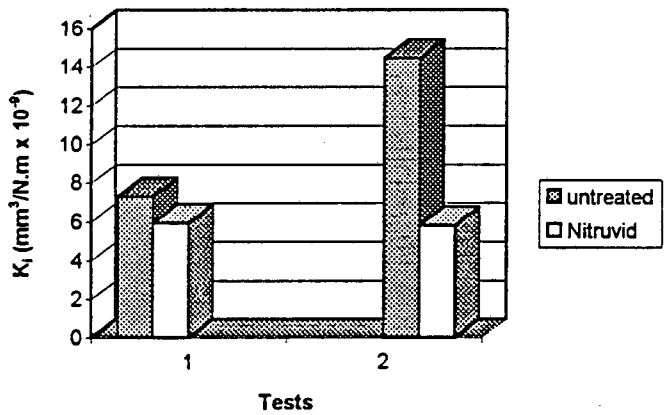

Fig. 9. Chart representation of the comparitive wear performance of untreated and ion implanted UHMWPE after 20 km.

Only two tests against polished counterfaces (R_a = 0.02 µm) covering 20 km have been conducted. The results, although varying substantially due to the difficulties encountered when measuring such low wear rates, favour the ion implanted UHMWPE.

4.2 Transfer layer formation

For UHMWPE worn against very rough counterfaces ($R_a \geq 0.54$ µm) the formation of a stable transfer layer was not found and very high wear rates result. Figure 10 is a SEM micrograph showing a rough (R_a = 0.65µm) stainless steel counterface after 20 km of sliding against UHMWPE. No transfer layer is visible. By contrast, figure 11 shows a stainless steel counterface of low initial surface roughness (R_a = 0.05 µm) after 100 km of

sliding against UHMWPE. The scratches seen on the same counterface in figure 3 are no longer visible due to the formation of the transferred polymer layer.

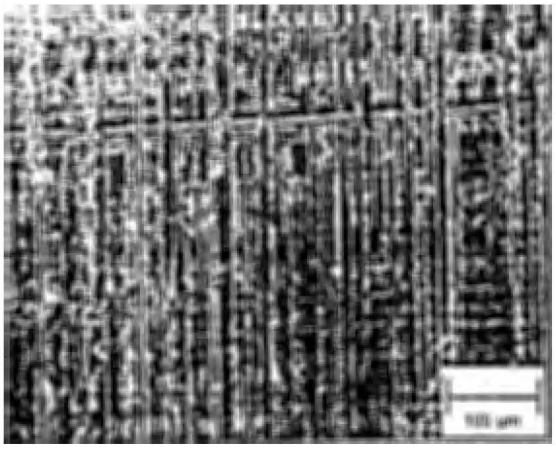

Fig. 10. Rough stainless steel counterface (R_a = 0.65 μm) after 20 km of sliding against UHMWPE No transfer layer has formed.

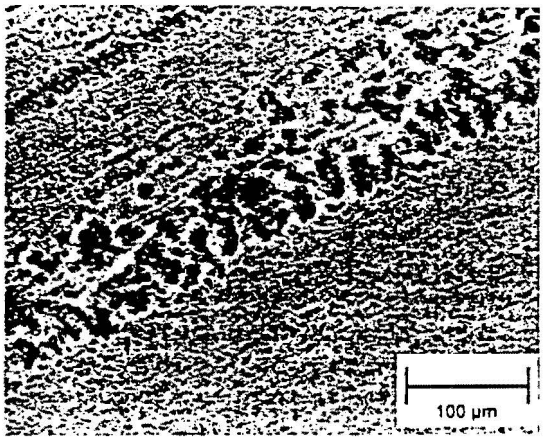

Fig. 11. Smooth stainless steel counterface (R_a = 0.05 μm) after 100 km of sliding against UHMWPE. The transfer layer, with some areas of rupture, is visible.

4.3 The nature of the worn UHMWPE surface

Examination of the worn surfaces revealed different surface characteristics encountered for specimens worn against different counterface topographies.

Surface ripples are associated with surface fatigue wear (Wang *et al*, 1997). This wear mode usually results in very low rates of wear. Most UHMWPE surfaces worn against very smooth counterfaces showed such rippled regions (figure 14 and 15).

Sliding against very rough parallel ground counterfaces shows no transfer layer formation. The UHMWPE wear surface shows signs of large plastic deformation, cracking in addition to abrasive tracks (figure 12).

When transfer layers are formed, the UHMWPE wear surface appeared much "cleaner" and ordered. Figure 13 shows polymer being sheared off the surface and surface cracks, evidence of the adhesive wear mechanism (counterface Ra = 0.36, random ground) prevalent when wearing against smoother counterfaces.

Fig. 12. UHMWPE wear surface after 20 km of sliding against a rough stainless steel counterface (R_a = 0.65 μm). Abrasive tracks and polymer cracking are very visible, leading to very high wear rates.

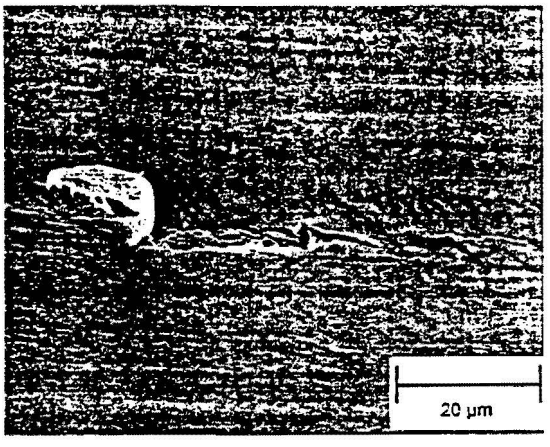

Fig. 13. Polymer shearing off the wear surface (counterface R_a = 0.36 μm, random ground, sliding distance covered = 100 km).

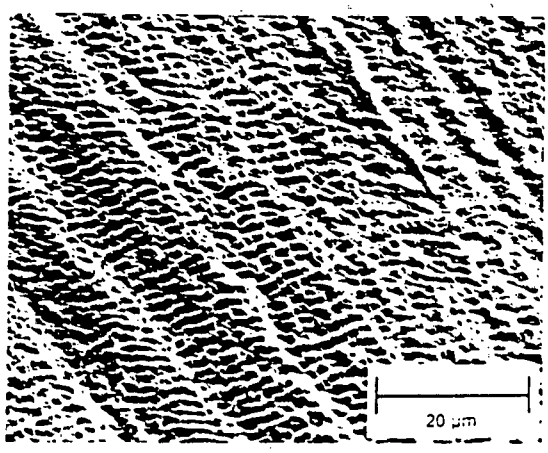

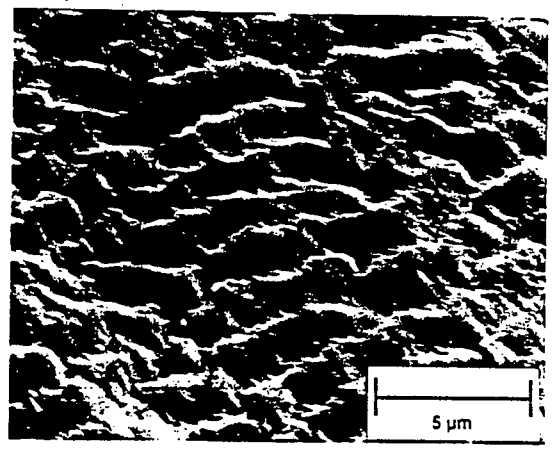

Fig. 14 and 15. Surface ripples associated with surface fatigue wear and very low wear rates (counterface R_a = 0.2 µm, parallel ground, sliding distance covered = 100 km). The sliding direction is perpendicular to the ripple direction.

5. Discussion

It is generally believed that low wear rates are only obtained in a polymer on metal sliding couple when a stable polymer transfer layer is formed on the metal counterface. The absence of such a transfer layer will result in much increased wear rates.

This transfer layer dependency of UHMWPE-on-metal wear has been graphically shown where for very rough counterfaces no stable transfer films are allowed to form and extremely high rates of wear result. The large increase in wear with increasing surface roughness has been reported elsewhere. Lloyd *et al.* formulated the relationship of steady state wear to surface roughness as

$$\text{Specific wear rate } (mm^3/N.m) = 1.1 \times 10^{-8} \exp(7.7R_a)$$

and also noticed a change of wear mechanism at approx. R_a = 0.4 µm. The steady state wear rates shown by the author conformed to the trend of the Lloyd *et al.* equation, although they were generally much lower because of the finer grade of UHMWPE used. Marcus (Marcus, 1992), using UHMWPE grade B15, achieved steady state wear rates very similar to those of the authors'.

The lack of transfer layer formation for rough counterfaces (R_a > 0.54 µm) may be explained by an inability of the larger surface corrugations to adequately restrain the polymer debris i.e. the wear product is easily removed from the valleys in-between the asperities, which is not the case when stable transfer layer formation is allowed.

The effect of surface roughness parameters such as shape, slopes, height distribution and radii of curvature of the metal asperities can be expected to play a critical role in mechanical interlocking in the early stages of wear, prior to transfer layer formation (Marcus *et al.*, 1994). Hence there is a difference in initial wear rate between UHMWPE against parallel ground and random ground counterfaces for equivalent R_a values, the wear against parallel ground counterafaces being higher due to the greater initial abrasive action of those counterfaces. Once a stable transfer film has formed, the comparative wear rates against the differently prepared counterfaces coincide well, in both cases being much lower than the initial wear.

At low counterface roughnesses (R_a < 0.3 µm), the dependency of the stable wear on the surface roughness becomes much reduced and may even rise for wear against very smooth counterfaces, this feature having been ascribed to the increased difficulty of coherent transfer layer formation upon such very low surface roughness counterfaces (Dowson *et al.*, 1978). However, this rise in wear usually only occurs below counterface roughnesses of R_a = 0.025 µm (Tanaka *et al.*, 1985).

Surface hardening UHMWPE by implantation with nitrogen ions has shown an improvement in wear after 20 km of sliding against suitably smooth stainless steel counterfaces. However, due to the small implantation depth achieved with the current test specimens, the hardened layer is easily removed during the initial high wear period. Even when wearing against smooth, polished counterfaces the layer is estimated to be worn away after 10 km. However, the reduction in this initial high period of wear can have a very significant influence on the overall polymer loss.

Higher accelerating voltages and greater implantation doses may lead to further improvements, even against rougher counterfaces. Rieu *et al.* have shown that for doses of 1.4×10^{17} ions/cm^2, nanohardness increases from 0.030 GPa to 0.090 GPa are registered at depths of 0.5 µm, whereas for the current implantation dose used by the author (1.0×10^{15} ions/cm^2) the surface hardened layer will not be deeper than 0.5 µm . For

increased doses, the hardened layer is thus much thicker and should last beyond the initial higher period of wear, resulting in not just lower initial and hence total wear, but also reduced steady state wear.

Acknowledgements
The authors gratefully acknowledge the financial assistance of Eskom and the Foundation for Research and Development.

References

[1] Jasty, M.; J. Applied Biomater., (1993),4 , pp.273-276.
[2] Liao, J.D., Rieu, J., Corre, Y., Rabbe, L.M., Boudoukha, L., and Paletto, S.; Proc. World Ceramics Congress, Int. Ceramic Fed., Florence, (1994).
[3] Wang, A., Essner, A., Polineni, V.K., Sun, D.C., Stark, C. and Dumbleton, J.H., New Directions in Tribology, Plenary and Invited Papers from the First World Tribology Congress, (1997), pp.443-458.
[4] Marcus, K. and Allen, C., Wear, (1994), 178, pp.17-28.
[5] Dowson D., Challen J.M., Holmes K., and Atkinson J.R., Proc. 3rd Leeds-Lyon Symp. on Tribology, MEP, London, (1978), pp.99-102.
[6] Marcus, K., Thesis, University of Cape Town, (1992).
[7]Tanaka K. and Yamada Y., Proc. Conf. on Wear of Materials, ASMA Trans., (1987), Vol. 101 pp. 407-414.